A STUDY OF DUCTED JETS INCLUDING
THE EFFECT OF DILUTE
POLYMER SOLUTIONS

A THESIS

Presented to

The Faculty of the Division of Graduate Studies

By

Rajagopala K. Menon

In Partial Fulfillment

of the Requirements for the Degree

Doctor of Philosophy in the

School of Aerospace Engineering

Georgia Institute of Technology

August, 1976

A STUDY OF DUCTED JETS INCLUDING

THE EFFECT OF DILUTE

POLYMER SOLUTIONS

D. P. Giddens, Chairman

J. E. Hubbartt

L. H. Bangert

Date approved by Chairman: 7/29/76

ACKNOWLEDGMENTS

I wish to express my sincere appreciation to my advisor, Prof. D. P. Giddens, for his advice and help throughout my research work. His efforts to generate interest in the field as well as his encouragement during the experimental studies made my research work a most pleasurable and rewarding experience.

I also wish to thank Dr. R. A. Cassanova for his help during various phases of the experimental study.

Sincere appreciation is also expressed to Prof. J. C. Hubbartt and Prof. L. H. Bangert for the comments on the original manuscript.

A large number of friends have stimulated interesting discussions as well as provided an atmosphere conducive to research. I wish to express my thanks to all of them.

Special permission was received from the Division of Graduate Studies to vary the format of this thesis from that required in the Thesis Manual (extra spacing between paragraphs and pagination) so that this thesis could be generated on the computer.

Finally, I am grateful to my mother for her encouragement in my academic pursuits and I dedicate this work to her.

TABLE OF CONTENTS

NOMENCLATURE

C_p	Pressure coefficient
C_F	Skin friction coefficient
C_1, C_2, C_3, C_D	Coefficients in two equation model
R	Resitance in equation (25)
T_s, T_f	Temperatures in equation (25)
U	Uniform value of outer velocity
U	Uniform value of jet exit velocity
U	Mean velocity in x-direction
U	Average velocity in the duct
U	Jet exit velocity at the axis
V	Voltage in equation (26)
W	Square of vorticity frequency
a, b, c, d	Coefficients in equation (23)
k	Turbulent kinetic energy
l	Mixing length
n	Parameter defined in equation (26)
r	Radial coordinate
u', v', w'	Turbulence velocities
x	Streamwise coordinate
k	von Karman constant
α	Temperature coefficient of resistance

SUMMARY

A theoretical and experimental study of a ducted jet has been conducted. The study was motivated by complications that occur during angiographic injections. The analytical study was done using the equations governing the flow obtained by making the boundary layer assumptions. The k-W model equations were employed to model the turbulent mixing of the ducted jet. The Patankar and Spalding method for coupled parabolic equations was adopted to solve the governing set of equations.

Computations were carried out for Reynolds number values of 1.70×10^{5} and 1.36×10^{4}. Comparison with experimental data indicated that the near field of jet expansion was sensitive to initial conditions. Depending upon the injection conditions, the pressure and friction coefficients may or may not exhibit local maxima distal to the injection plane. It was also observed that by exercising considerable care in selecting the initial conditions the k-W model of turbulence was successful in predicting the flow with reasonable accuracy.

In vitro measurements of the angiographic injection situation were done for a Reynolds number of 1.36×10^{4} using

a conical hot film probe. Measurements were made by traversing the probe radially at eight axial locations. Mean and turbulence velocities and turbulence energy spectra were obtained from the measurements. Experiments were carried out using both water and dilute solutions of Polyox WSR-301 as the mixing medium.

The measurements indicated that the outer flow was not much influenced by the jet expansion. The same result was observed from the computed value of pressure and skin friction coefficients. Near field energy spectra in the wake of the lip of the jet tube exhibited a spike indicative of the dominant eddy size in the mixing layer.

To find the influence of the polymer on confined jets, the results of polymer solutions and water were compared. The centerline velocity indicated a faster decay for the case of polymer solution, in the near field mixing. This behaviour is similar to the centerline variation for free jet mixing of polymer solutions. Further, the higher turbulence intensity for the case of dilute polymer solutions supports the free jet nature of mixing of the ducted jet in the initial region of mixing. Radial variation of turbulence intensity exhibited the influence of the polymer in the mixing layer. Far downstream, for the fully developed case, the turbulence intensity near the wall is higher for the case of polymer solution. In the developing region of the flow the polymer solution exhibits a higher energy content in large scale eddies than does the water flow. This suggests the tendency to enhance mixing may be through the mechanism of larger eddy transport. In conclusion, polymer solutions may aid in obtaining better angiograms by improving the mixing characteristics of the contrast media.

CHAPTER I

INTRODUCTION

One of the more common arterial diseases, atherosclerosis, occurs from hardening of the fatty deposits in the inrer layers of an artery. These deposits, called plaques, can accumulate to such an extent that blood supply to distal regions is severely compromised. A common way of diagnosing this disease is by the method of angiography. In many cases of angiographic procedures the first step is to expose an artery (either in the arm or leg) and a catheter is introduced into the vessel by puncturing the arterial wall [1]. The flexible catheter is maneuvred into the artery so that its tip reaches the region of interest (e.g. coronary artery) where the study is to be made. Then, after positioning the catheter, a bolus of radiopaque fluid is injected into the blood vessel. An X-ray picture, known as an angiogram, outlines the region of the blood vessel containing the radiopaque contrast medium.

These intravascular injections are usually made under high pressure producing a jet of fluid mixing with the blood flow in the vessel. The forces resulting from this rather violent fluid injection may fragment or dislodge atheromatous plaques, resulting in subsequent transport of emboli downstream. These may partially or totally occlude the smaller distal vessels. In cerebral angiography such a situation can result in permanent disability or even death of the patient [2-5].

Typical values of injection rate may be between 6 and 10 cc/sec whereas the catheter tube radius may lie between 0.6 mm and 1 mm. This suggests that the injection velocities could be as high as 12 m/sec. These are extremely large values of velocity compared to the flow velocity in the vessel. In such clinical situations, the existence of a recirculating zone due to jet mixing is a strong possibility.

The serious nature of the complications is a very strong motivation to study the injection problem in detail. From a fluid mechanical standpoint a study of the structure of the flow field is of great interest since such a study will enhance the knowledge about the nature of mixing, influence of various parameters on flow field development, and lead to a better understanding of the injection procedure. This may also suggest improvements from a clinical standpoint. For example, the need for obtaining a good contrast medium, so as to obtain a clear angiogram, points towards the need for better mixing. This in turn could be achieved from the knowledge gained by the understanding of the fluid dynamical aspects of the angiographic injection situation.

Further, it would be most encouraging if one could suggest possible ways of reducing the trauma due to the fluid dynamics of the procedure. It is in this context that the phenomenon of drag reduction exhibited by dilute solutions of certain high molecular weight polymers is of relevance. Toms [6] was the first to make quantitative flow measurements using dilute polymer solutions. Since then a wide variety of experiments have explored the various aspects of drag reduction effect. Some of the additives such as Separan [7], DNA [8] and Polyox [9] exhibit drag reducing effect for the case of blood flow through a pipe . Since these polymers have a tendency to lower the shear stress at the wall (for pipe flow, at least), it was decided to undertake a study to determine if the presence of drag reducing polymers created a favorable modification of the flow fielc in angiographic injections.

Fluid mechanically, the angiographic injection can be considered to be similar to a ducted jet. The problem of such a confined jet has many interesting aspects of interest in fluid mechanics in the sense that it has regions similar to entrance flows, jet expansions, and fully developed shear flows. The interaction among these makes the problem fascinating, as well as complex in analysis. The presence of the duct wall boundary distinctly alters the nature of flow from that of a free jet because of the continuous momentum transfer to the wall from the fluid medium. In addition, the mixing of two shear layers (wall boundary layer and the mixing region of the jet) further complicates the flow structure. The assumption of the jet being concentric to the duct may not be the exact modelling of the angiographic injection, but is a reasonably accurate first approximation to study the problem, and is adopted here.

The initial attempts to study the problem were to divide the flow into distinct regions where simplifying assumptions could be applied. A majority of the studies have been on mixing of air jets with air as the surrounding medium. Many of the initial analytical studies are related to the study of a jet in a unconfined co-flowing stream. Squire and Trouncer [10] used an integral momentum approach to study the case of a turbulent axisymmetric jet in a coflowing stream of constant velocity. The radial variation of velocity in the mixing region was assumed to follow a cosine form and the turbulence model was Prandtl's mixing length model.

Experimental measurements by Forestall and Shapiro [11] provide concentration and velocity profiles. Helium was used as tracer gas (for the jet) and air as the mixing medium. The results were compared with those obtained using Squire and Trouncer's method. By properly selecting the proportionality factor in the turbulence model a fairly good agreement for the jet half-width is obtained. Since the jet is confined, the analytical approach is valid at best only in the region where confinement effects are small.

Mikhail [12] employed the integral form of equations of motion, assuming the nature of the velocity profile, to study the ducted jet. By making suitable assumptions (velocity constant in the potential core and in the secondary potential flow region) the equations were linearized. The computations were carried out using a mixing length model for turbulence. Good agreement in mean velocity values between computations and his experiments in air was obtained by appropriately choosing the proportionality factor, the value of which was not constant with axial distance, in the mixing length model.

Craya and Curtet [13] developed an analytical method for confined jets. Integral forms of momentum and moment of momentum equations were used in this study. The excess velocity profile is taken as a member of a two - parameter family of curves. For studying two dimensional, as well as axisymmetric, jet flow cases the excess velocity was taken to be self preserving and the co-flowing stream was assumed potential. The results are valid, at best, up to the point where the free shear flow reaches the wall boundary layer. Experimental studies by Becker et al. [14] brought out the importance of a single parameter (Craya-Curtet parameter, Ct) as the possible criterion for similarity. The experimental studies of Curtet [15] were done for two dimensional (mixing medium-water), and Curtet and Ricou [16] for axisymmetric, (mixing medium - air) jet expansion. Abramovich [17] obtained a solution for co-flowing free streams using an integral form of the equations of motion. The confined jet problem was then analyzed by approximating the velocity field at every cross section of the mixing chamber by that of a free jet. Another integral approach is that by Hill [18] who used free jet data to do the computations.

Alpineri [19] conducted experiments for the case of carbon dioxide and hydrogen jet mixing with air. His calculations, based on the assumption that transport coefficients can be taken to be independent of the radial coordinate, gave results of mean velocity and concentration in good agreement with his experimental values. Weinstein, et al. [20] conducted experiments for the case in which the co-flowing stream moved faster than the jet. A recent experimental study of the ducted jet problem gives detailed information about mean and turbulent flow quantities. The study of ducted jet mixing for air by Razinsky and Brighton [21] was carried out for a wide range of radius and velocity ratios. The analytical study of Exley and Brighton [22] used integral forms of equations of motion. To obtain the results, the shape of the velocity profiles in the duct wall boundary layer (one-seventh power law profile) and in the jet mixing zone were assumed. Brandon [23] used very simple models for the eddy viscosity (constant and proportional to half radius) and compared experimental and theoretical values of total pressure distrubution. Hedges and Hill [24] have made measurements of a compressible jet mixing in a duct of converging-diverging geometry. For comparison a finite cifference scheme was used to rewrite the governing equations. A mixing length model was used in the equations and the value of the proportionality factor was suitably chosen in the computations. Minner [25] studied incompressible jet mixing in a constant diameter duct. He calculatec radial and axial eddy viscosity distributions from the mean velocity and Reynolds stress profiles obtained experimentally.

In summary, it should be pointed out that the results obtained by Razinsky and Brighton [21] for air are detailed and are of interest here. Their experimental results will be used as a check for the computational technique to be adopted. Previous efforts on the computational side suffer from various shortcomings. All of them employ a very simple model to simulate the turbulent mixing procedure, with the result that the coefficient or the proportionality factor cannot be chosen a priori. Further, the integral methods require the knowledge of the nature of the velocity profile. Such approaches are accurate only sufficiently far downstream of the jet exit and the results are not very reliable in the initial mixing region.

The research efforts referenced above were all for the case of a pure solvent (air or water) as the mixing medium. The next step is to review the efforts for polymer solutions as the mixing medium. Since the study by Toms [6] for a fully developed pipe flow, various aspects of the drag reduction phenomenon have been investigated. Still, it is far from being fully understood. The interest in this field has grown considerably in recent years with the result that various flow situations have been studied. This has resulted in a tremendous growth of literature in this field, raising many interesting cuestions about the phenomenon of drag reduction. Fortunately, excellent review papers have helped put the problems in a proper perspective. The two papers by Lumley [26,27] were more in the initial stages of the study of drag reduction. A more recent review by Hoyt [28] presents the state of the art as well as current theories to explain the phenomenon. Gadd [29] and Granville [30] also have given reviews of the progress in drag reduction research. Darby [31] has briefly reviewed several of the theories proposed to explain drag reduction.

The problem of the expansion of a jet of dilute polymer solution has been studied only by few and, interestingly, the results are not in agreement. All research to date has been for a free jet expanding into a stationary ambient fluid, with one exception. For example, a simple visual study of a round submerged jet was made by Gadd [32]. Comparison of jet expansion of water and a 30 parts per million (ppm) solution of Polyox suggested suppression of small scale eddies. Another visualization by A.White [33] showed that solutions of guar gum up to 500 ppm concentration had no visible effect on the jet spreading. He also found that solutions of Polyox exhibited turbulence suppression for concentrations greater than 10 ppm but this effect disappeared for aged solutions of Polyox. The first quantitative measurements were made by D. A. White [34] who used a recirculating flow system. His study of free round jets expanding into a stagnant medium showed that a jet of Polyox had a greater spreading angle than that of water. However, solutions of Guar gum and HEC did not show any such behaviour. D. A. White used a pitot tube to make measurements. It is well known that hot wire anemometers and pitot tubes exhibit anomalous behaviour when used in polymer solutions [35,36] . As was shown by A. White the aging of the solution also affects the observations. Hence, the observations of D. A. White must be approached cautiously. To eliminate the dependence of measurements on physical properties of the fluid, optical methods of measurements have been developed. Vlasov, et al.[37] studied the expansion of a round jet using a Laser Doppler Velocimeter (LDV). Their observations with solutions of guar gum showed that center line velocity for the solution case decayed faster than that for water (as observed by D.White with Polyox). The turbulence measurements at the center line indicated an increased level of turbulence for the case of guar gum solution. More recently, Barker [38] used the LDV to study round jets of dilute polymer solution. His experiments with a jet nozzle diameter of 0.64 and 1.91 cm for solutions of Polyox did not indicate any changes from the results obtained for water. However, when a tube of length 63 cms and diameter 0.63 cm was added on to the nozzle so that the flow at the end of the tube was a fully developed pipe flow, jet spreading was found to be larger than that for water. It was also found that polymer additives reduce the center line velocity and increase the turbulence at the center line during the early growth of the jet. These observations give support to his opinion that the inconsistencies of previous experimental results were due to the dependence of downstream flow upon initial conditions. The only previous study of polymer injection along a duct center line was by Wells and Spangler [39]. Their aim was to find the effects of injecting the polymer solution at the wall and along the center line of a pipe with water flowing through. The injection was done into a fully developed pipe flow and the effectiveness of polymer injection was observed through static pressure measurements at the wall. The measurements show the polymer to be more effective for the case of injection at the wall than for injection along the center line.

In summary, there have been no attempts to analyze in detail the flow situation in angiographic injections. As for the fluid mechanics literature in the case of pure solvents, it can be shown that the methods of prediction, with the exception of two [23,24], use an integral form of the equations of motion followed by a suitable assumption for the velocity profile in the region of study. The assumption made on the nature of the profile indicates that the results are good only sufficiently downstream of the jet exit. Further, excluding two of the approaches [22,24] all the others have not taken account of the interaction of the jet mixing layer with the boundary layer on the duct wall. The results obtained using these methods are good only till the jet spreading reaches close to the wall. Finally, all of them adopted a simple model to simulate the turbulent mixing procedure. Methods using a simple mixing length model had to choose the proportionality factor to obtain good agreement between experiment and theory. Others assumed the nature of variation of eddy viscosity in the region of study. Besides the obvious lack of generality in prediction capability of these models, they are of dubious validity in computations for a complex, ducted jet flow.

As far as experimental studies are concerned, mean and turbulent quantities are provided in sufficient detail for air mixing. Investigations using liquid as the mixing medium have also been carried out. However, conditions of Reynolds number close to situations in clinical angiography are of interest and the need for experimental study of flow under such conditions is evident. No detailed quantitative measurements for the case of a ducted jet using dilute polymer solutions have been made. In addition, the conventional methods of measurement are solution dependent and sometimes exhibit anomalous behaviour.

Keeping these points in view, the aims of the present investigation are as follows.

1. To develop a computational procedure which

incorporates a detailed advanced turbulence model for describing certain classes of angiographic injection flows. Some possible values of jet injection velocity could be as high as 12 m/sec and in such a situation a recirculation region exists in the flow field. However, the motivation here is to develop a method for situations in which there is no recirculation.

2. To experimentally simulate the injection flow problem so that the measurements can be compared with theoretical predictions.

3. To compare the injection of a pure solvent with that of a polymer solution into a co-flowing, confined stream.

It is clear that in a clinical situation such as angiography the injection conditions are varied and the flow field is complex. Because of these, the present study has been limited to the experimental and theoretical description of a single set of conditions which is typical of certain clinical injections. However, the various possibilities associated with angiographic injections - retrograde injection, side-hole catheters, small vessel visualization - are numerous. Thus the example selected for study does not provide exhaustive coverage of angiographic modelling but is only a representative situation. It is expected that this study would improve the knowledge of angiographic injection procedures.

CHAPTER II

ANALYTICAL METHOD

The approach used for the analytical study is described in this chapter. The first section outlines the modelling of the problem and the second is concerned with the numerical scheme adopted in the computation.

Theory

In the previous chapter it was shown that the angiographic injection, with certain reasonable simplifications, may be modelled by a ducted jet expansion flow. Thus, the flow problem of interest is an axisymmetric jet mixing with the confined flow in a circular duct, the jet being taken to be concentric with the outer duct. Certain simplifying assumptions have been made for the flow. These are

1. The circular duct is of constant cross section with rigid boundaries.

2. The mixing is considered to take place between streams, jet and the confined flow, of the same fluid.

Based upon these, the present approach can be considered as the first step in understanding the clinical situation. The geometry of the flow problem is as shown in Figure 1. The jet issues from the inner circular tube. The flow is incompressible. Cases selected for the analytical study are such that there is no recirculation created by injection. Further, previous experimental measurements [19,20] have shown that the radial variation of static pressure of the flow is almost negligible. In the light of these, the boundary layer assumptions are applied to the full Navier-Stokes equations of motion for axisymmetric flow.

The problem is to be studied for sufficiently high Reynolds numbers that the flow is turbulent throughout. The need for turbulent modelling arises from the necessity for closure in the formulation of a turbulent flow problem. Since the ways in which turbulence closure can be accomplished are varied [40], the choice for turbulence modelling is not unicue. The most useful model of turbulence in a given class of flows is that which gives acceptably accurate results with the minimum number of differential equations. The simple mixing length model is restrictive in application because of its drawbacks. First, agreement between theory and experiment must usually be obtained by suitably adjusting the proportionality factor in the expression for mixing length and hence the correct

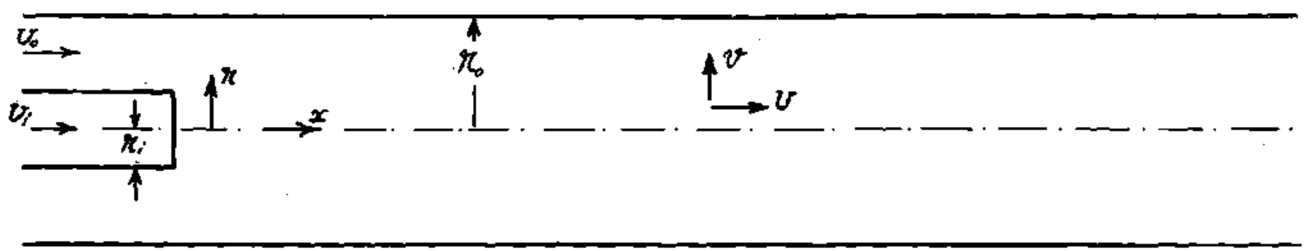

Figure 1. Flow Geometry.

value of this factor for a flow is not known a priori. Further, the mixing length approach deals with only the "localness" of turbulence and ignores the history of turbulence [41]. It is found that one equation models require ad hoc adjustment of the empirical input and are, in this sense, not substantially better than Prandtl's mixing length model. As the number of equations increase there is an increase in the need for intuition in constructing individual terms of the equation and in the empirical knowledge required for setting the values of constants which are introduced [41]. Previously, three equation models have not given results superior to those of two equation models [41]. Two equation models have been shown to give acceptable accuracy in a wide variety of turbulent flows with a reasonable amount of computational effort [42]. Therefore, such a model was selected for the present study.

Specifically, the two equations are those governing k, the kinetic energy of turbulence, and W, which can be considered proportional to the square of the mean frequency of turbulence. The aspect of interest here is that the length scale is not prescribed algebraically but is determined from k and W values. A discussion of the k-W model may be found in the literature [42,43].

Turbulent viscosity is defined by

$$\mu_T = \rho k^{1/2} l \tag{1}$$

where the mixing length "l" is given by

$$l = k^{1/2} / W^{1/2} \tag{2}$$

The governing equations of motion are

$$\frac{d}{dx}(Ur) + \frac{d}{dr}(vr) = 0 \tag{3}$$

$$\rho U \frac{dU}{dx} + \rho v \frac{dU}{dr} = -\frac{dp}{dx} + \frac{1}{r}\frac{d}{dr}(r\tau) \tag{4}$$

$$\rho U \frac{dk}{dx} + \rho v \frac{dk}{dr} = C_\mu \rho \frac{k}{W^{1/2}} \left(\frac{d^2 U}{dr^2}\right)^2 - C_D \rho \frac{k^{3/2}}{l}$$

$$+ \frac{1}{r}\frac{d}{dr}\left(\frac{r\mu_{eff}}{\sigma_k}\frac{dk}{dr}\right) \tag{5}$$

$$\rho U \frac{dW}{dx} + \rho v \frac{dW}{dr} = C_1 \rho \frac{k}{W^{1/2}} \left(\frac{d^2 U}{dr^2}\right)^2 + C_3 \rho \frac{k^{1/2}}{l}\left(\frac{dU}{dr}\right)^2$$

$$- C_2 \rho \frac{k^{1/2}}{l} W + \frac{1}{r}\frac{d}{dr}\left(\frac{r\mu_{eff}}{\sigma_W}\frac{dW}{dr}\right) \tag{6}$$

The quantities $C_1, C_2, C_3, C_D, C_\mu$ are coefficients in the turbulence model. The effective viscosity is μ_{eff} which has laminar, as well as turbulent, contributions. The computational procedure to be adopted was developed by

Patankar and Spalding for boundary layer flows [44]. Basically, the method uses a modified von Mises transformation which results in the flow regime lying between fixed ordinates ($\omega=0$ and $\omega=1$) in the transformed plane.

The transformation is from the (x,r) plane to the (x,ω) plane, where ω is given by

$$\omega = \frac{\psi - \psi_I}{\psi_E - \psi_I} \tag{7}$$

Here, ψ is the stream function, defined mathematically by

$$\frac{d\psi}{dr} = \rho U r \tag{8}$$

$$\frac{d\psi}{dx} = -\rho v r \tag{9}$$

The stream functions at the inner and outer boundaries ψ_I and ψ_E, are taken to be functions of x only. Hence, the flow region lies between $\omega=0$ and $\omega=1$. From the definition of ψ, the relations

$$\frac{d\psi_I}{dx} = - r_I \dot{m}_I'' \tag{10}$$

$$\frac{d\psi_E}{dx} = - r_E \dot{m}_E'' \tag{11}$$

must hold, where $\dot{m}''_I$ and $\dot{m}''_E$ are the mass transfer rates across I and E surfaces.

The transformed equations in (x-ω) plane are

$$\frac{dU}{dx} + \frac{r_I \dot{m}''_I + \omega(r_E \dot{m}''_E - r_I \dot{m}''_I)}{(\psi_E - \psi_I)}\frac{dU}{d\omega} = \frac{d}{d\omega}\left[\frac{r^2 \rho U \mu_{eff}}{(\psi_E - \psi_I)^2}\frac{dU}{d\omega}\right] - \frac{1}{\rho U}\frac{dp}{dx} \tag{12}$$

$$\frac{dk}{dx} + \frac{r_I \dot{m}''_I + \omega(r_E \dot{m}''_E - r_I \dot{m}''_I)}{(\psi_E - \psi_I)}\frac{dk}{d\omega} = \frac{\rho U r^2 \mu_{eff}}{(\psi_E - \psi_I)^2}\left(\frac{dU}{d\omega}\right)^2 - C_D\frac{k^{3/2}}{Ul}$$

$$+ \frac{d}{d\omega}\left[\frac{r^2 \rho U}{(\psi_E - \psi_I)^2}\mu_{eff}\frac{dk}{d\omega}\right] \tag{13}$$

$$\frac{dW}{dx} + \frac{r_I \dot{m}''_I + \omega(r_E \dot{m}''_E - r_I \dot{m}''_I)}{(\psi_E - \psi_I)}\frac{dW}{d\omega} = -C_2\frac{W^{3/2}}{U}$$

$$+ \frac{\rho U r^2 C_1 \mu_{eff}}{(\psi_E - \psi_I)^4}\frac{d}{d\omega}\left[\frac{d}{d\omega}\left(\rho U r\frac{dU}{d\omega}\right)\right]^2 \tag{14}$$

$$+ C_3\frac{\rho^2 U r^2}{(\psi_E - \psi_I)^2}\frac{k^{1/2}}{l}\left(\frac{dU}{d\omega}\right)^2 + \frac{d}{d\omega}\left[\frac{\rho U r^2 \mu_{eff}}{(\psi_E - \psi_I)^2}\frac{dW}{d\omega}\right]$$

Thus, the differential equations with U, k and W as the dependant variables are the governing equations for the flow. The next step is to describe the domain of interest as far as computations are concerned. Since the center line is the axis of symmetry, the inner (I) and outer (E) boundaries of the region of study are as shown in Figure 2,

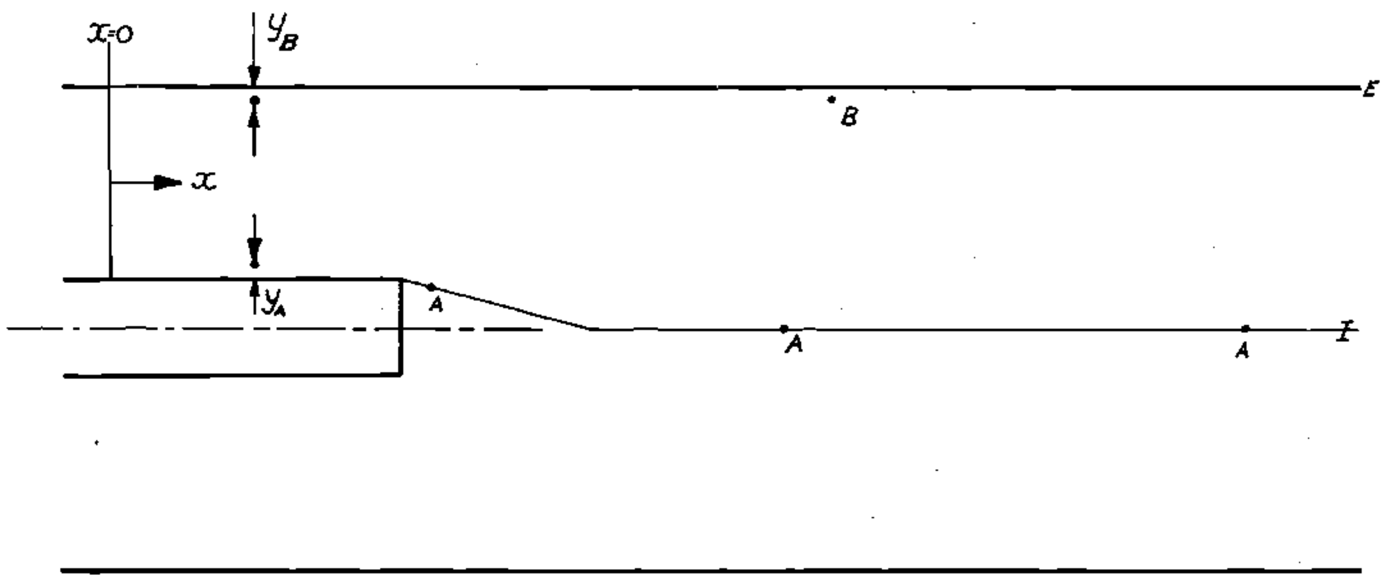

Figure 2. Computational Geometry.

where AA is the boundary of the potential core of the jet. The inner boundary I is, in sequence, composed of the inner tube wall, a free boundary and finally, the symmetry line. The outer boundary E is coincident with the wall boundary.

To mathematically define the problem completely, conditions along these boundaries must be specified. At the center line the radial symmetry provides the boundary condition for the dependent variables. As the free boundary is approached, the radial gradients tend to zero. Using this, the equations for k and W are simplified (analogous to obtaining inviscid the momentum equation from boundary layer equations) to provide the conditions for a free boundary. Specifying conditions for the wall boundary requires some special attention. At the wall the mean, as well as fluctuating, velocities go to zero. It is also known that close to the wall there is a viscous sublayer where the viscous behaviour is dominant. If this region is included in the domain of interest, then problems arise as far as k and W equations are concerned. This is because the equations governing k and W, derived for high Reynolds number flows, become less accurate as the viscous sublayer is approached. One way to deal with this is to make the coefficients (C' s) a function of local Reynolds number, based on distance from the wall. Instead of adopting such a complex procedure, for which there are few guidelines, the approach is to redefine the domain of study so that it does not include the viscous region. In other words, an effective boundary for k and W is defined such that it lies just outside the laminar region, in the fully turbulent flow (point B in Figure 2). Thus, the computational boundary is different from the geometric one when the wall is the boundary.

To summarize, the boundary conditions are as follows:

Center line: for any property Z,

$$\frac{dZ}{dr} = 0 \tag{15}$$

Free boundary:

$$\frac{dk}{dx} = -\frac{C_D}{U} k W^{1/2} \tag{16}$$

$$\frac{dW}{dx} = -C_2 \frac{W^{3/2}}{U} \tag{17}$$

Wall boundary: at a distance y from the wall

$$k = \tau / (\rho C_D^{1/2}) \tag{18}$$

$$W = \frac{\tau/\rho}{C_D \kappa^2 y^2} \tag{19}$$

where τ is the shear stress at that y.

With the specification of the boundary conditions the problem is fully defined mathematically. The coefficients C in the transport equations are not unique and have been obtained from the best comparison of calculated and experimental results [41,42]. For almost all the flows studied, the values of these coefficients are not dependent on the type of flow. For the case of pipe flow, it is found that the value of C_3=1.04 gives the best agreement between theory and experiment. However, for a free jet the value C_3 must be taken to be 1.48 for best agreement. This suggests that the value of C_3 must be taken differently for wall turbulence flow and for free turbulence and is a shortcoming of the k-W model. Since the ducted jet has a combination of the two, some numerical experiments were done with the coefficients. Although the dependence of the fully developed flow far downstream on this variation of C_3 was negligible, the properties in the developing region were noticeably affected. The most appealing effort was with C_3 varying radially as well as axially from the value for jet flow to that for pipe flow. Since the flow far downstream is a pipe flow, the value of C_3 in this region should be 1.04. There is a location of maximum pressure coefficient, beyond which the value of C_3 decreases monotonically. Thus, C_3 was allowed to vary linearly from that for a free jet at the jet exit to that for pipe flow at this location of maximum pressure coefficient. The radial variation was also taken to be linear from the value at the axis to the pipe flow value of C_3 near the duct wall.

The value of σ_k and σ_W are also to be prescribed. From inspection, it can be seen that these quantities, which are present in the diffusion term in the transport equations, are analogous to a Prandtl number. Further, for free turbulent mixing very good agreement between theoretical and experimental results are obtained when these values are approximately unity. For the case of wall turbulence it is possible to obtain a compatibility relation among the empirical constants, in the region close to wall, from the equation for W. This relation is obtained in the shear layer close to the wall by neglecting the convection terms and using wall function expressions for various quantities in the equation [42]. For the case of two-dimensional flow the compatibility condition is given by

$$\left(\frac{4}{\sigma_W} + C_1 C_D\right) k^2 + C_3 C_D^{1/2} - C_2 / C_D^{1/2} = 0 \qquad (20)$$

Thus, it can be seen that by specifying the values of the coefficients C the value of σ_W is prescribed. However, the corresponding value thus obtained for σ_W is approximately 3. Therefore, the values of σ_W near the wall and near the center line are different. The procedure adopted is to allow σ_W to vary between these two limits. The variation is taken as [42]

$$\sigma_W = (\sigma_W)_0 + (\sigma_{W_{WALL}} - \sigma_{W_0}) \left(l / k C_D^{1/4} y \right)^n \tag{21}$$

where n=3 and σ_{W_0} is the value for free turbulence and is equal to 0.9.

For the case of axisymmetric flow the compatibility relation from the equation for W (at y close to the wall) is

$$\left(\frac{4}{\sigma_W} + C_1 C_D - \frac{2}{\sigma_W} \frac{y}{R} \right) k^2 + C_3 C_D^{1/2} - C_2 / C_D^{1/2} = 0 \tag{22}$$

The value of σ_W near the wall found from this equation is used in equation (21) to obtain the variation of σ_W.

Numerical Scheme

In the previous section it was shown that the three coupled partial differential equations (12-14) describe the flow mathematically. For the sake of discussion, it is possible to rewrite the equations in the general form

$$\frac{\partial \phi}{\partial x} + (a + b\omega)\frac{\partial \phi}{\partial \omega} = \frac{\partial}{\partial \omega}\left(c\,\frac{\partial \phi}{\partial \omega}\right) + d \qquad (23)$$

Here, ϕ represents U,k or W and a,b,c,d are coefficients.

The next step is to express the general partial differntial equation in finite difference form. Since the equations are parabolic, they can be solved by a marching integration procedure. More specifically, at every step of integration the values of ϕ will be known at discrete values of ω for a particular value of x; the task will be to obtain the values of ϕ at the same values of ω, but for a slightly higher value of x (next x-step value).

By selecting the number of points needed in the radial direction the grid points in the ω direction are obtained. The grid network is shown in Figure 3. To obtain the finite difference equations, the usual procedure is to replace the partial derivatives by expressions using various difference schemes. The partial derivatives in ω are evaluated at x_D rather than at x_U because of the increased numerical stability and higher accuracy observed for simple cases. Rather than using the conventional form to obtain finite difference equations, the procedure adopted here is to obtain a miniature integral equation by integrating the equations over a small control volume. Specifically, to write the equations at ω_i, the integration is performed over the shaded area (bounded by lines joining middle points between ω_i and ω_{i+1} and ω_{i-1} and ω_i) in Figure 3. To obtain the difference equation the nature of variation of ϕ between grid points must be assumed. In most cases there are enough grid points so that the assumption of a linear variation of ϕ in the ω-direction between grid points is sufficiently accurate over most of the flow region. However, close to the wall boundary there is a steep variation in ϕ and so this region must be dealt with separately. The variation in the x-direction is considered to be step-wise: that is, except at x_U, the value of ϕ between x_U and x_D is equal to the value of ϕ at x_D. Further, in order to obtain linear equations in the coefficients a,b,c are all evaluated at the upstream x location where ϕ values are known. An advantage of generating a microintegral equation is that it ensures that conservation will be satisfied over the region of analysis. By interpreting some of the integrals physically, better approximations or modifications can be introduced to increase the accuracy of the scheme [43].

Near the boundary, the region of integration becomes a half-grid interval. The variation in ϕ is accounted for by introducing a fictitious value of ϕ, given by ϕ_2, such that

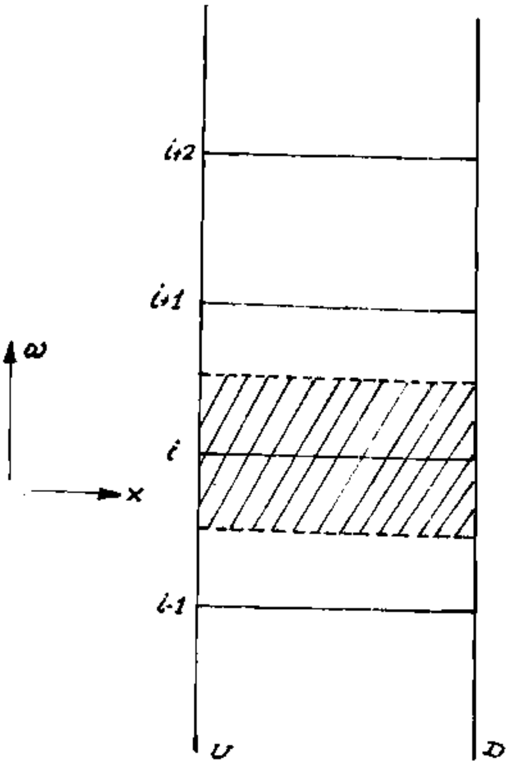

Figure 3. Grid Network.

this value ϕ_2 is provided from a linear interpolation of ϕ between points 2 and 3 using the correct slope and value of at the midpoint ω_{25} [44]. This is illustrated in Figure 4.

Another factor to be considered is the flux of ϕ across the constant ω line closest to the boundary. For example, in the case of the momentum equation the question of writing momentum transport across boundaries in terms of known quantities arises. When the boundary is wall, some functional relationships are needed to do this. Initially, the conventional form of the law of the wall was used as the wall function for obtaining shear stress. Yajnik and Afzal [45] have pointed out that the constants in the law of the wall were obtained from the the best fit of data over a large Reynolds number range and thus may not have good accuracy at all Reynolds numbers. They have developed an expression using the method of matched asymptotic expansions in which the so-called constants become parameters of Reynolds number. This modified form of the law of the wall was used in the computations. For the case of the k and W equations the conditions near the wall were obtained from the shear stress at the point close to the wall (effective boundary point), from equations (18,19).

By forming the microintegral equations and simplifying

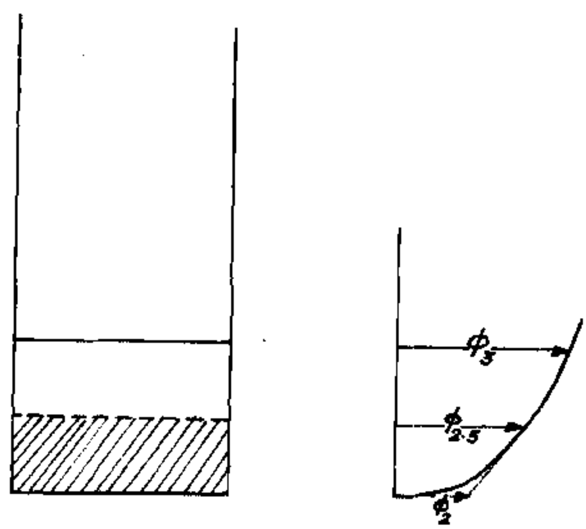

Figure 4. Grid Near Wall Boundary.

them using the assumed nature of ϕ variation, a tri-diagonal system of equations was obtained:

$$\phi_i = A_i \, \phi_{i+1} + B_i \, \phi_{i-1} + C_i \tag{24}$$

The boundary conditions provide the two known values of ϕ in the above system of equations. They were solved for by a simple recursion relation. The procedure is repeated for the next x-location and thus the values are obtained over the region of interest by marching downstream.

CHAPTER III

EXPERIMENTAL PROCEDURE

The modelled flow problem of a ducted jet was investigated both analytically and experimentally. The experimental setup along with the instrumentation and procedure adopted is described in this chapter.

A schematic of the arrangement for the experimental studies is shown in Figure 5. The jet and the co-flowing stream are supplied through circular tubes which are concentric to one another. A plexiglas tube of one inch internal diameter serves as the duct or outer tube. The ends of this tube are sheathed inside the PVC pipes such that the plexiglas tube is free to translate back and forth, the purpose of which will be explained shortly. As shown in Figure 5, at the measuring station the probe could be inserted through the hole on top of the plexiglas tube. The probe is held at this position with the help of couplings which permit only a vertical motion. This allows a radial traverse of the probe at any axial location. To make measurements at different axial stations, the probe station has to be placed at these locations. This is achieved by sliding the duct tube (plexiglas), along with

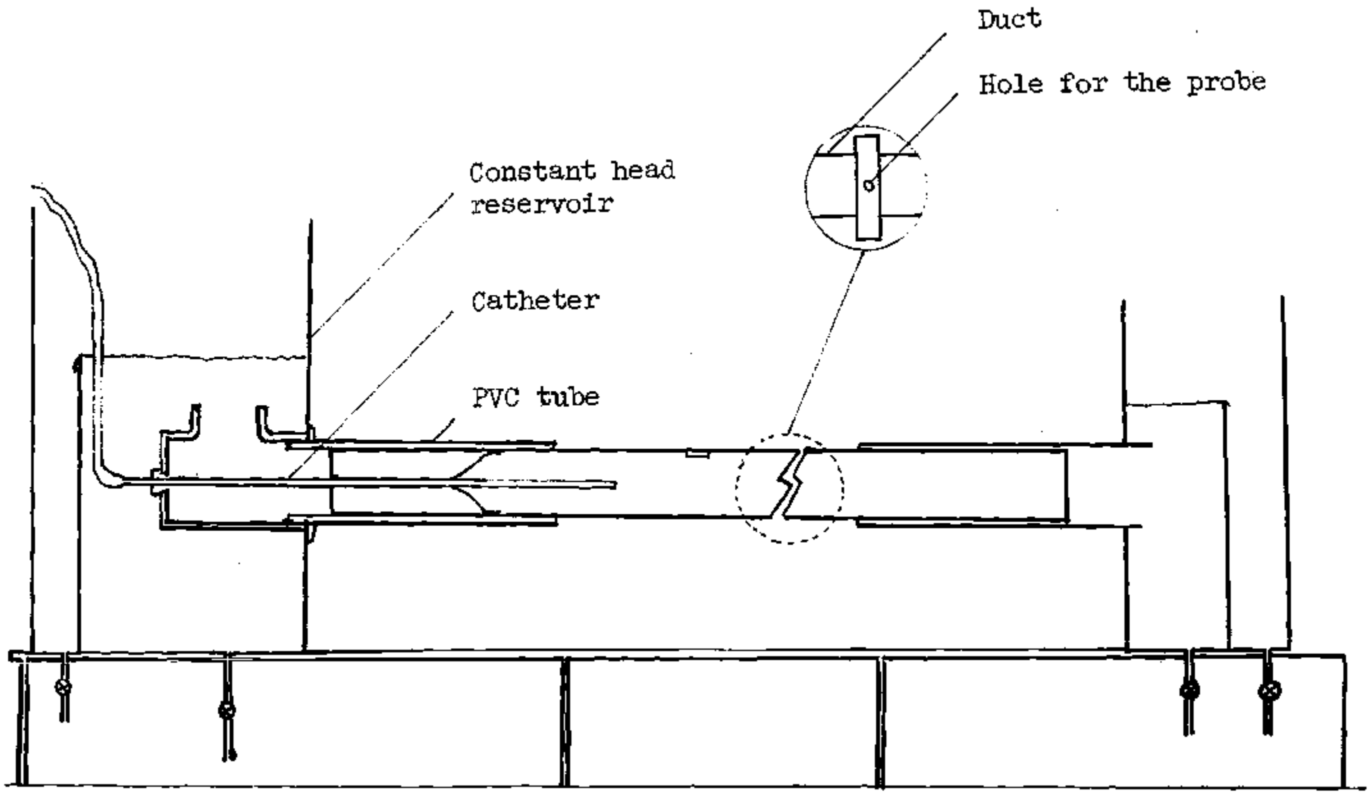

Figure 5. Schematic of the Experimental Arrangement.

the probe, in or out of the PVC tubings so that the probe is brought to the desired location. The advantage of having a trombone-like movement is that measurements using the probe could be made at any desired axial position. The setup allows the probe station to be anywhere from 1.5 inches upstream of jet exit to 35 inches downstream of jet exit. The PVC pipes, each of which is 47 inches long, end in reservoirs maintained at constant head upstream as well as downstream.

The primary (jet) as well as secondary (outer) flows are supplied from constant head overflow reservoirs. The outer flow reservoir head is supplied through two lines of PVC tubing from a main tank of about 800 liters capacity. All containers, as well as supply lines, which are metallic and in contact with water were coated with MIRA-PLATE epoxy coating to prevent surface reactions from taking place. The jet exits from a metallic tube 56 inches long and 5/16 inch in external diameter with a wall thickness of 0.035 inch. This tube is made concentric with the outer tube by three prongs welded to the the catheter tube. These prongs (1/32 inch diameter) are attached to the jet tube six inches upstream of jet exit.

A check of the effect of the support prongs on the flow was made with the probe located one inch upstream of jet exit and in the wake of the prongs. The change in velocity fluctuation values with this probe location was hardly noticeable.

The upstream end of the catheter tube passes through a circular alignment disc, concentric with the duct. The jet flow is supplied by a reservoir which is connected to the main tank. The catheter tube is connected to this reservoir through flexible tubing. A recirculating flow system was not used due to the possibility of polymer degradation occuring when solution is pumped. Thus, the total running time (approximately 30 minutes) is determined by the capacity of the tank, which gradually empties as the test proceeds.

Instrumentation

The need for measuring mean velocity arises because this is a suitable quantity for comparison between theory and experiment. Detailed comparisons suggest the need for knowing the value of turbulent fluctuating velocities. Further, these measurements are useful in making comPARAtive studies for water and polymer solutions and, hence, to find the influence of polymers. Some of the previous studies [38] did not show influence of polymers on mean and turbulence velocities. Thus, it would be wise to make energy spectral measurements so as to describe the turbulence in finer detail. In view of this, turbulence energy spectra were obtained for the case of water as well as polymer solutions. In summary, the quantities to be measurec are the mean and turbulence velocities as well as the turbulence energy spectra.

It was mentioned earlier that hot wire measurements in dilute polymer solutions are concentration dependent and may exhibit anomalous behaviour. However, it has been pointed out by Patterson [46] and Rodriguez, Patterson and Zakin [47] that wedge and cone probes do not, in general, suffer from these anomalous characteristics when used in polymer solutions. Further, it has been found by Warschauer, Vijge and Boschloo [48] that wedge-shaped sensors appeared sensitive to fouling by small particles even in water which had been filtered to better than 50 m. Because of these previous results, the conical probe was selected for the present experiments. In a preliminary study, Koletty [49] has calibrated a DISA conical probe in dilute polymer solutions and exhibited repeatable calibration curves.

Hot Film Anemometer System

Velocity measurements were made using commercially available conical hot film probes made by DISA and Thermo Systems Incorporated. Probe circuitry included a Constant Temperature Anemometer and a Linearizer, both made by DISA.

Principle of Operation. The measurement of fluid velocity by use of hot film (or hot wire) anemometry is based on convective heat loss from the heated sensing surface to the surrounding fluid. In general, the heat loss depends on temperature, geometrical shape, and dimensions of the sensor, and on the velocity and thermodynamic properties of the fluid being studied [50,51]. This discussion will concentrate on the conical hot film probe which is shown in Figure 6.

The flow sensor is a vacuum-sputtered film of either nickel or platinum deposited on the conically shaped end of a quartz rod. The film thickness is only a few thousand angstroms to minimize thermal inertia. Electrical insulation from the surrounding fluid medium is achieved by overcoating the film with a 1 or 2 micron thick layer of quartz. This thickness of quartz is sufficiently thin so that damping of the dynamic heat transfer is not a factor in the frequency response of the sensor.

The sensor element is heated to the desired temperature by current supplied from an anemometer, basically consisting of a Wheatstone bridge in which the sensor forms part of one bridge arm and an amplifier. The current flowing through the bridge heats the sensor, and the amplifier output voltage is a measure of the heat loss from the sensor. The system can be operated either in a constant current mode or

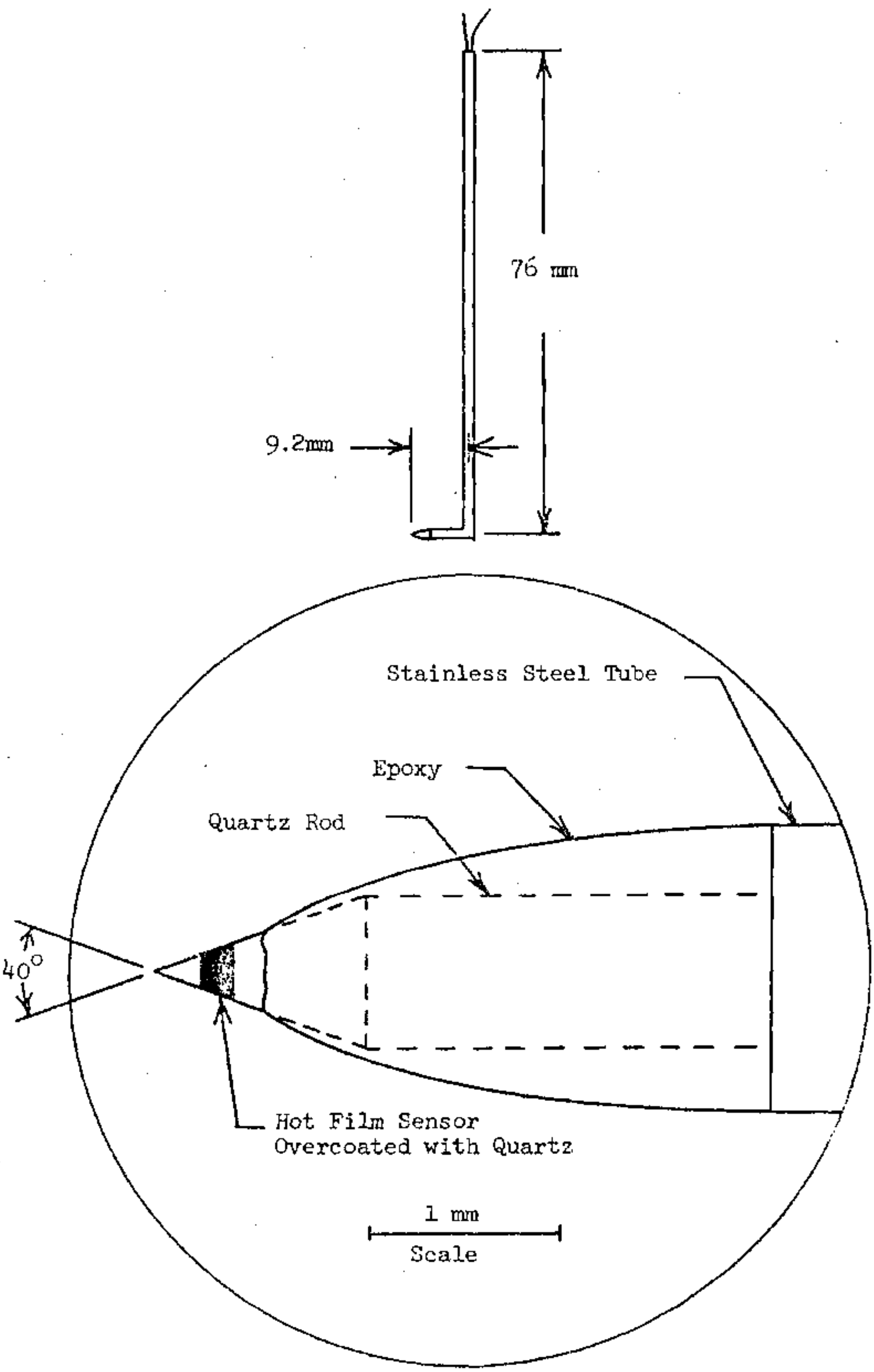

Figure 6. Conical Hot Film Probe.

a constant temperature mode. In the constant current mode, the heating current to the sensor is held constant and the probe temperature is allowed to vary with flow velocity. In the constant temperature mode, the probe temperature, or probe resistance in the bridge, is held constant. The bridge voltage necessary to maintain this constant resistance is a measure of the heat transfer and hence, also the fluid velocity. Of the two modes, the constant temperature system has inherently better frequency response, greater sensitivity and less chance of probe burn-out.

The most desirable sensor operating temperature is chosen by consideration of several factors: (1) the sensitivity required, (2) fluid temperature, and (3) in case of liquids, the temperature at which bubbles tend to form. The overheat ratio is defined as:

$$R_H / R_C = 1 + \alpha \left(T_S - T_f \right) \tag{25}$$

where R_H = operating resistance of the sensor

R_C = resistance of sensor at fluid temperature

α = temperature coefficient of resistance of sensor at the fluid temperature

T_S = sensor temperature

T_f = fluid temperature

Of great importance in preserving probe sensitivity and calibration repeatability is the use of the same overheat, R_H/R_c, in the calibration and use of the probe. For use in water, satisfactory results were obtained with an overheat ratio of 1.01.

In general, the bridge voltage output is related to the fluid velocity by the relation

$$V^2 = V_o^2 + K\,U^{n_o} \tag{26}$$

where U = fluid velocity

V = bridge voltage at velocity U

V = bridge voltage for U = 0

K and n_o are constants which depend on the thermodynamic properties of the fluid, probe geometry and the overheat ratio.

A linearizer circuit is employed to transform the nonlinear anemometer output voltage into a voltage which is linearly related to the fluid velocity. In these experiments a DISA Model 55D10 linearizer was used.

Hot Film Probe Calibration. The relationship between the anemometer bridge voltage and the fluid velocity was determined for each probe by calibration in a fluid (water or polymer solution) flow whose velocity is known.

The probes were calibrated using a calibration apparatus. This apparatus consists of a circular channel machined in a one inch thick plexiglas disc which in turn is rotated by a system of stepped pulleys and a variable speed motor. The channel design allows calibration with as little as 200 cc of fluid. The probe was inserted into the rotating fluid and rigidly held in place. It was determined experimentally that the probe wake did not perturb the flow over the probe. The rotational speed, and therefore the fluid velocity at a known radius, was measured with a timing mark on the disc and a manual timer accurate to 0.1 sec. The rotational speed was determined by timing ten revolutions. Calibrations were also done using a larger tank of about three liter capacity. Here also, the probe was held stationary and the tank was rotated to obtain various flow speeds at the probe loaction. The calibrations obtained using this large tank and the spinning table were almost identical. Hence, only the spinning table was used because of the greater convenience. Calibrations were made using water as well as a polymer solution of 50 ppm concentration. A typical probe calibration curve is shown in Figure 7.

At high speeds large velocity variations produce only

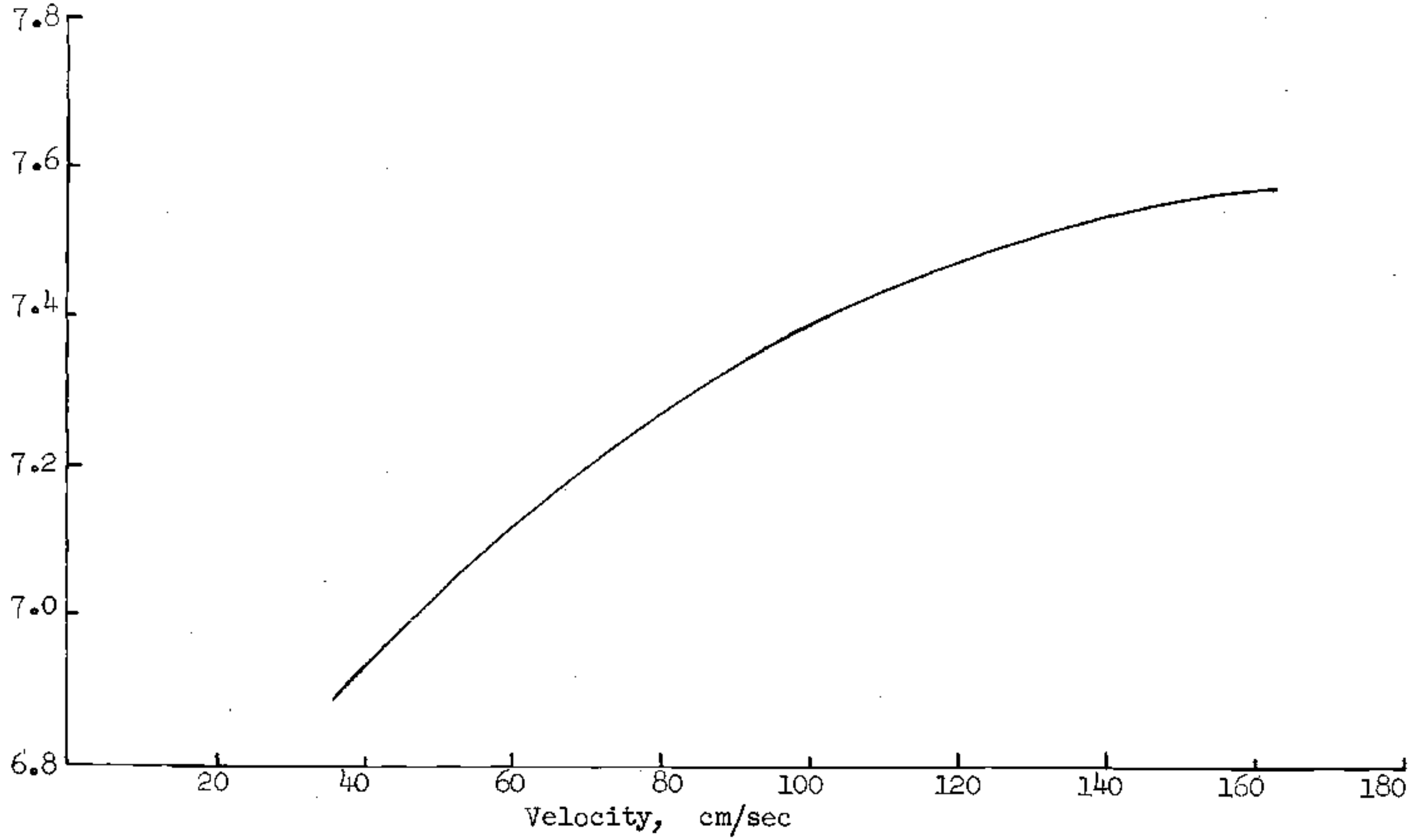

Figure 7. Probe Calibration Curve

small voltage variations. In other words, a small error in the voltage output measurement can produce large errors in the calculation of velocity fluctuations.

The linearizer fits an exponential function to the calibration curve and its output gives the instantaneous velocity values at the probe location. The exponential factor can be set on the instrument [52,53]. Once this is done, the output from the linearizer directly provides the velocity.

Operating procedure. Of utmost importance for accurate velocity measurements is to maintain tha same probe overheat in the application of the probe as was used in the calibration. The overheat used (1 per cent) was the same for water and the polymer solution.

The variation in fluid temperature has a significant effect on the probe sensitivity if the probe operating resistance is not adjusted to yield the correct overheat ratio. For this reason the probe resistance was checked often and the operating resistance adjusted if necessary.

Another factor in calibration repeatability is the deposition of contaminants on the probe surface. If a contaminant, such as a dust filament, adheres to the surface the probe sensitivity is reduced. This response is easily detected as a sudden decrease in anemometer output.

Bubbles occasionally formed on the sensor surface, even for the low 1 per cent overheat. Past experience indicates that bubble formation occurs when the quartz overcoating or the epoxy sealer on the lead elements does not completely insulate the sensor or leads from the conducting fluid. The water was not distilled or demineralized and would have significant conductivity to enhance bubble formation from electrolytic action. Once bubble formation occured at frequent intervals, the probe calibration is unreliable.

Digital Voltmeter

The outputs from anemometer as well as linearizer were displayed using digital voltmeters. A Fluke Model 8000A and an integrating voltmeter (HP Model 2401C) were used .

Fourier Analyzer System

The output from the linearizer was fed into the Fourier analyzer system for data reduction. The 5451A system has the following units [54].

Model 180 AR/DR Oscilloscope Model 2100 Computer

Model 2752A Teleprinter

Model 5460 A Display plug-in unit

Model 5465 A ADC plug-in unit

Model 5475 A Control Unit

The system performs analyses of time and frequency data containing frequencies from dc to 25 kHz. This was generally employed to obtain energy spectra in which the input that varies with time is broken down to its component frequencies. However, since the system has programmable capability the input data could be analyzed or processed to obtain various features about the input signal.

To obtain a reliable power spectrum repeated samples of the input can be taken and the power spectra can be added together over and over again so that a valid statistical sampling is obtained. This method of averaging was employed to obtain mean and turbulence velocities as well as energy spectra of turbulence. A sample program usec for data analysis is given in Appendix I. The Fourier Analyzer system utilizes a finite fast Fourier transform to obtain the energy spectrum [54].

Preliminary Studies

Before studying the ducted jet case, the accuracy of the system as well as the procedure was estimated by studying the case of fully developed pipe flow. The probe was located near the downstream end of the pipe. The output signal from the linearizer was averaged using an integrating voltmeter as well as the Fourier Analyzer system. The results agreed to within 3 per cent. The accuracy of the averaging program used in the Fourier analyzer was also tested by inputing known signals. The program reproduced the input value within 1 per cent. Because of the accuracy and the convenience, only the averaging program was used later. The program provided both mean velocity as well as the mean square value of the input signal. The value of the fluctuating velocity was computed from these two outputs from the Fourier analyzer. It should be noted, however, that the sensing element of the probe is on the surface of a cone and so the probe senses fluctuations which are a measure of turbulence rather than any single component of fluctuating velocity. The volume flow rate was calculated by integrating the velocity profile obtained experimentally. This was compared with the flow rate measured by timing the flow into a graduated flask. The 5 per cent difference was considered to be satifactory. Mean velocity traverses made along the horizontal and vertical diameters gave assurance of axial symmetry of the flow. Finally, the radial mean velocity profiles agreed very well with the logarithmic form of the law of the wall for the flow Reynolds number.

Polymer solution Preparation

The polymer used for the experimental study was Polyox-WSR 301. To prepare a solution of concentration of 50 ppm by weight, the first approach used was to make a concentrated solution of Polyox and then dilute it suitably.

Obtaining approximately 800 liters of homogeneous polymer solution of 50 ppm concentration by the dilution technique was found to be extremely difficult. The main difficulty was in obtaining a homogeneous mixture.

The second approach was to make the polymer solution by direct mixing. In this case the polymer was sprayed on to the water in the reservoir while water is being added on. By carefully controlling the spraying of the polymer, a solution was prepared. Care had to be taken in adding the polymer so that no lumps, due to uneven spraying, were formed in the solution.

Solutions prepared by the second method were found to be homogeneous. The homogeneity of the solution was checked by taking samples at various depths of the main reservoir (800 liter capacity) and measuring flow rate in a simple pipe flow apparatus. A pressurized flask of capacity 1 liter serves as the upstream reservoir for this pipe flow setup. Polyox solution of 50 ppm concentration was made in the flask by direct mixing of the polymer. The flow rate obtained using this sample is taken as the standard against which other values of flow rate are compared. For this pipe flow setup, the increase in flow rate (between water and polymer solution) due to the presence of polymer was found to be about 0.5 liters per minute.

The criteria for no degradation was that the increase in flow rate, due to the presence of the polymer, should be above 0.48 liters per minute. For all the experiments of the ductec jet flow with polymer solution the flow rate in the pressurized system was obtained before and after taking all the (velocity) measurements. Only those for which the two values agreed to within 5 per cent were accepted. To find the amount of degradation created by flow through supply lines from the tank, the solutions collected at the exit of these lines were used in the pressurized pipe flow system. The effect was found to be negligible. In conclusion, it should be mentioned that the solution preparation procedure was tedious and time consuming and the probability of failure was not low.

CHAPTER IV

DISCUSSION OF RESULTS

The results from the analytical method of study and those obtained by using the hot film anemometer are presented in this chapter.

Analytical Approach

Study of High Reynolds Number Ducted Jet

The method of analysis to predict detailed flow properties was described in Chapter II. Conditions corresponding to the experiments of Razinsky and Brighton [21] were selected as the first case for the numerical calculations. Both jet and secondary flows were supplied by converging nozzles in such a manner that the velocity profiles at the exit plane were essentially flat, except for the presence of a very thin boundary layer. The computations were performed for the following set of parameters:

$$U_i = 45.7 \text{ m/sec}$$

$$U_i / U_o = 3.0$$

$r_o / r_i = 3.0$

Reynolds Number of the flow = 1.70×10^5

The various symbols were explained in Figure 1. The reason for selecting this set of conditions was that the experimental results indicate a strong mixing taking place as suggested by a peak in the value of the pressure coefficient. For lower values of the velocity ratios the variation of pressure coefficient C is almost monotonic. Furthermore, for higher values of velocity ratio, there is a possibility of a recirculation zone, where the boundary layer assumptions inherent in the present theoretical treatment are not valid.

Also required for the program, aside from the parameters mentioned earlier, are the initial values of the turbulence quantities. However, the initial values of longitudinal turbulence intensity in the annulus at the jet exit plane were given from the experiment. If the flow were isotropically turbulent, then k would be equal to $3/2\ u'^2$. Annular and channel flows are not isotropic, and usually k has a somewhat smaller value. In the present computational scheme, a value of k equal to 90 per cent of the isotropic value (with u' being obtained from the experimental data) was assumed at a station two duct radii upstream of the exit plane, and computations proceeded downstream. To test the sensitivity of the flow on this assumption, the value was perturbed to 85 percent and the computations repeated. Very little change was found in the calculated flow conditions at the exit plane. Thus, the idea of starting the computations two duct radii upstream of the jet exit indicates that the flow has "sufficient time" to adjust to the conditions at the boundary of the annulus. The input values of W are obtained by specifying that the mixing length in the annulus region is 1 per cent of the annulus width.

The values of k and W selected were

$$k = 0.650 \quad m^2/sec^2$$

$$W = 5.0 \times 10^7 \quad sec^{-2}$$

These, combined with the flow velocities, define the inlet conditions completely. The values chosen for the various coefficients in the two equation model were

$$C_D = 0.090$$

$$C_1 = 3.500$$

$$C_2 = 0.175$$

$$C_{3_p} = 1.040$$

$$C_{3_{jet}} = 1.400$$

The governing equations were solved by the method described in Chapter II. The results obtained from the computations are shown in Figures 8 - 10. The radial variation of mean velocity is compared with predicted values at two axial stations - one in the early developing region and the other far downstream of jet exit. However, in the region very close to jet exit the agreement was not as good. The reasons for this will be discussed shortly. Figure 9 gives the variation of pressure coefficient, C_p, in the streamwise direction. The location of the peak in C_p is approximately nine duct diameters from the jet exit plane. Comparison with experimental results shows that the theory predicts the rise and the peak in the curve very well and also the slope of the curve (pressure gradient) far downstream of the peak. The intermediate region shows that the analysis overestimates the axial extent of high pressure zone. Far downstream the flow becomes a fully developed pipe flow and the experimental measurements agree very well as far as mean velocity and pressure gradient are concerned. Another interesting observation is the peak in the value for

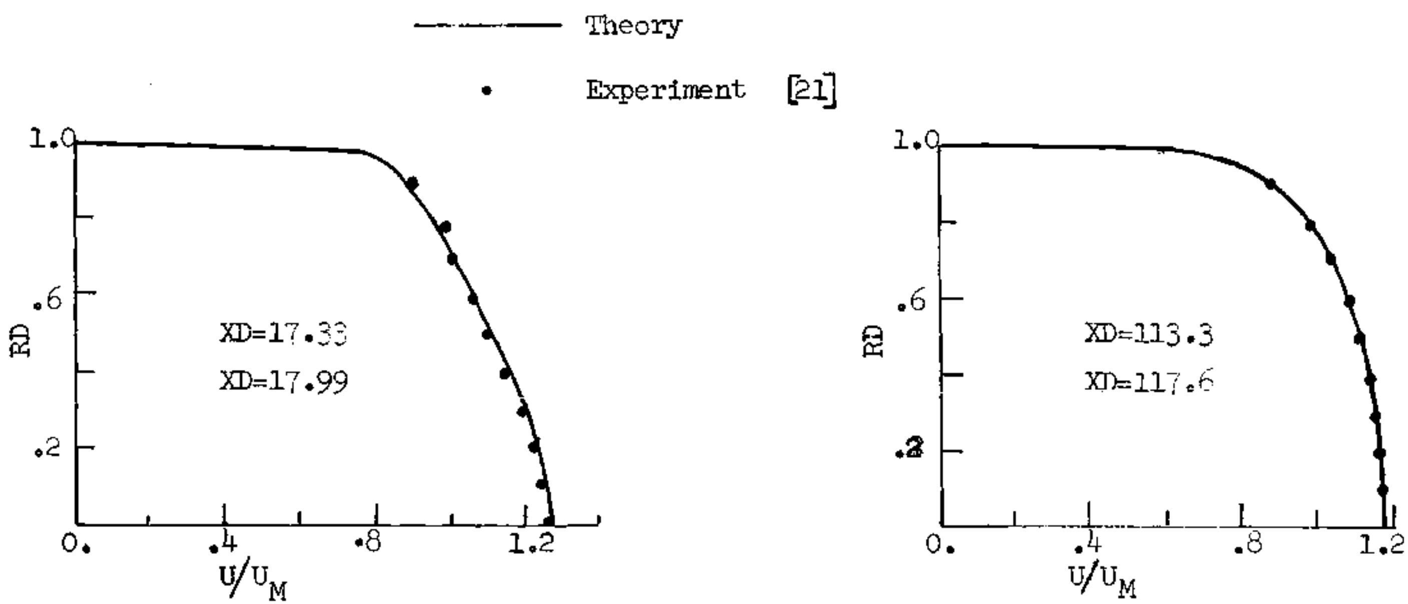

Figure 8. Comparison of Mean Velocity Profiles, Re=1.7 x 10^5
$U_i/U_o=3.0$; $r_o/r_i=3.0$

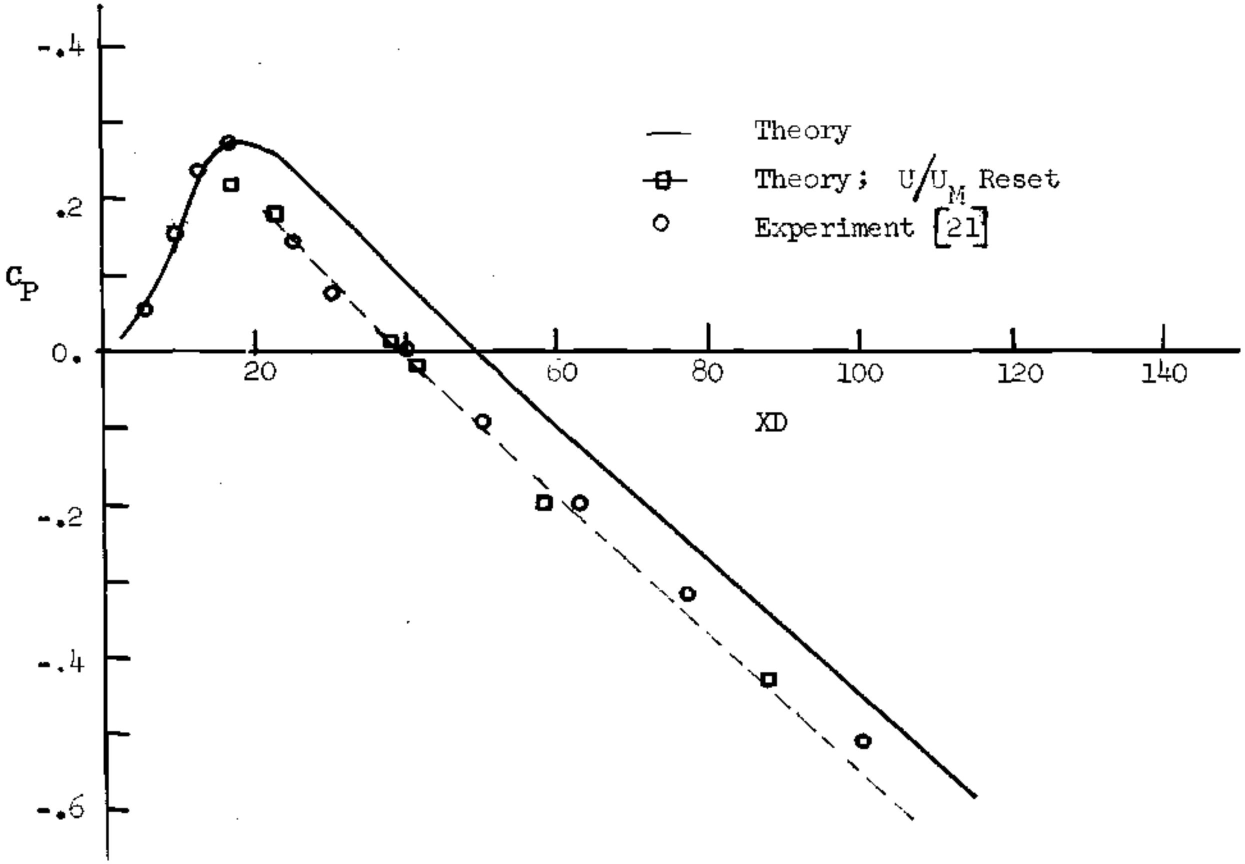

Figure 9. Axial Variation of Pressure Coefficient, $Re=1.7 \times 10^5$

$U_i/U_o=3.0$; $r_o/r_i=3.0$

C_f shown in Figure 10. The proximity of the axial location of the maxima in C_p and C_f indicates the influence of jet mixing with the outer flow. In clinical angiographical situation the possibility of tissues breaking loose from the wall is of prime concern and so the occurence of a possible peak in stress at the wall is of great interest.

Effect of Initial Conditions

Discrepancies between the experimental results and theory may be due to the arbitrariness in the initial conditions. In the actual experiment the jet tube wall has a finite thickness and hence there is a wake downstream of the jet wall. Experimental measurements [21] indicate a very sharp peak in turbulence intensity in the wake region. Since there are no experimental results available for v' and w', there is no way of computing the value of k at the jet exit plane so as to account for the thickness of the lip of the jet. Further, in moving downstream from the jet exit plane some uncertainty arises in specifying the value of k at the first grid point, which is on the potential core boundary. At the exit plane, the core diameter is almost the same as the diameter of the jet tube and the computational scheme takes the properties to be constant radially in the core. This introduces a very large amount of error in k values because of the boundary layer on the inside wall of the jet tube. Experimental results [21] indicate that the turbulence intensity increases to a value

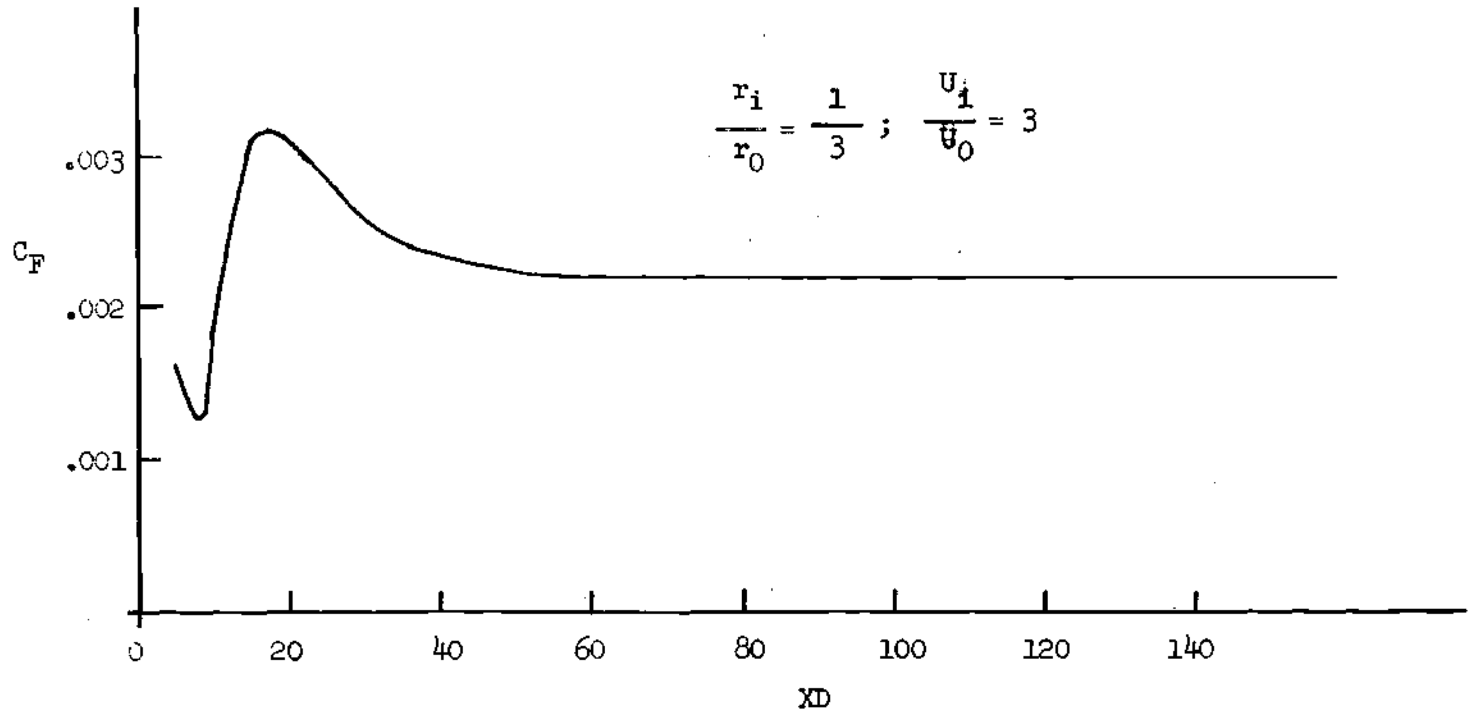

Figure 10. Axial Variation of Skin Friction Coefficient.

ten times that in the core, in the very small boundary layer region from the inside wall. Since this value affects the decay of potential core width, the necessity of selecting the right value, which is not known, becomes important. Although there are some guidelines - such as measurement of u', v' and w' - for obtaining a proper value of k, there are none for obtaining values for W. Thus, a certain amount of arbitrariness is always present in the input to the turbulent quantities.

One way of alleviating some of this arbitrariness is to input into the computational scheme the measured values of various quantities at some point downstream of jet exit. Thus, some of the influence of the finite thickness of the jet tube wall will be accounted for. The ideal situation would be to input measured mean as well as turbulent velocities and the distribution of W. Since all these are not available experimentally, the best that could be done was to input the radial distribution of velocity. The axial station XD = 3.33 was selected for this input station. The method was to replace the computed values of mean velocity and then continue marching downstream. The effect on C_p is shown in Figure 9. The results indicate that the agreement between theory and experiment has improved downstream of the maxima. There is some discrepancy near the maximum value. However, the important thing to note is that, by compensating somewhat for the influence of the wake region on the mean velocity, the C_p values show considerable change and better agreement in the region where there was discrepancy previously. This suggests that the arbitrariness in input data can contribute considerably to difference between theoretical and experimental results in the near field mixing region.

Finally, the influence of specifying the values of k also was evaluated. A 10 per cent difference (which is easily within the range of measurement accuracy) in turbulence intensity at the jet exit plane was found to cause about 10 per cent difference in the rate of decay of center line velocity in the devoloping region for this experimental setup. There was also some influence on the wall shear stress values but was not substantial enough to be distinct in the plot. Thus, it can be said in conclusion that the arbitrariness in the input data affects the results in the developing region of the jet to a large extent. However, the results far down stream reach fully developed values in all cases.

Study of Angiographic Injection Model

The comparison of theory and experiment just described gave considerable experience in using the computational program and provided insight into the requirements for the primary thrust of the research, namely, modelling turbulent angiographic injections.

Next the analytical procedure was applied to study the mixing problem for the geometry of the experiment. However, there are some differences in the geometry of the present experimental arrangement and that of Razinsky and Brighton that must be accounted for in the computations. For the current setup the flow does not enter through nozzles, but through pipes. In other words, the outer flow at the jet exit plane is through a circular annulus with the result that the velocity profile at this plane is not uniform. Also, the jet issues through a circular pipe so that the velocity profile of the jet flow is more like that for a fully developed pipe flow - and not a flat profile. Hence, there is no potential core in the present experiment and this must be incorporated into the computations. The method adopted is as follows. The jet, for the sake of computation, is assumed to have a flat profile at the jet exit plane and this uniform value was calculated from the jet flow rate. Then, the values for mean velocity obtained by the computational procedure were replaced by the values obtained experimentally at a station downstream of jet exit plane. This approach partially accounts for the influence of the jet lip on the mean velocity (as discussed previously) as well as the fact that the jet issues as a fully developed pipe flow. However, the same cannot be done for k and W values, since these were not directly measured. Thus, the procedure was to replace the value of the mean velocity at a station two duct radii downstream of jet exit plane, while not altering W and the turbulence intensity from their calculated values.

The initial conditions used as input to the program were obtained from experimental measurements at a station 2.33 duct radii upstream of jet exit plane. The value of k was estimated (to be a uniform value) from the values of turbulence intensity measurements. As before, the value of W was calculated from the concept that the mixing length should be a fraction of the physical dimension (annulus width) of the flow.

The parameters as well as the initial conditions of the flow are as follows.

$$U_i / U_o = 1.5$$

$$r_i = 0.308 \text{ cms}$$

$$r_o = 1.270 \text{ cms}$$

$$k = 0.005 \text{ m}^2/\text{sec}^2$$

$$W = 5.02 \times 10^3 \ \sec^{-2}$$

$$\text{Reynolds number of the flow} = 1.360 \times 10^4$$

The governing equations were solved by the marching procedure and at the station two duct radii downstream of jet exit the value of U/U_M is replaced by the values obtained experimentally.

The results of the computation are given in Figures 11 - 17. The radial distributions of mean velocity at the different axial positions are shown in Figures 11 - 14. The mean velocity variation shows the mixing between the two streams. The mean velocity profile at XD = 2.0 is the value from experimental measurements and is used for replacing the U/U_M values obtained by the marching scheme. The local minima in the velocity profile at XD = 3.0 is caused by by the boundary layer wake. This local minima is gradually smoothed as the jet flow moving downstream mixes with the outer flow. The profile at XD = 10.0 is smooth, suggesting that the flow is gradually reaching a fully developed pipe flow profile. The results for the farthest station downstream, XD=60.0, indicate that the velocity profile corresponds to one for fully developed pipe flow. The streamwise variation of pressure coefficient is shown in Figure 15. The variation is monotonic for these

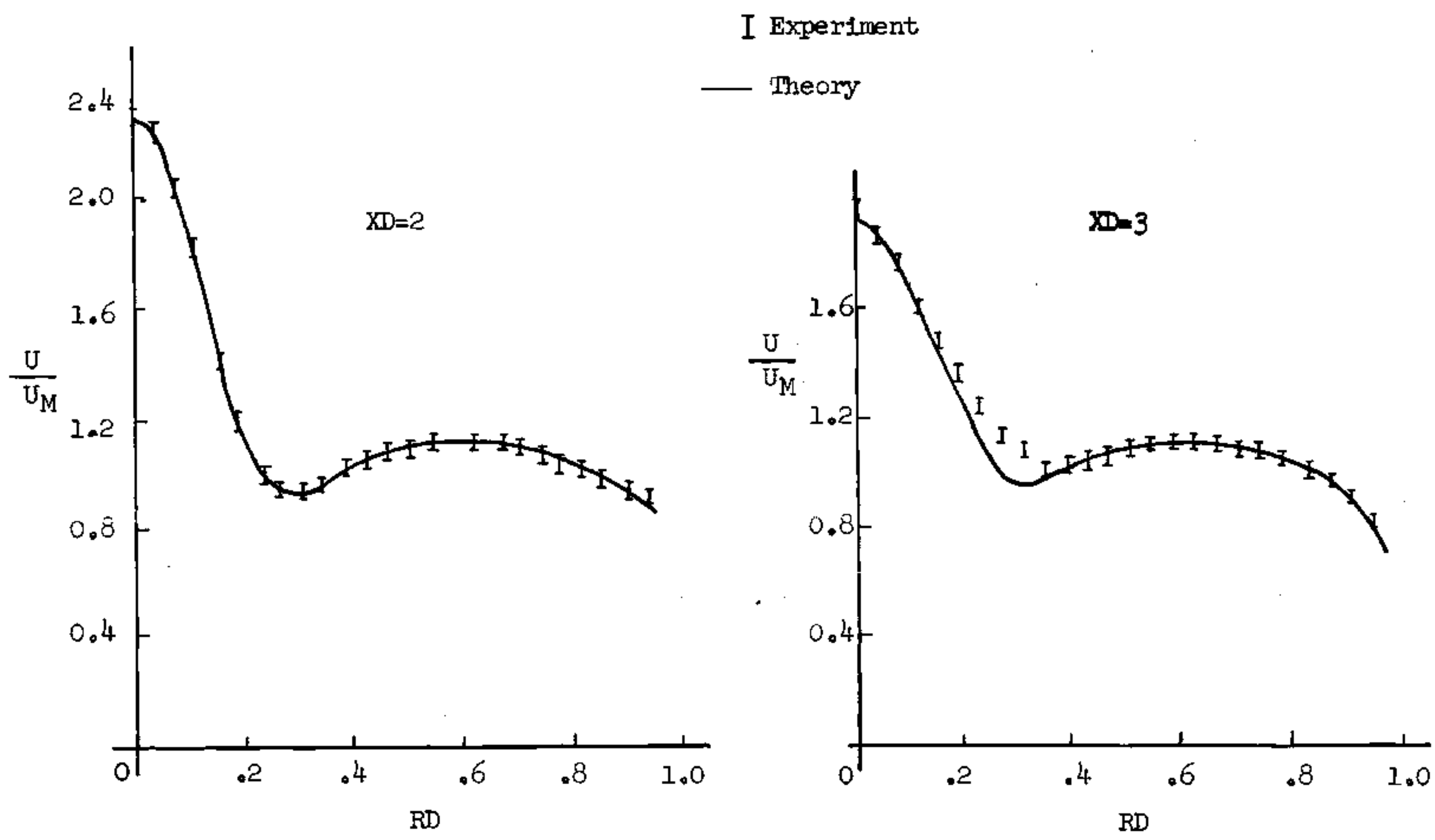

Figure 11. Radial Mean Velocity Profiles, Water I.

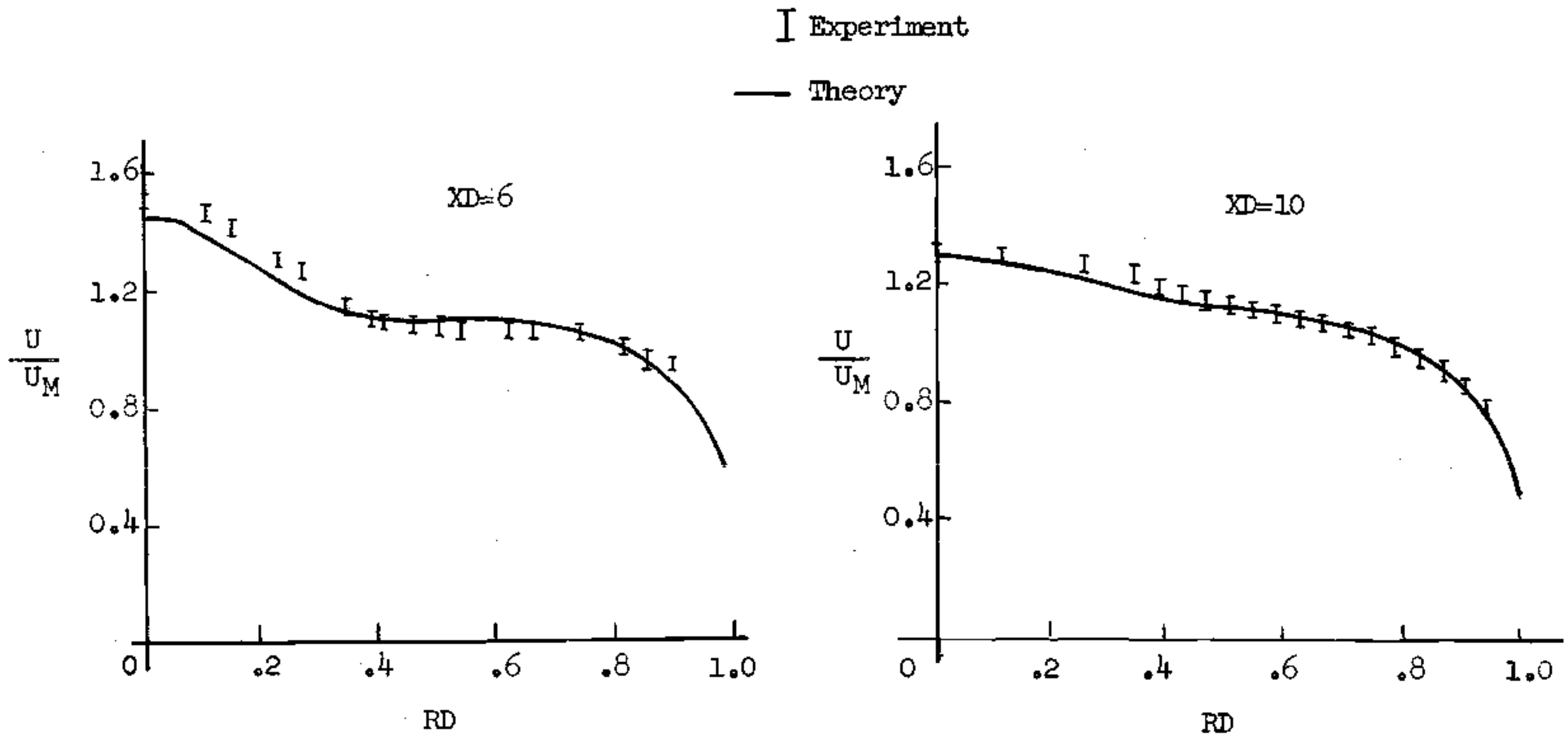

Figure 12. Radial Mean Velocity Profiles, Water I.

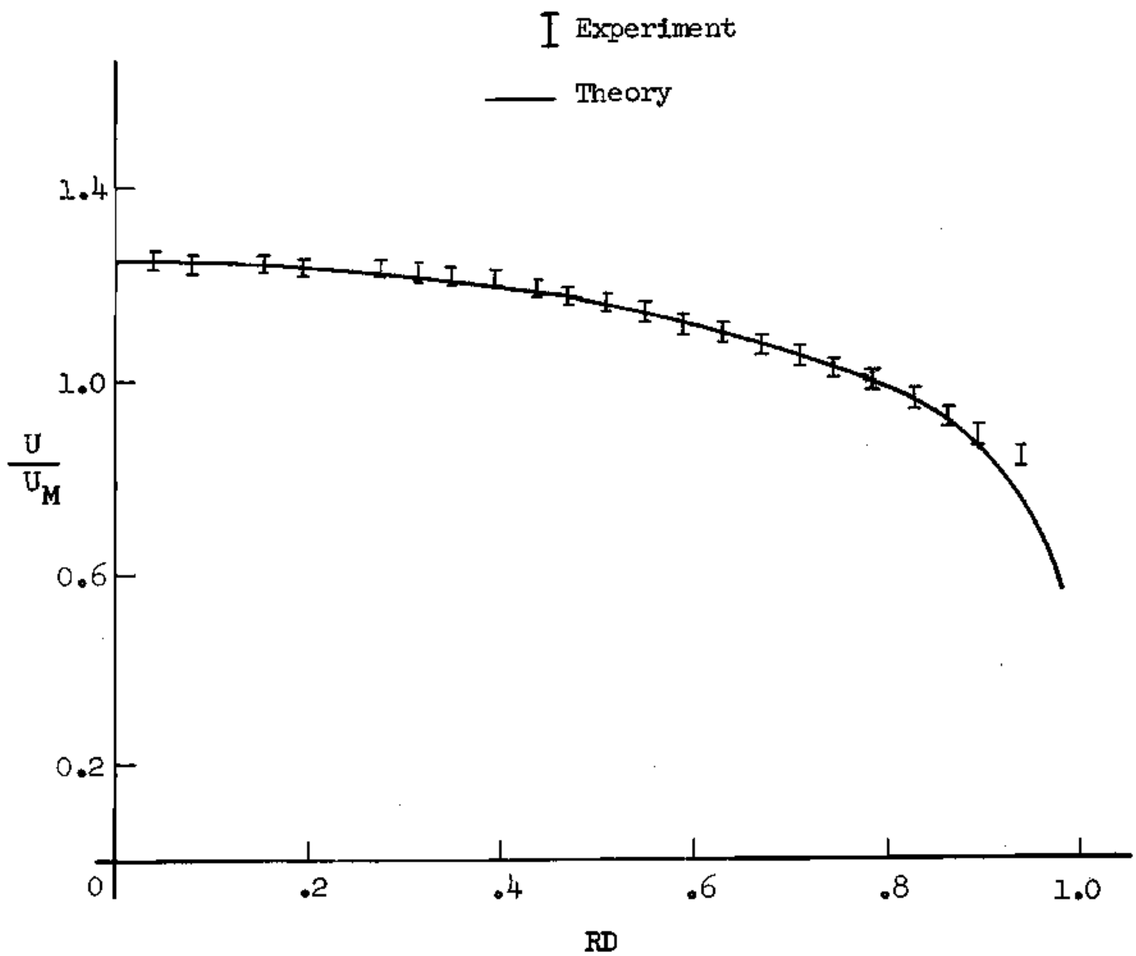

Figure 13. Radial Mean Velocity Profiles, XD=20.0, Water I.

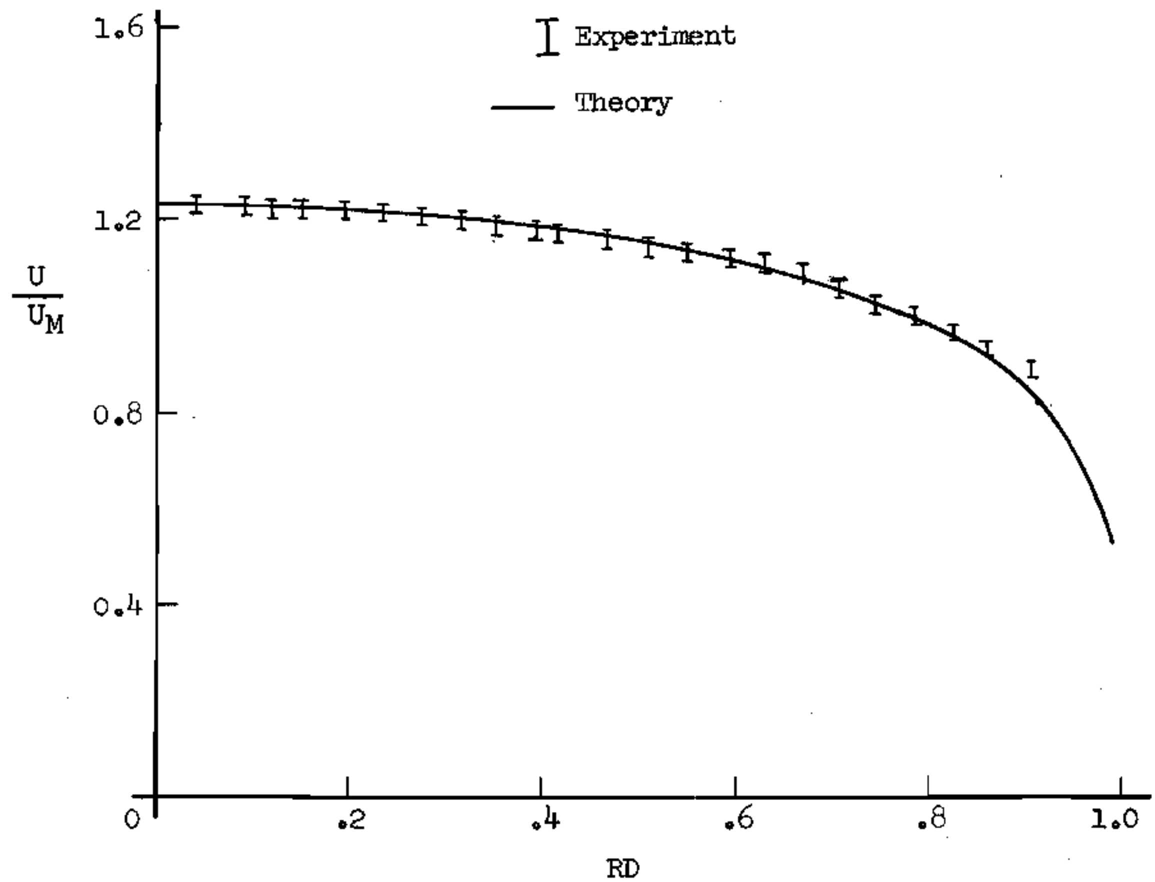

Figure 14. Radial Mean Velocity Profiles, XD=60.0, Water I.

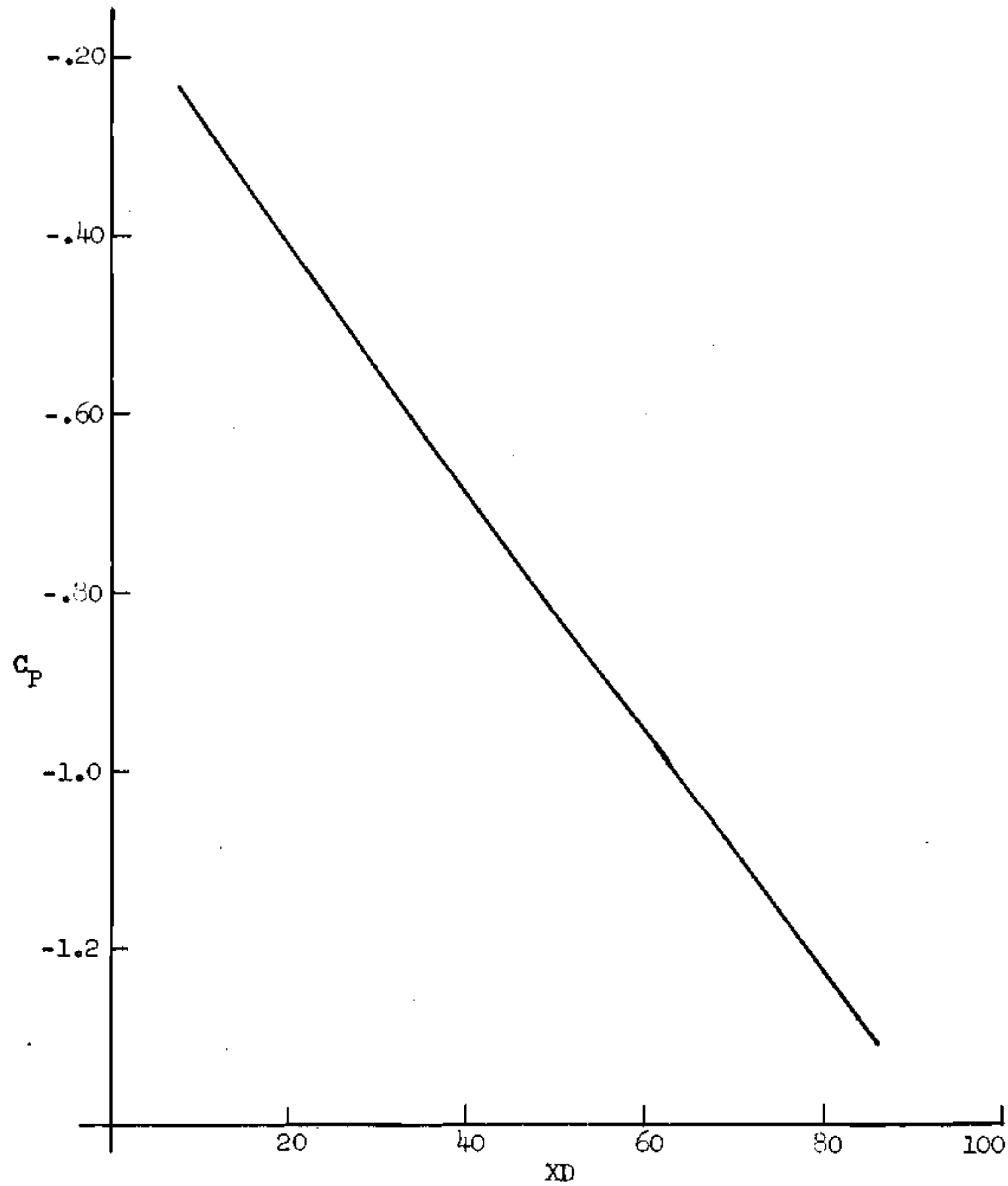

Figure 15. Axial Variation of Pressure Coefficient, Water I, Re=1.36 x 10^4

conditions suggesting that the outer flow is only slightly affected by the jet flow. The gradient of C_p approaches the value for a fully developed pipe flow as the computations proceed downstream. The variation of the skin friction coefficient C_f, shown in Figure 16, does not exhibit a maxima. This likewise suggests that the outer flow is only slightly influenced by the jet momentum. The streamwise decay of centerline velocity is also obtained from the computation and is illustrated in Figure 17. The results indicate a smooth decay of center line velocity.

Experimental Results

The details of the experimental setup as well as the instrumentation used were described in Chapter III. As mentioned before, the mean and turbulent quantities were obtained by ensemble averaging of the signal. The number of samples chosen was fifty, each sample having a 0.256 second duration. Experience proved that results obtained with this combination did not change appreciably when the sampling time or number was increased. Another factor influencing the selection of sampling parameters was the time limitation or the duration of a given experimental run imposed by the reservoir size. When employing polymer solutions, it was desirable to complete measurements at all radial stations (for a given axial location) in a single run, so that the same polymer solution batch could be used. Thus, total time

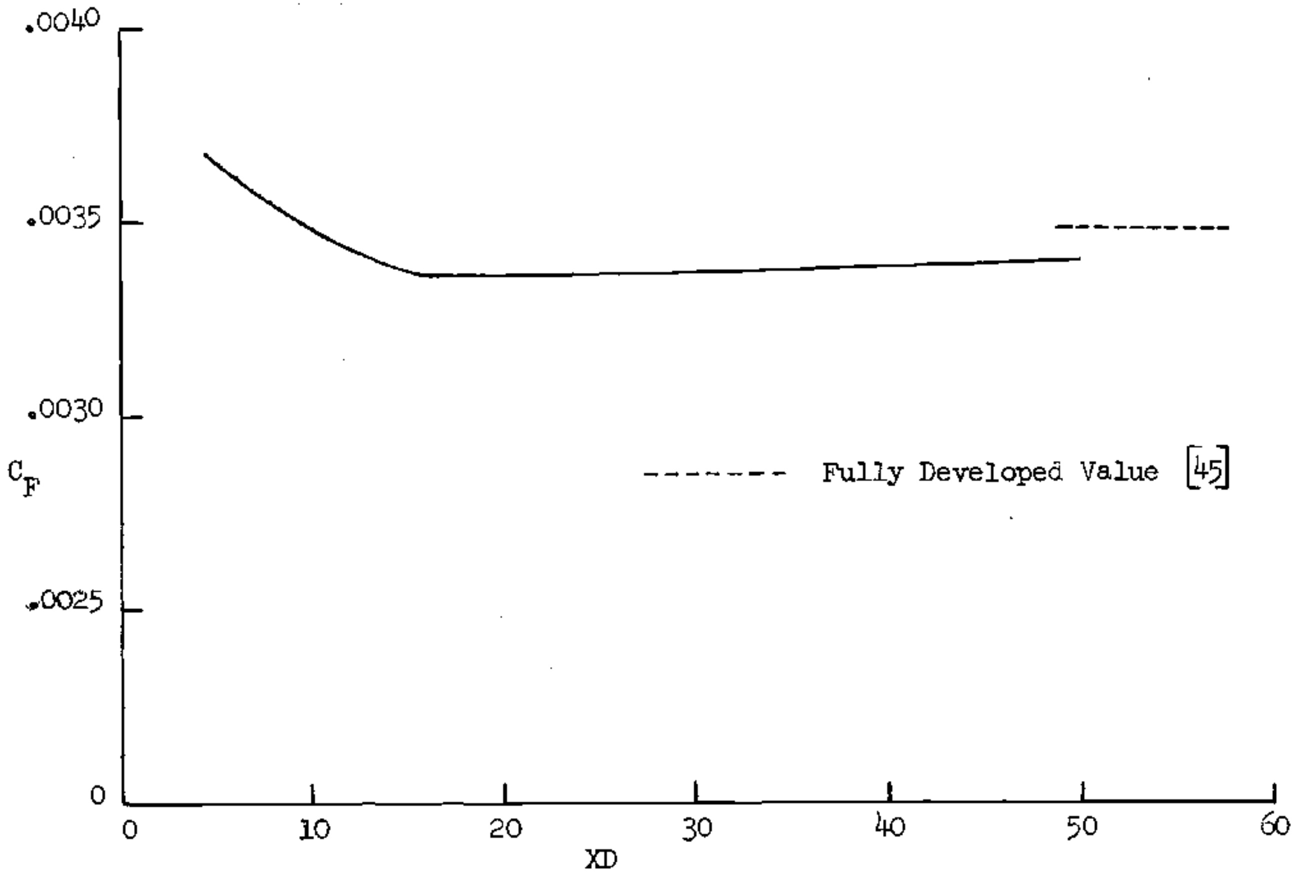

Figure 16. Axial Variation of Skin Friction Coefficient, Water I, Re=1.36 x 10^4.

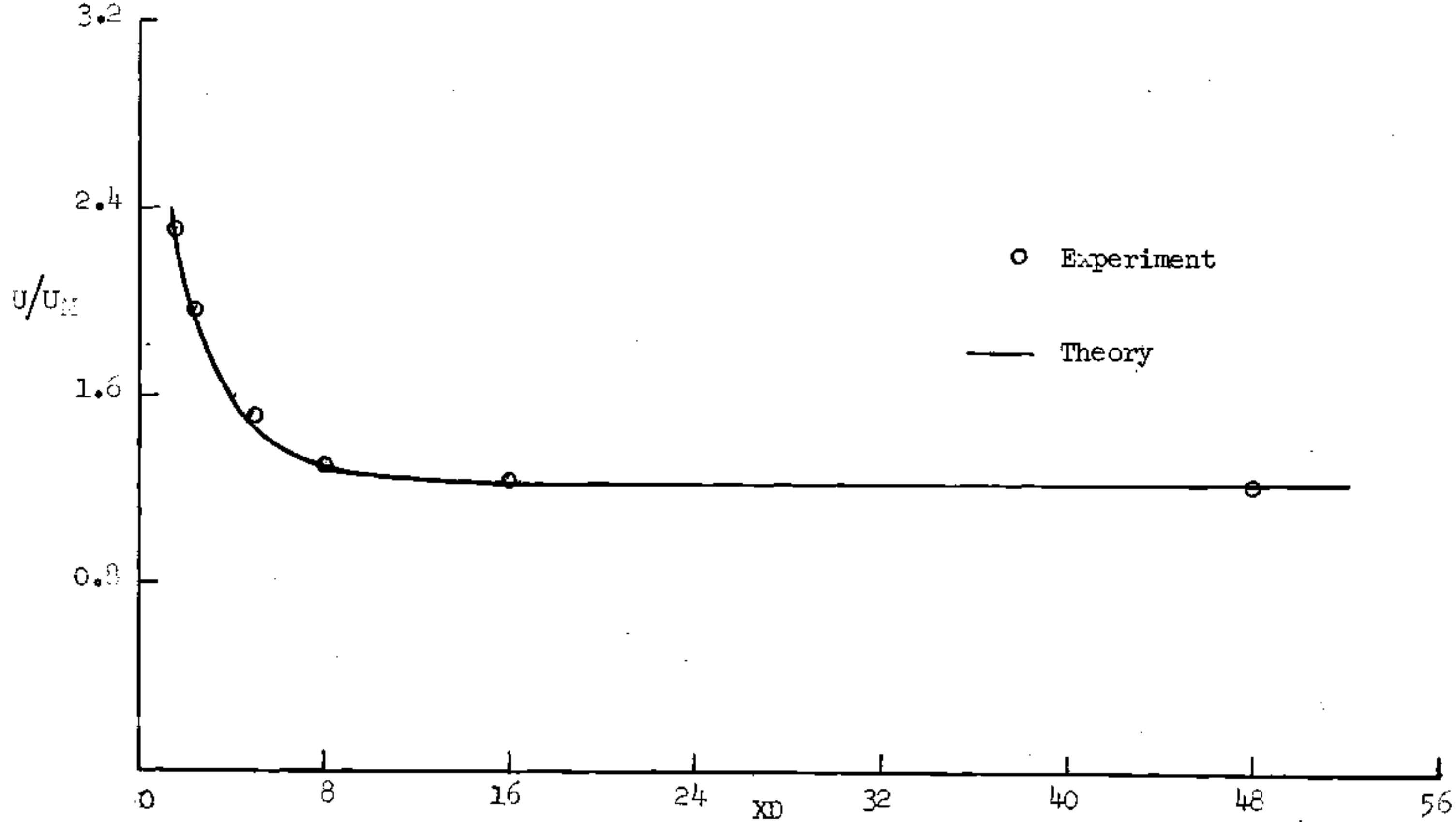

Figure 17. Axial Variation of Centerline Velocity, Water I, Re=1.36 x 10^4

available to record data was limited to 30 minutes.

Based on the number of radial positions at each axial station and the sampling time required at each point, the block size for the Fourier Analyzer was selected. Considering all factors, the maximum frequency selected for the Fourier Analyzer was 1000 Hertz and the block size selected was 512. This set of parameters provided sufficient time for the probe traversal from top wall boundary to a point close to the bottom wall boundary of the pipe.

The flow rates for water and polymer solution were 16.0 and 17.5 liters, respectively.

Mean and Turbulence Velocity Measurements

Water Experiments and Comparison with Theory. The velocity profiles obtained from the measurements are given in Figure 11 - 14. These show the radial distribution of mean velocity at six axial locations. The experimental values shown in Figure 11 were used to replace the values at XD = 2.0 obtained from the computations by the marching procedure, and the computations were carried out to obtain the various values downstream of this location. The comparison between theory and experiment in Figure 12 for XD = 3.0 indicates the agreement is not as good in the region of RD = 0.20 to RD = 0.40 as it is over the remainder of the tube radius. This may be due to the fact that the effect of the finite lip thickness of the jet tube - that is, the wake of the lip - was not incorporated into the program fully. Results obtained at XD = 6.0 indicate the spreading of the effect of the lip of the jet to other regions also. Figures 13 ind 14 indicate good agreement between theory and experiment. The last measuring station is 30 diameters downstream of jet exit and the mean velocity values have almost reached the values for fully developed pipe flow. It should also be pointed out that the radial location closest to wall produces errors in measurements because the probe is touching the wall surface [54]. This very likely contributes to the discrepancy between theory experiment at this point.

Figure 17 shows good agreement between the centerline mean velocity values obtained from theory and experiment.

Figure 18 indicates the radial variation of the fluctuation intensities at the various measuring stations. The values of the intensity were measured by the conical probe and hence are a measure of turbulence rather than the value of any particular component of turbulence velocity. Since the computations provide only the value of turbulence kinetic energy, the values of turbulence velocity fluctuations cannot be obtained unless the ratio of their

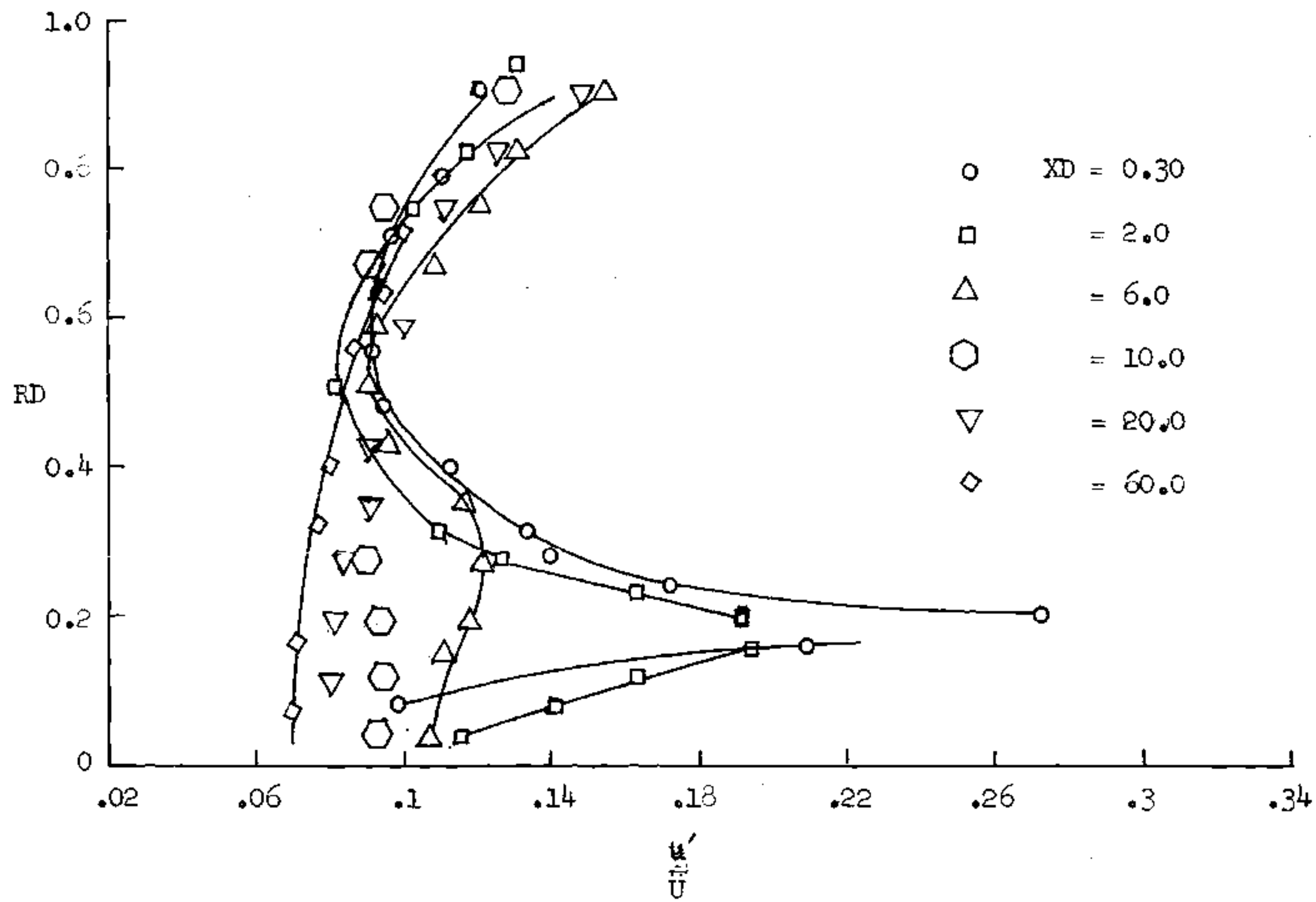

Figure 18. Radial Variation of Turbulence Intensity, Water I, Re=1.36 × 10^4

magnitudes are known. Since the centerline values of the fluctuation velocities (ie u',v',w') are in general approximately the same in pipe flows as well as in a free jet flow, the value of the turbulence intensity at the center line was calculated based on this assumption of isotropy. Although this is not precisely true, the comparison of this value with that obtained by the hot film probe is quite useful and is illustrated in Figure 19. The profile variations suggested by experiment and theory are very similar.

Polymer Solution Experiments. The next phase in the experimental procedure was to study the mixing with a dilute polymer solution as the mixing medium. The inner flow (jet flow) and the outer flow are both polymer solutions with a concentration of 50 ppm of Polyox WSR-301. The measurements were made with a conical hot film probe which was calibrated in a polymer solution of the same concentration. All procedures adopted for data reduction were the same as those for water. The experiments were conducted keeping the pressure heads same as that for water resulting in an increased flow rate. The flow rate for the case of polymer solution was 17.5 liters/minute.

Figure 20 shows the radial variation of the mean velocity at various axial locations. The jet velocity is higher than that for water because of the higher flow rate.

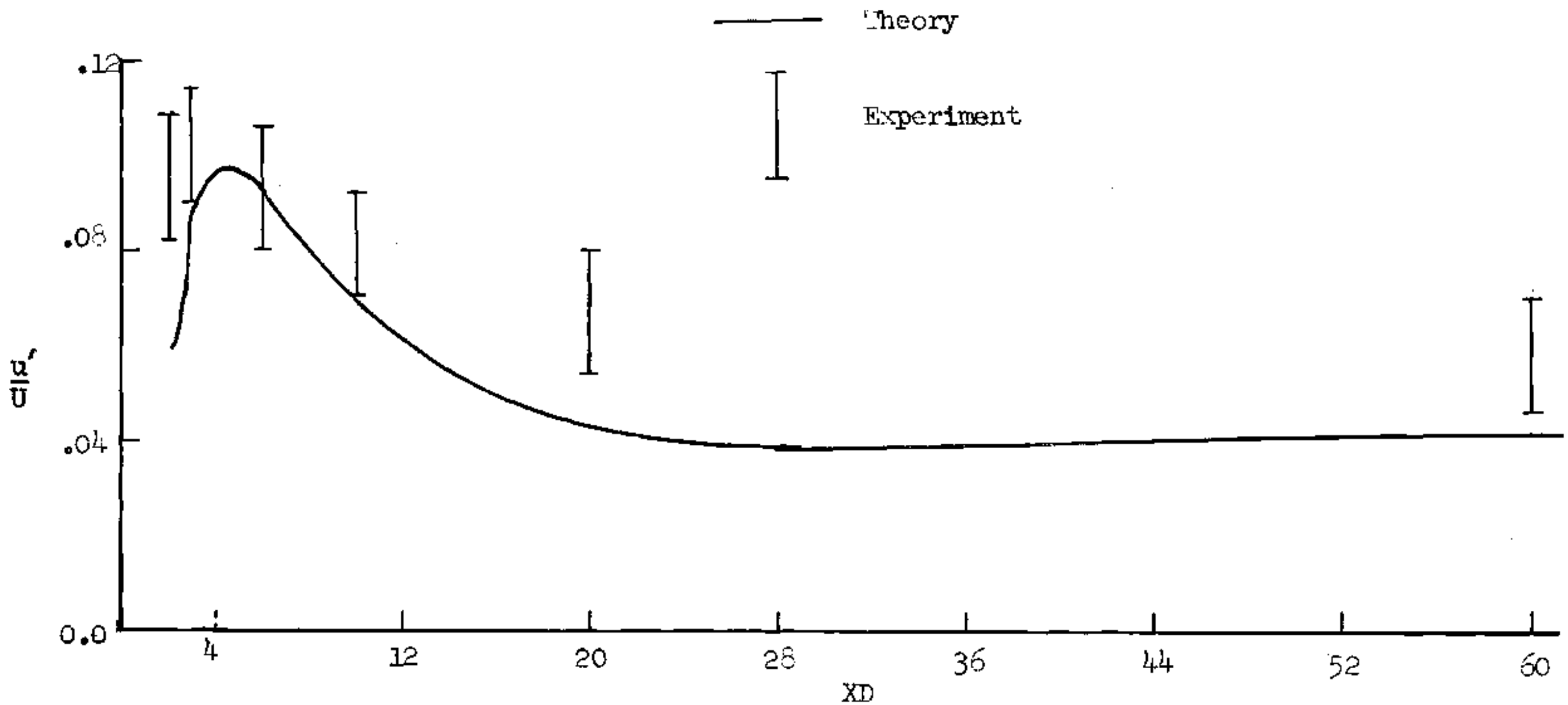

Figure 19. Axial Variation of Centerline Turbulence Intensity, Water I, Re= 1.36×10^4

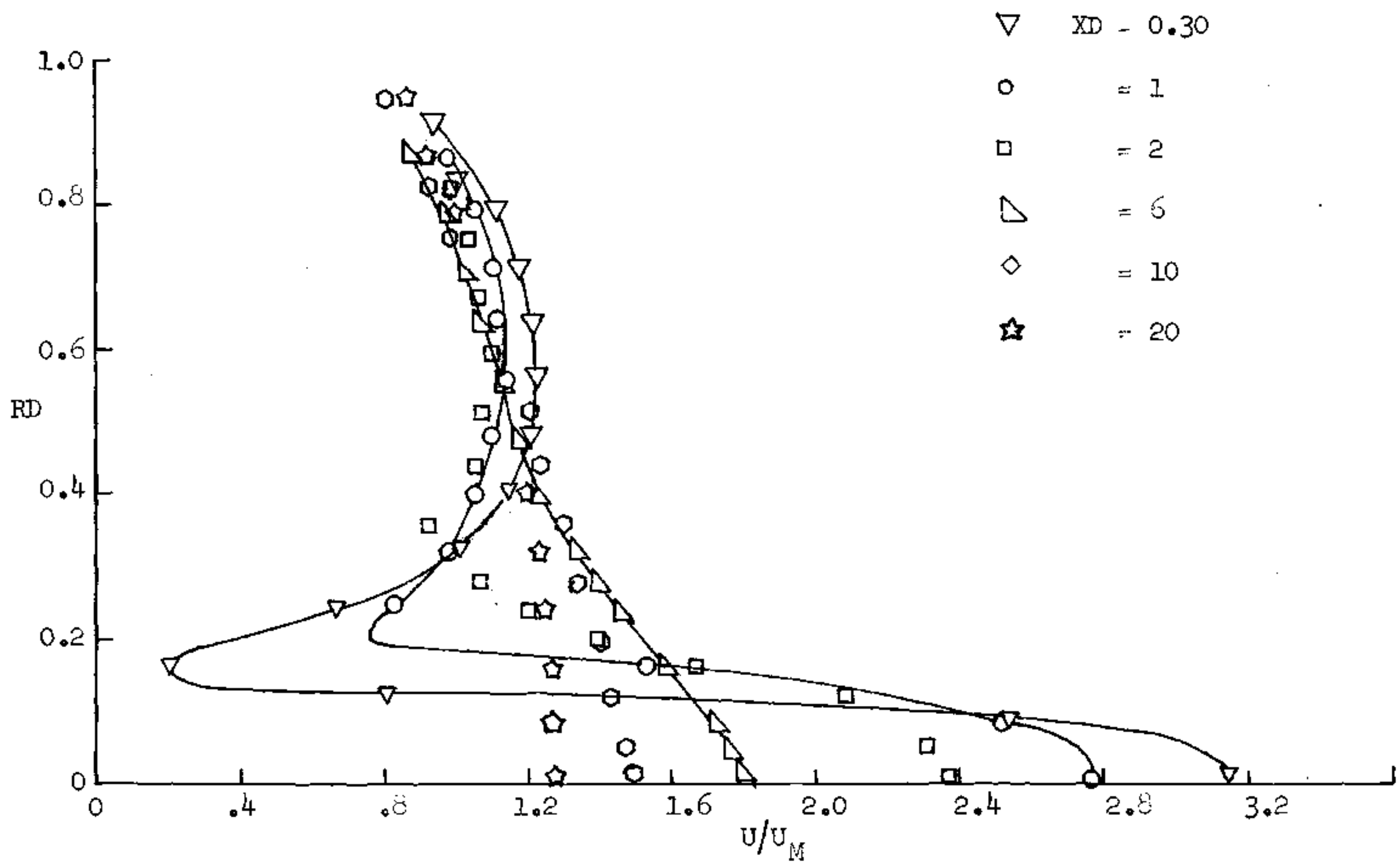

Figure 20. Radial Mean Velocity Profiles, Polymer.

The mean velocity in the outer region is almost the same as that for water case. This is because the polymer is more effective for a tube of small diameter than for a large one in the same Reynolds number range. This is known as the diameter effect [28]. Figure 20 clearly indicates the different regions of the flow. The wake of the jet tube lip at the first axial station (XD = 0.30) is prominent. As the jet mixes with the outer flow the steep gradients gradually are smoothed out and the velocity approaches the fully developed pipe flow profile.

The measured values of the turbulent intensities for the polymer mixing are shown in Figure 21. The intensity values in the mixing region are higher than that for water. This high jet velocity (and so higher velocity ratio of inner to outer flow) results in a more intense mixing and thus has higher turbulence intensities in this region. Another interesting observation is that the turbulence intensities near the wall are higher than that for water. This is in agreement with the behaviour of polymer solutions in pipe flows, as noted by Rudd [56]. This further indicates that in the developing region the conditions near the wall remain similar to those for pipe flow. By the time XD = 20.0 is reached the sharp peaks existing near the jet exit are smoothed out. Although the mean velocity indicates smooth profiles at XD = 10.0 the turbulence intensity does not show

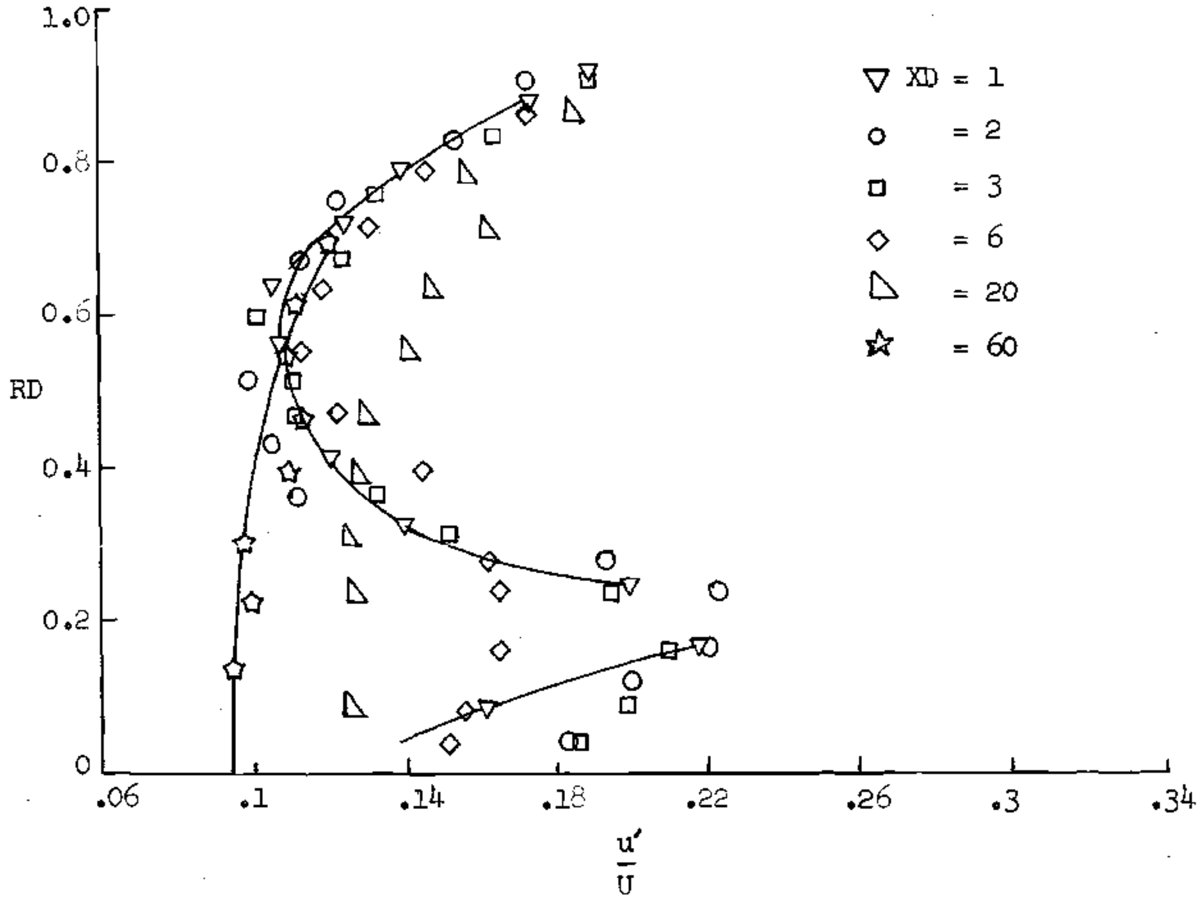

Figure 21. Radial Variation of Turbulence Intensity, Polymer.

a smooth variation until XD = 20.0. This agrees with the generally accepted concept that turbulence quantities take a greater time to reach developed flow values than do mean quantities. At XD = 60.0 the turbulence intensity profile is uniform near the center, but there is a steep increase in the intersity values as the duct wall is approached. The values of u'/U at the center line for water and polymer solution at this axial station are not very different.

The previous two sections dealt with the mean and turbulent flow velocities obtained for the case of water and polymer solution. The effect of polymer on the variation of these quantities can be studied by making a direct comparison. It should, however, be emphasized that for both the cases the pressure heads (for jet and outer flow) were kept the same.

<u>Comparison of Water and Polymer Results</u>. It was found that for the polymer solution turbulence intensities were higher close to wall as well as in the wake region. To illustrate the influence of this, the streamwise variations of center line velocity were plotted in Figure 22. The velocity values were non-dimensionalised by the velocity at jet exit (U_I) for each case. Thus, the non-dimensional centerline velocity at the jet exit for water as well as polymer solution is unity. As the jet develops, the nondimensional value decreases monotnically from $U/U_I=1.0$

to a value of about 0.4 for the case of the polymer solution and to approximately 0.45 for the case of water. This suggests that the center line velocity decays faster for polymer solution than for water. However, it should be pointed out that the flow rates, and hence the initial conditions, for both cases are not the same. To reduce the effect of differences in initial conditions, another set of experiments was done using water. In other words, a new set of measurements for water was taken so that the initial conditions and hence the the flow rates, were close to those for the polymer solution. It was seen earlier that the presence of polymer resulted in a large increase in the jet flow velocity and only a small increase in the outer flow velocity. So it was decided to increase the pressure head of the jet flow supply reservoir so that the jet exit velocity at the center line is close to the value for the case of polymer solution. This arrangement for water with higher head will be referred to as Water II. Water experiments with the same head as for polymer will be referred to as Water I, for consistency. For the experimental setup the center line velocity for polymer at the first axial station (XD = 0.30) was 199.0 cms/sec and that for Water II was 194.0 cms/sec. Mean and turbulence quantities were measured at the various axial stations and the data reduction procedures adopted were the same as before.

The streamwise variation of U/U_{*} for Water II is shown in Figure 22. Comparison of the values for polymer and Water II indicate that the center line velocity decays significantly faster for the case of the polymer solution suggesting a quicker mixing of the jet with the surrounding medium. Barker's [37] measurements for submerged jet using a Laser Doppler Velocimeter also reported a quicker decay of the center line velocity. The turbulence intensity values at the center line for the three cases of Water I, polymer and Water II are shown in Figure 23. The intensity values for polymer solution are higher than those for water. Further , it can be seen that the turbulence intensity reaches a peak value during the early growth of the jet and then decreases. Also, the peak value of intensity is clearly larger than that for water. Similar observations were reported by Barker [37]. Thus, the results show that the center line behaviour in the initial region is similar to that of a submerged jet issuing as a fully developed pipe flow. It should be noted, however, that although the center line mean velocity close to the jet exit for polymer and Water II are approximately the same, the presence of polymer does affect the turbulence structure [28].

Figure 24 shows the radial distribution of the mean velocity at three axial locations, for the cases of Water I,

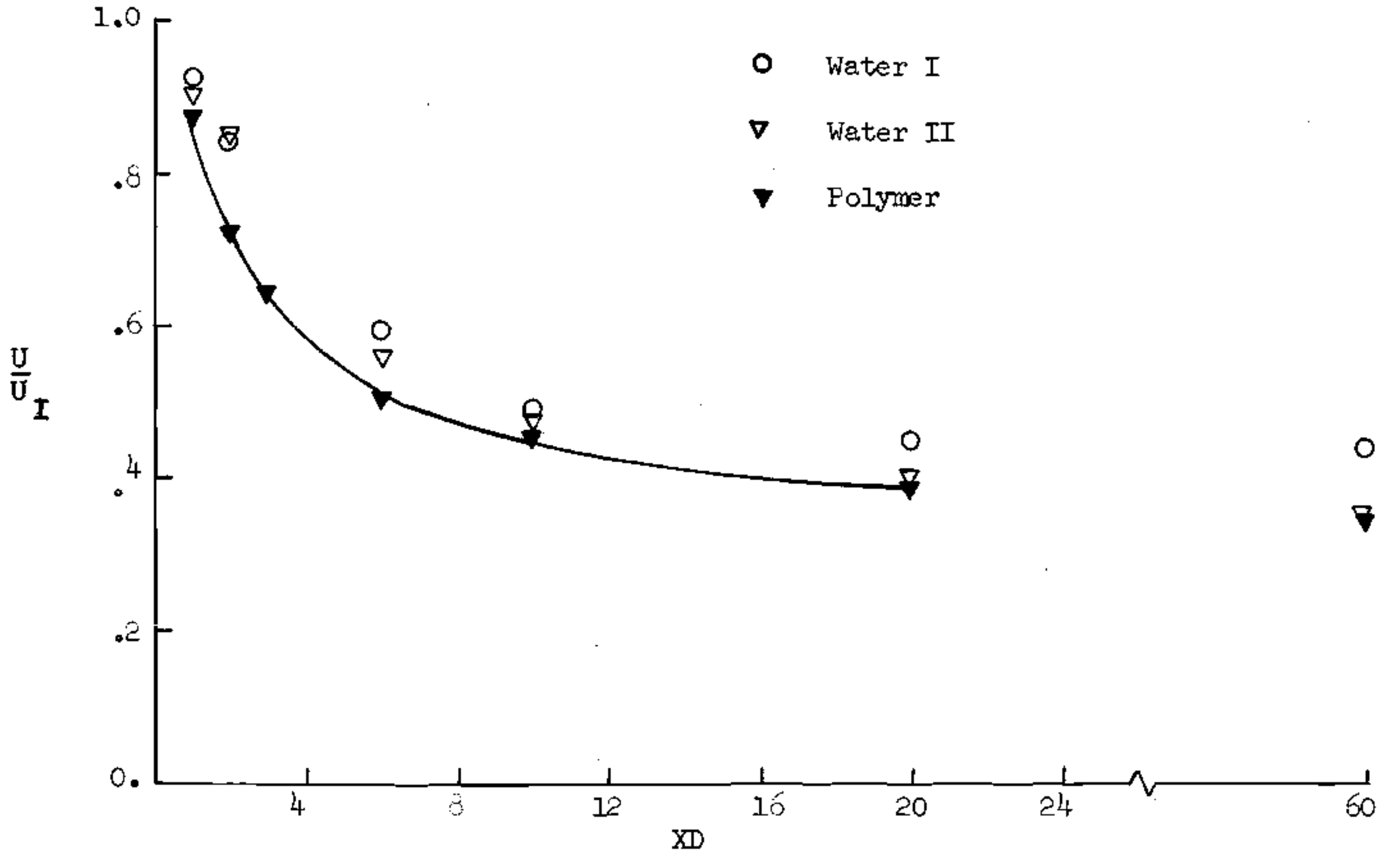

Figure 22. Comparison of Centerline Velocities, Water I, Water II and Polymer

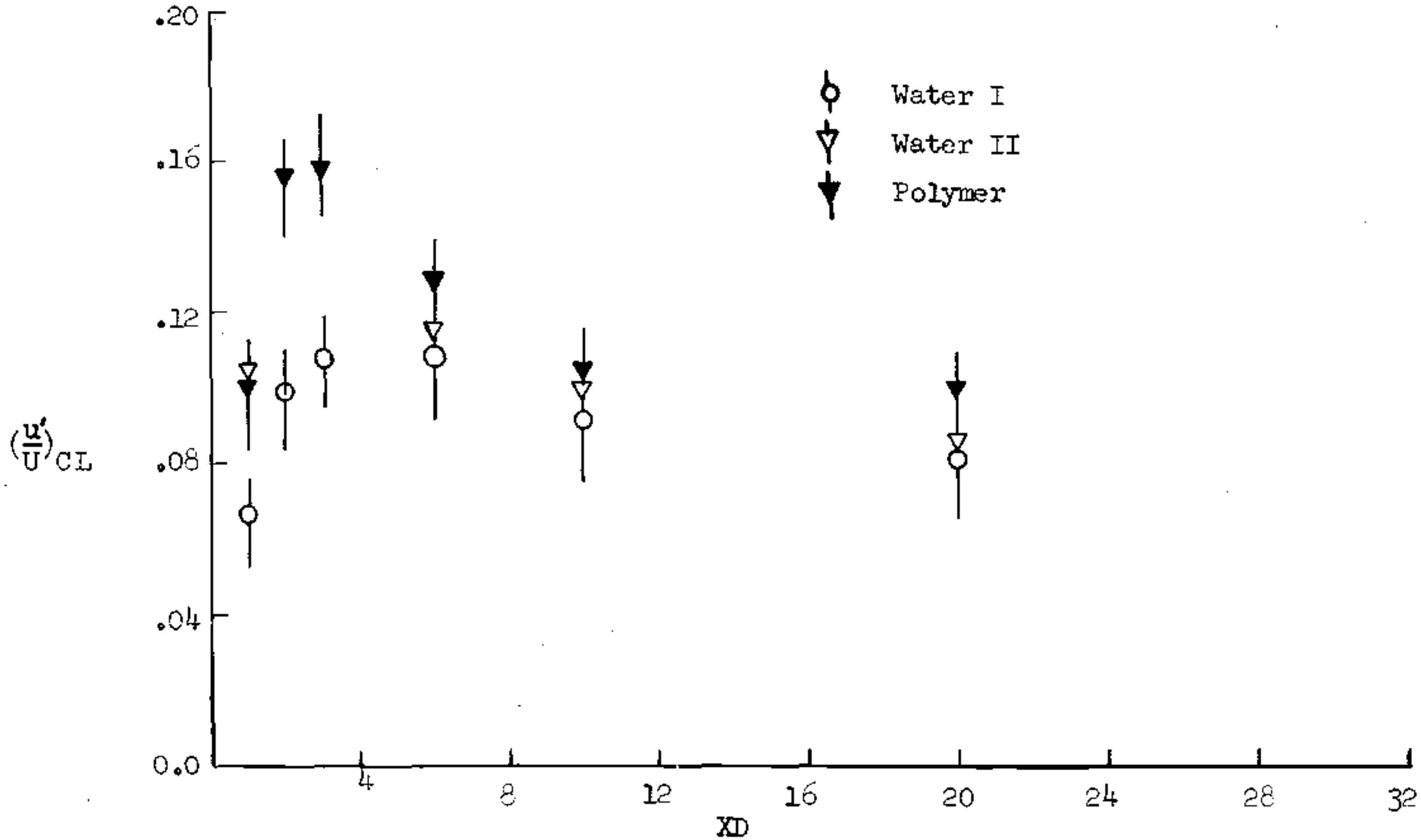

Figure 23. Comparison of Centerline Turbulence Intensities, Water I, Water II and Polymer.

polymer and Water II. The plots indicate that there is very little difference in mean velocity variation in the region near the duct wall, at all three axial stations. This also suggests similar axial variation of mean velocity near the wall. This happens because, in the outerflow region, the conditions are only very slightly influenced by the presence of polymer. Also , since the jet flow affects the outer flow only slightly, the higher jet velocity for Water II has little influence on the behavior near wall as far as mean velocity is concerned. Moving radially toward the center line the difference in mean velocities is significant. At XD = 2.0 it can be seen that the presence of the polymer results in a faster axial decay of mean velocity. This is observable in the region from the primary mixing zone to the axis (RD = 0.45 to RD = 0.0). At XD = 10.0 the influence is still observable in this region. This suggests the polymer is influential in the near field mixing zone. The mixing finally results in reaching fully developed pipe flow conditions for XD = 60.0. The velocity profiles for polymer and Water II are very close to each other in this location.

The axial variation of mean velocity at the center line suggests that the polymer jet decays faster than that for water. The radial distribution of turbulence intensity at each axial station should also indicate the effect of mixing. Figure 25 shows this distribution at XD = 1.0. It

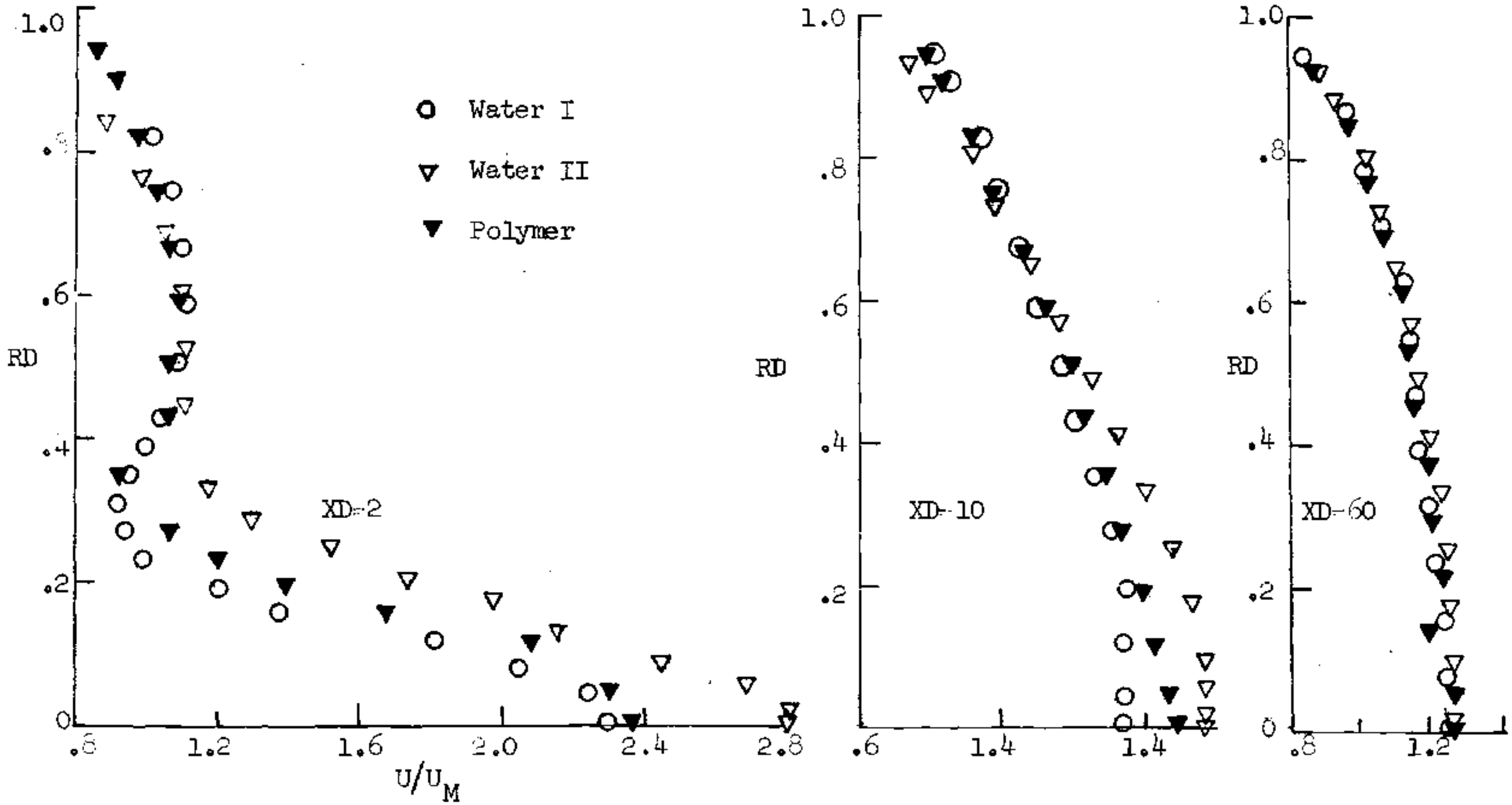

Figure 24. Comparison of Radial Mean Velocity Profiles, Water I, Water II and Polymer.

can be seen that the intensities for the polymer case are higher in the mixing layer than those for Water II. Also the effective mixing layer width or the wake behind the lip of the jet is larger for polymer than for Water II. This could be interpreted as due to the thickened boundary layers on the walls (inner and outer) of the jet tube due to the presence of the polymer. Some influence of the higher intensity values in the lip wake is felt in the outerflow as indicated by the higher intensity values in the region RD = 0.3 to RD = 0.6. Additional comparisons are given at XD = 6.0 and XD = 10.0 in Figure 26. The high intensities are seen to be gradually reduced by the mixing. However, the intensity values for the polymer are still higher, from center line to a region in the mixing layer where RD = 0.3 at XD = 6.0. Beyond this the intensity values are not very much different for polymer and Water II. Figure 27 shows that the data obtained at XD = 10.0 and XD = 20.0 exhibit scatter. The mean velocity profile at XD = 10.0 (Figure 24) shows flow adjustment to fully developed pipe flow starting to take place. Correspondingly, the turbulence intensity profiles at XD = 10.0 and XD = 20.0 do not exhibit any local extrema. Thus, the profiles suggest that the flow nature is similar to that of a developing pipe flow. The radial turbulence intensity profile shown in Figure 27 at XD = 60.0 vary smoothly. Near the wall the polymer solution has higher values than Water II. However, near the centerline

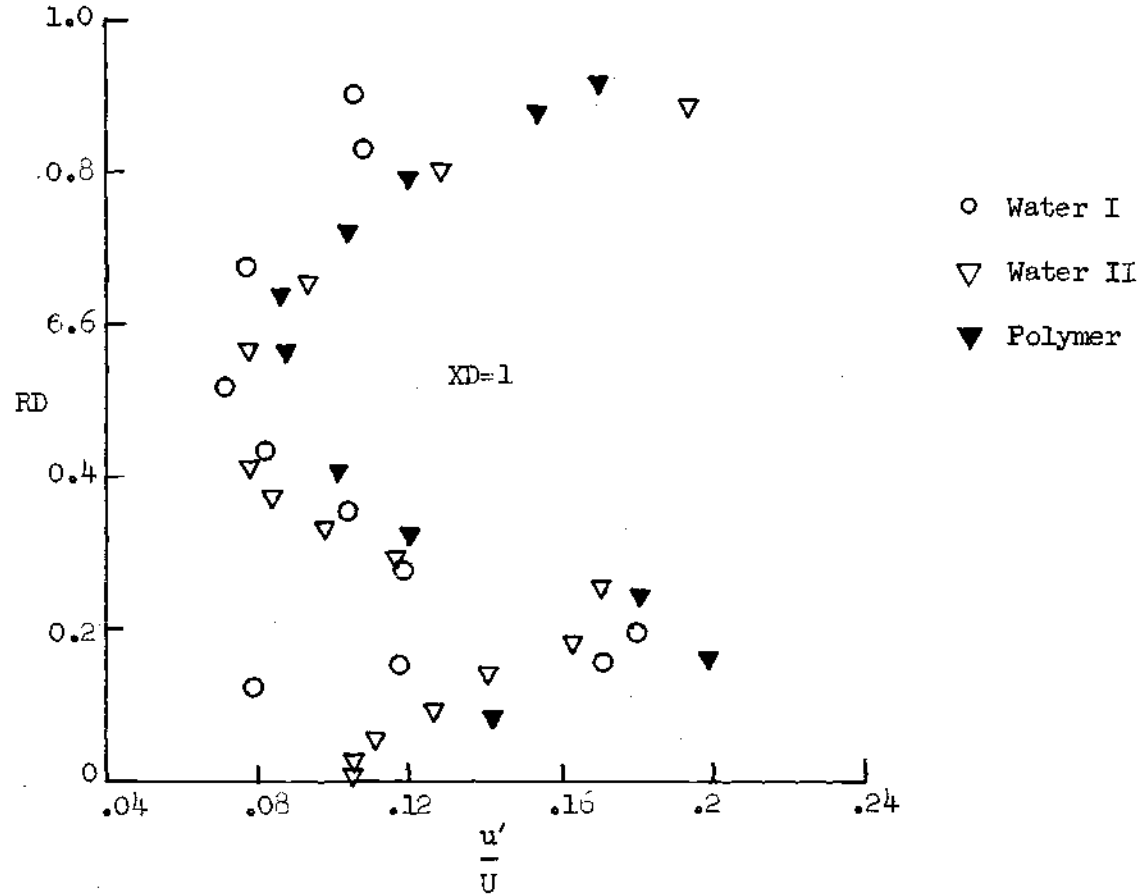

Figure 25. Comparison of Radial Turbulence Intensity Profiles, Water I, Water II and Polymer.

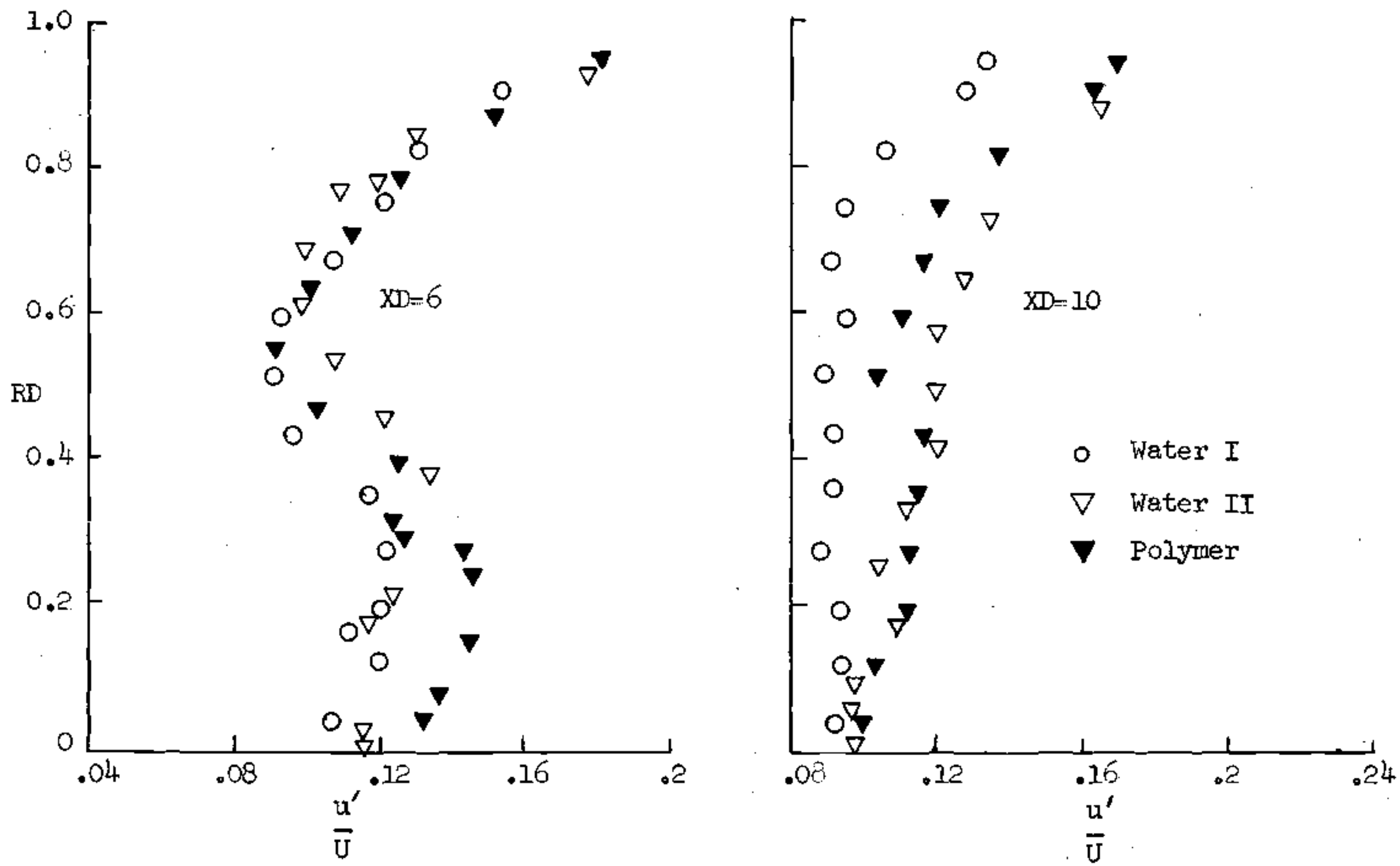

Figure 26. Comparison of Radial Turbulence Intensity Profiles, Water I, Water II and Polymer.

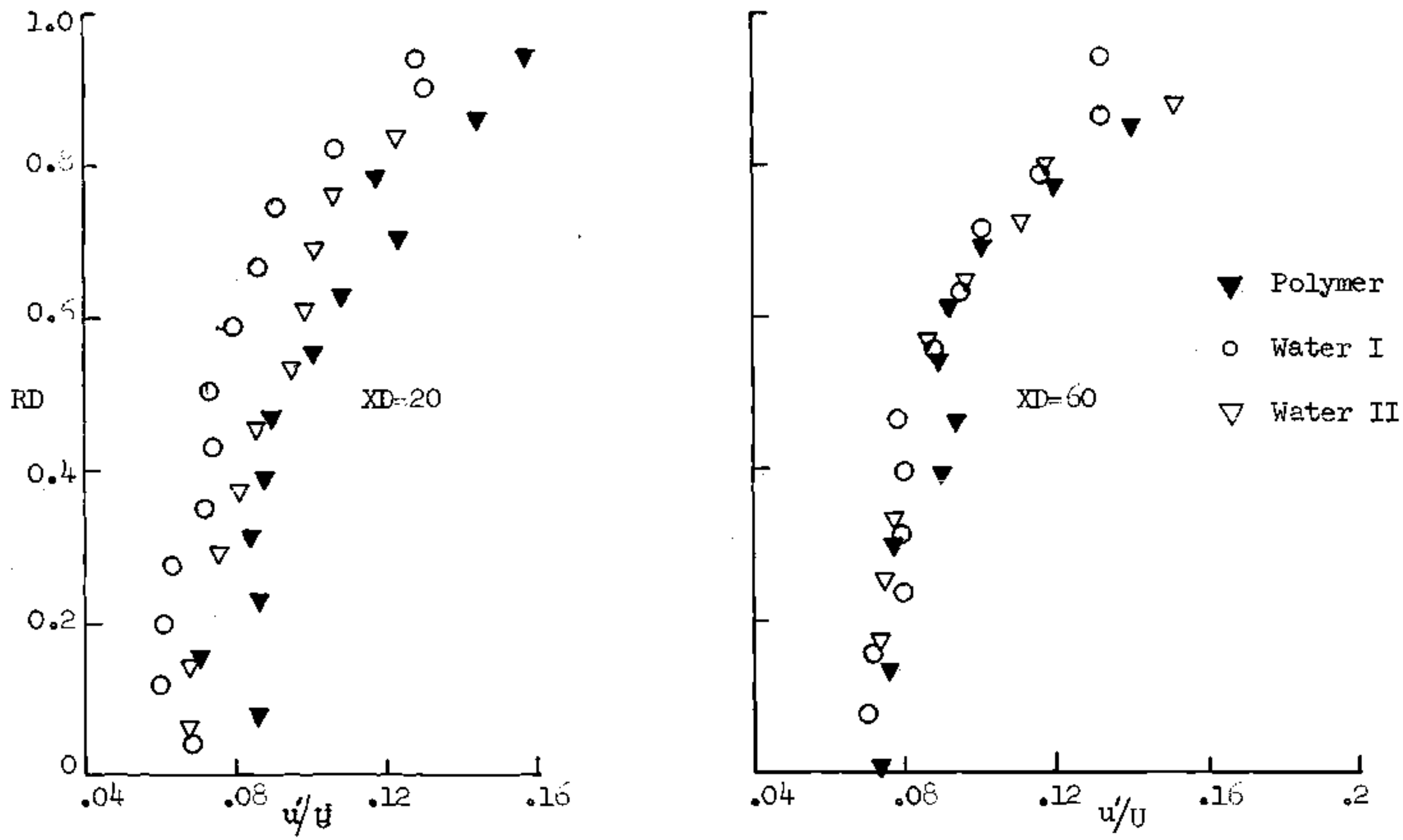

Figure 27. Comparison of Radial Turbulence Intensity Profiles, Water I, Water II and Polymer

they are very close to each other. Rudd [56] made measurements using a laser Doppler velocimeter in a pipe flow and observed that the intensity values for polymer solution to be higher near the wall and lower near the axis than for water. The profiles of Figure 27 showed the same behaviour near the wall as suggested by Rudd.

<u>Energy Spectra Measurements</u>

The energy spectra of the fluctuating velocities is obtained by performing a Fourier analysis of the output signal from the linearizer.

The maximum frequency setting was 1000 Hertz and the block size chosen was 512. According to Shannon's sampling theorem, it is necessary to sample a segment of data at twice the rate of the highest frequency desired. Therefore, if energy spectra to 1000 Hertz are needed, the linearizer output must be converted to digitized data at a rate of 2000 points per second. For a block size of 512 in the Fourier Analyzer system, the sampling time required to fill one block with data is 0.256 (512/2000) seconds. Since this is a relatively short time for turbulence sampling, a large number of samples was taken and ensemble averaged to obtain a reliable statistical result. Further, the resolution in the frequency domain is the inverse of sampling time, so that this value is approximately four Hertz. After the analysis of the output signal, the spectrum is given by values at discrete frequency points (separated by approximately four Hertz in frequency space). The amplitude (or the value of the ordinate) is taken as the total area in the channel of width of approximately four Hertz [54].

The sum of the ordinates at the discrete frequency values, over the entire frequency range, simply gives a measure of the energy content of turbulence, since the conical probe senses fluctuations which in general are a measure of turbulence. Patterson, Zakin and Rodriguez [47] found spectral shapes obtained by conical probes to be similar to the u'^2 spectra. Therefore, the spectra here also have been referred to as u'^2 spectra, it being understood that this is not precisely correct. Checks using upper frequency limits from 500 to 5000 Hertz showed no effect on the spectral content below 5000 Hertz. Also various attempts to improve the signal to noise ratio were unsuccessful in producing useful data for frequencies greater than 500 Hertz. The reference voltage, for energy spectra in decibels, of 1 volt corresponds to a velocity of 1 m/sec.

<u>Spectra for Water</u>. The (u'^2) spectra at the various axial stations were obtained at the centerline and at a point close to the wall. In some cases spectra at other radial locations were also obtained.

The spectra at the measuring station closest to the jet exit are shown in Figure 28. The spectrum at the wall shows the energy content for eddies of small frequency falling off quickly with increase in frequency . However, at the center line the decrease in (u'^2) spectrum with frequency is much slower. In fact, the ordinate values drop by only six db in a frequency range from four to about 200 Hertz. The drop in (u'^2) values from 200 Hertz to 1000 Hertz is by about 20 db. Comparing the two spectra it can be seen that at the center line the energy content in the eddies of large scale is lower and that for small scale eddies is higher. It should also be noted that the spectra at the centerline and near the wall intersect at a frequency of about 85 Hertz. It should be added, however, that at this axial station (closest to jet exit) the spectra at the center line is measured in the primary flow (or jet flow) whereas the spectra near the wall is obtained at a location in the secondary flow (annular flow) distinctly different from the jet flow.

Figure 28 also contains the spectrum at a radial location RD = 0.236. One of the interesting characteristics here is the "spike" in the spectra at a frequency of approximately 200 Hertz. This radial station corresponds to a location in the wake of the lip of the jet, that is to

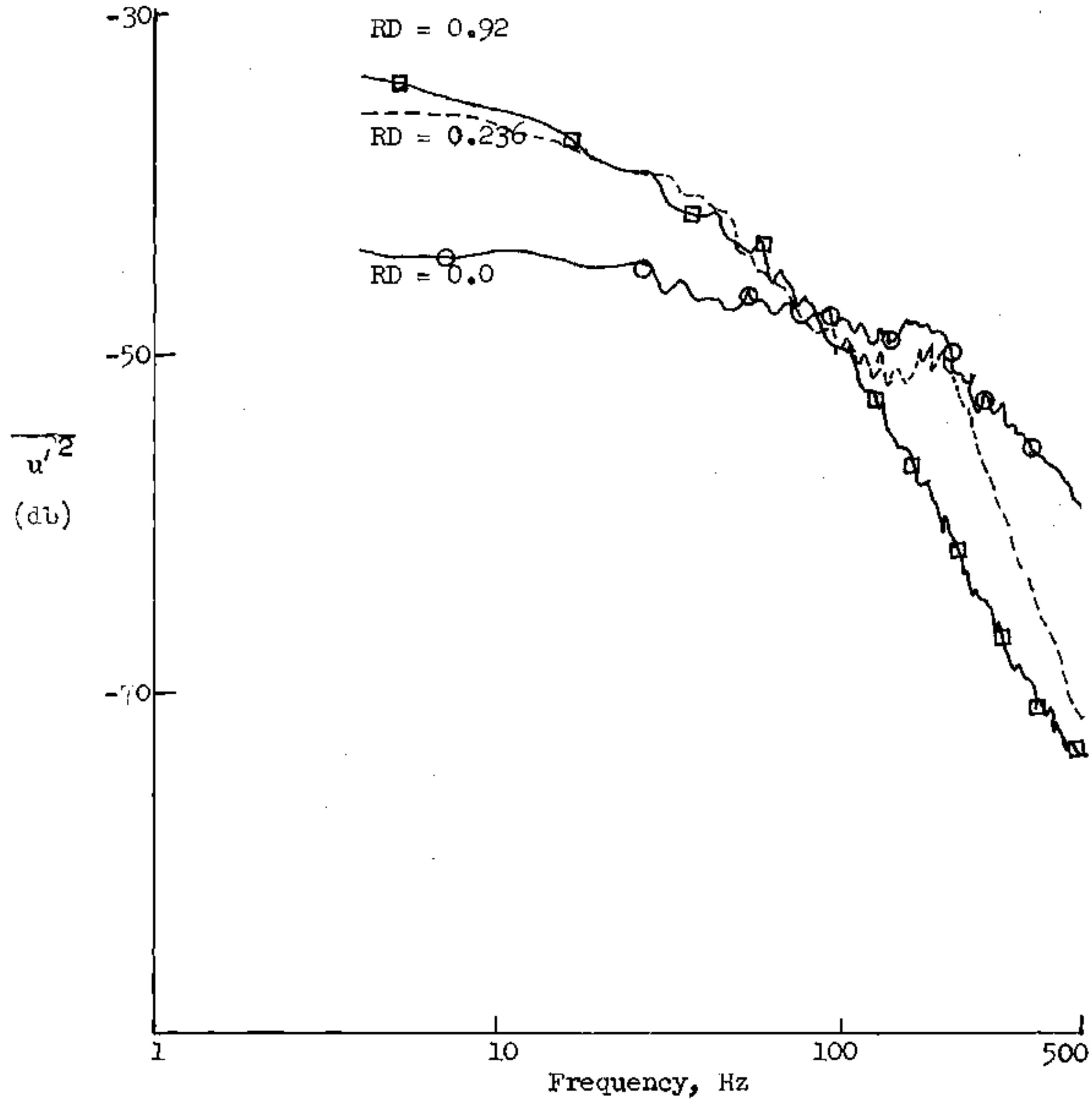

Figure 28. Energy Spectra for Water I, XD=0.30.

say, in the mixing layer. The presence of "spike" has also been observed in two dimensional mixing layers [57]. A peak in the energy spectra has also been observed for jets [58] and is thought to be indicative of vortex ring shedding. Although the present flow situation does have aspects of jet flow and mixing layers, the nature of the flow structre is much more complex. First, the presence of a coflowing stream distinctly alters the turbulence structure from that of a simple free jet. Second, the presence of the wall confinement alters the turbulence structure. Finally, it should also be pointed out that the primary flow does not exit through a nozzle and hence does not have a potential core. In fact, at the exit of the jet tube the flow is a fully developed turbulent shear flow. Keeping these differences in mind, it is easy to see that the comparison with previous observations in jets and shear layers would be naive and possibly erroneous. However, the presence of dominant eddy sizes in the mixing layer can produce a "spike" in the turbulent spectra. The presence of the spike could thus be thought of as due to the eddy structure in the mixing layer.

The spectra obtained at the axial location XD = 1.0 are shown in Figure 29. The spectrum obtained at a point close to the wall, at the centerline, and at the radial location RD = 0.158 are shown in this figure. The qualitative nature

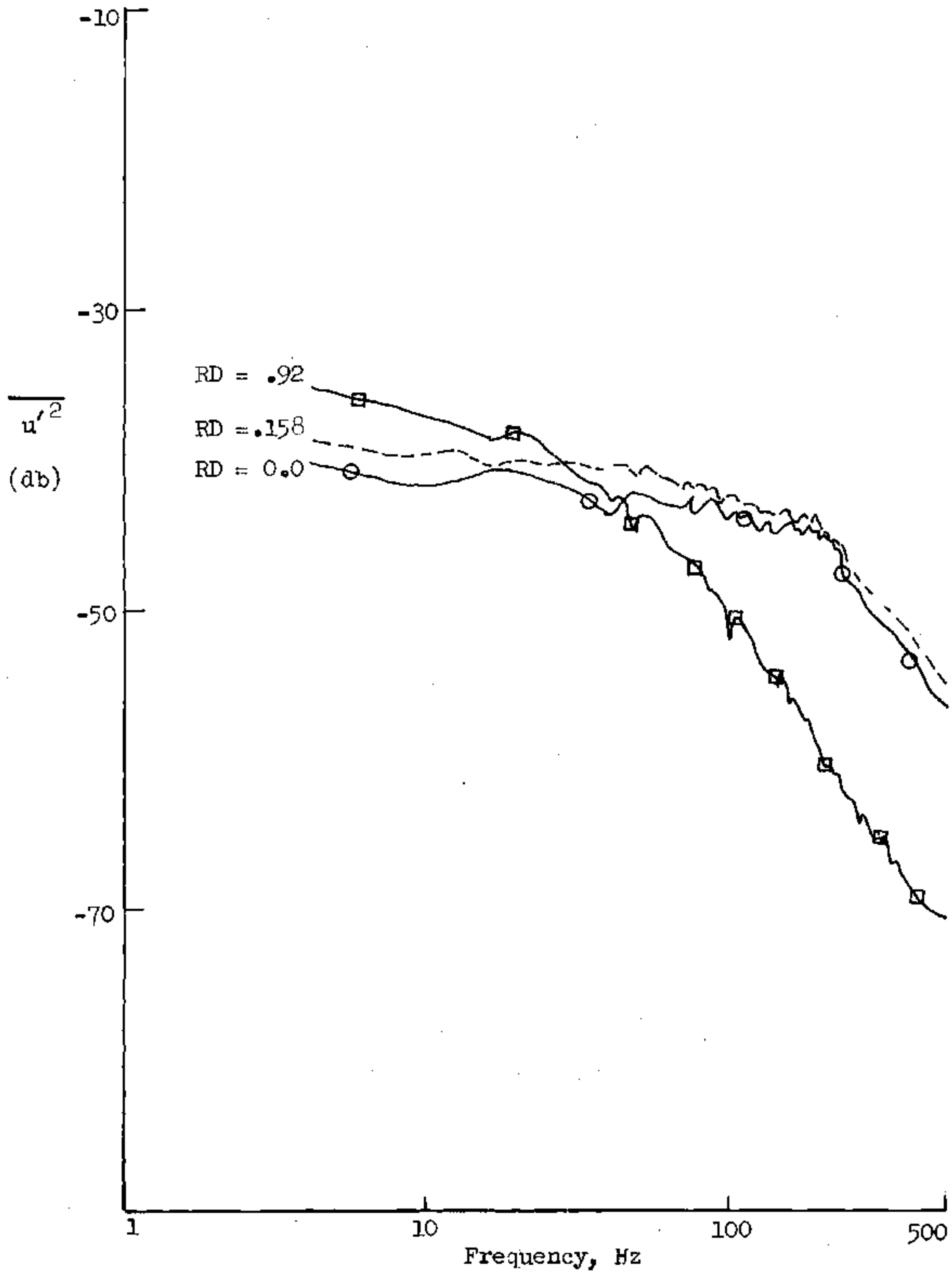

Figure 29. Energy Spectra for Water I, XD=1.0.

of the curves is similar to that observed at XD = 0.30. The spike in the spectra, although somewhat smoothed out, is visible at the center line as well as at RD = 0.150 and this occurs at approximately the same frequency range as for XD = 0.30. However, the relative intensity of the spike is much less at the downstream location. This is indicative of the mixing taking place, thus smoothing out the sharp gradients.

Figure 30 shows the spectra obtained at the axial location XD = 2.0. The most obvious feature of these curves is the abscence of the spike in the spectra. This is understandable because as the jet expands downstream the gradients in the flow occurring in the mixing layer region are reduced and the flow eventually tends toward a fully developed pipe flow. Another point of interest is the frequency at which the spectra at the center line and the spectra close to the wall intersect. The magnitude of the frequency value keeps decreasing as the measuring station moves downstream. This suggests a variation in either the spectra near the wall or those at the center line or both. To determine this the spectra obtained close to wall as well as at the center line at the first three stations (XD = 0.30, 1.0 and 2.0) were compared.

Figure 31 shows the spectra close to the wall and Figure

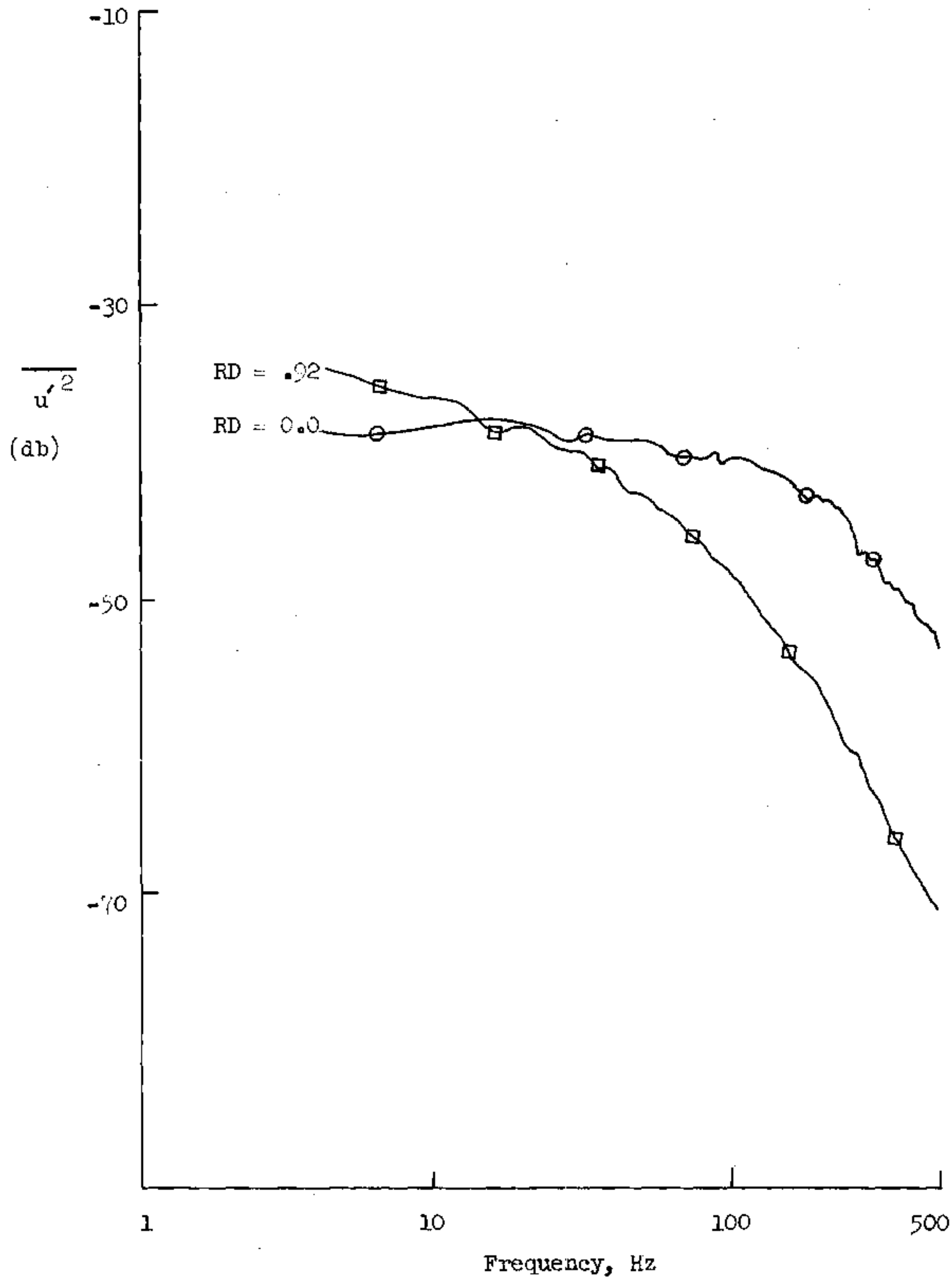

Figure 30. Energy Spectra for water I, XD-2.0.

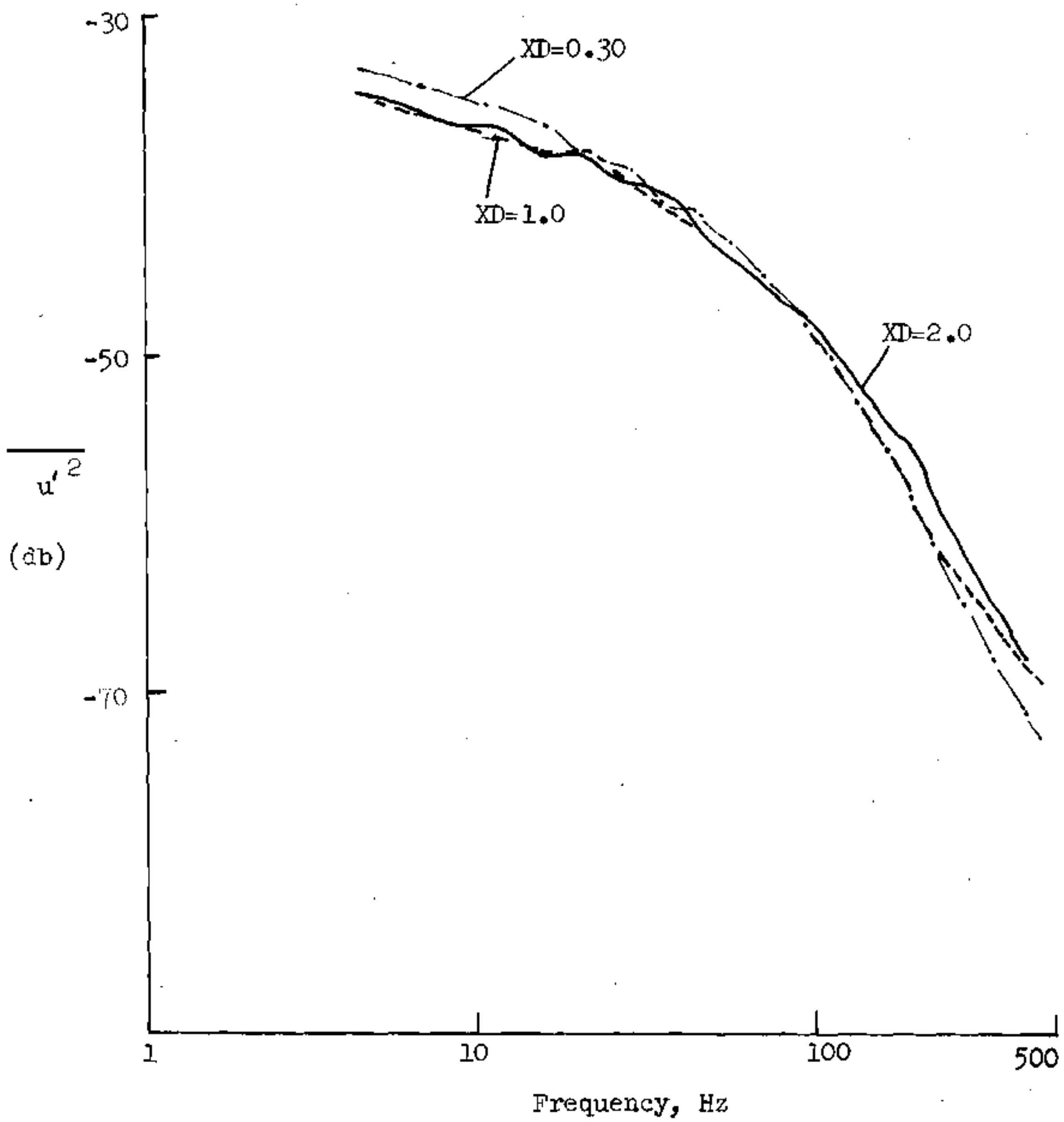

Figure 31. Energy Spectra for Water I, RD=0.92.

32 shows the spectra at the center line for the various axial locations. The spectra at the point close to the wall are almost the same whereas those at the axis show gain in energy as the mixing of the two streams take place. The turbulent energy due to mixing is redistributed and is manifested by an increase in energy (with XD) at the center line spectra. As far as the spectra near the wall are concerned, the shapes are very similar to those corresponding to pipe flow for the particular mass flow rate. Since the jet flow influence on the outer flow is very small, especially close to wall, the changes in spectral shape are negligible.

Figure 33 shows the energy spectra obtained at the axial location XD = 6.0 . Comparison of the spectra at the center line and a point close to the wall shows an adjustment of flow conditions taking place.

Figure 34 shows the energy spectra obtained at XD = 10.0. The spectral shapes at the centerline and close to the wall indicate that the flow development is acting to smooth out the velocity gradients.

Figures 35 and 36 show the energy spectra obtained at XD = 20.0 and 60.0, respectively. The spectra at the center and close to the wall do not intersect and the shapes are

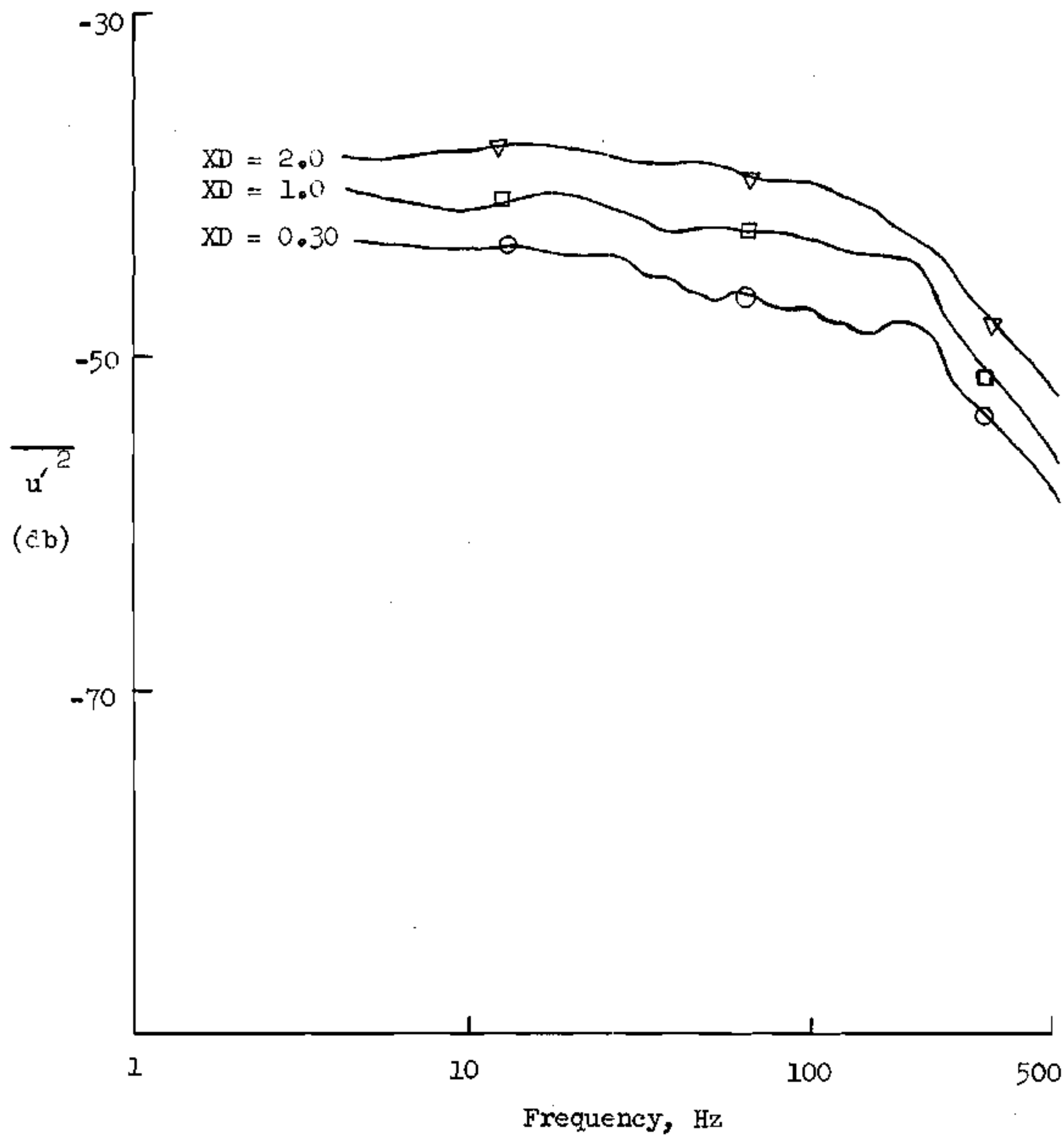

Figure 32. Energy Spectra for Water I, RD=0.0.

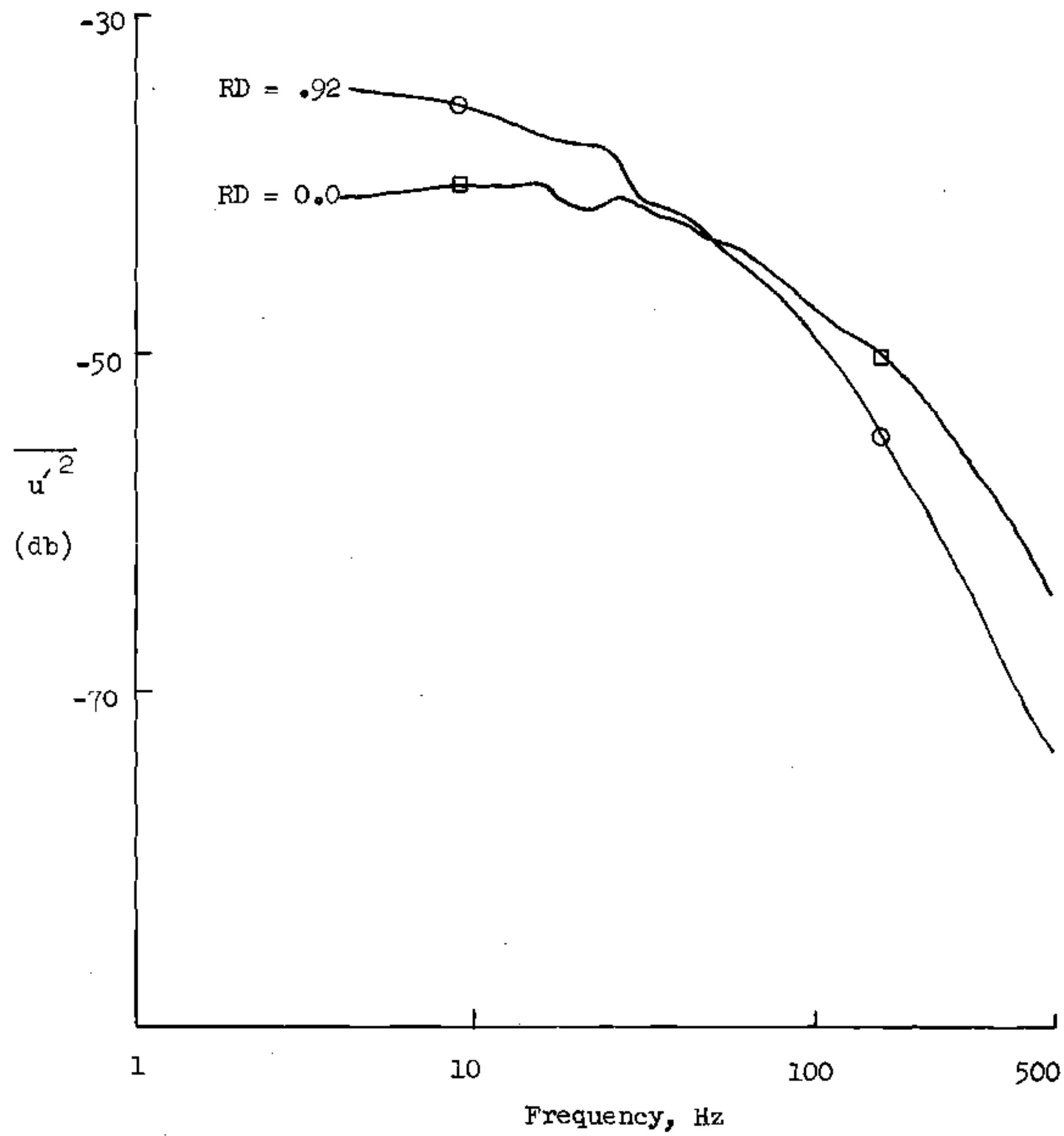

Figure 33. Energy Spectra for Water I, XD=6.0.

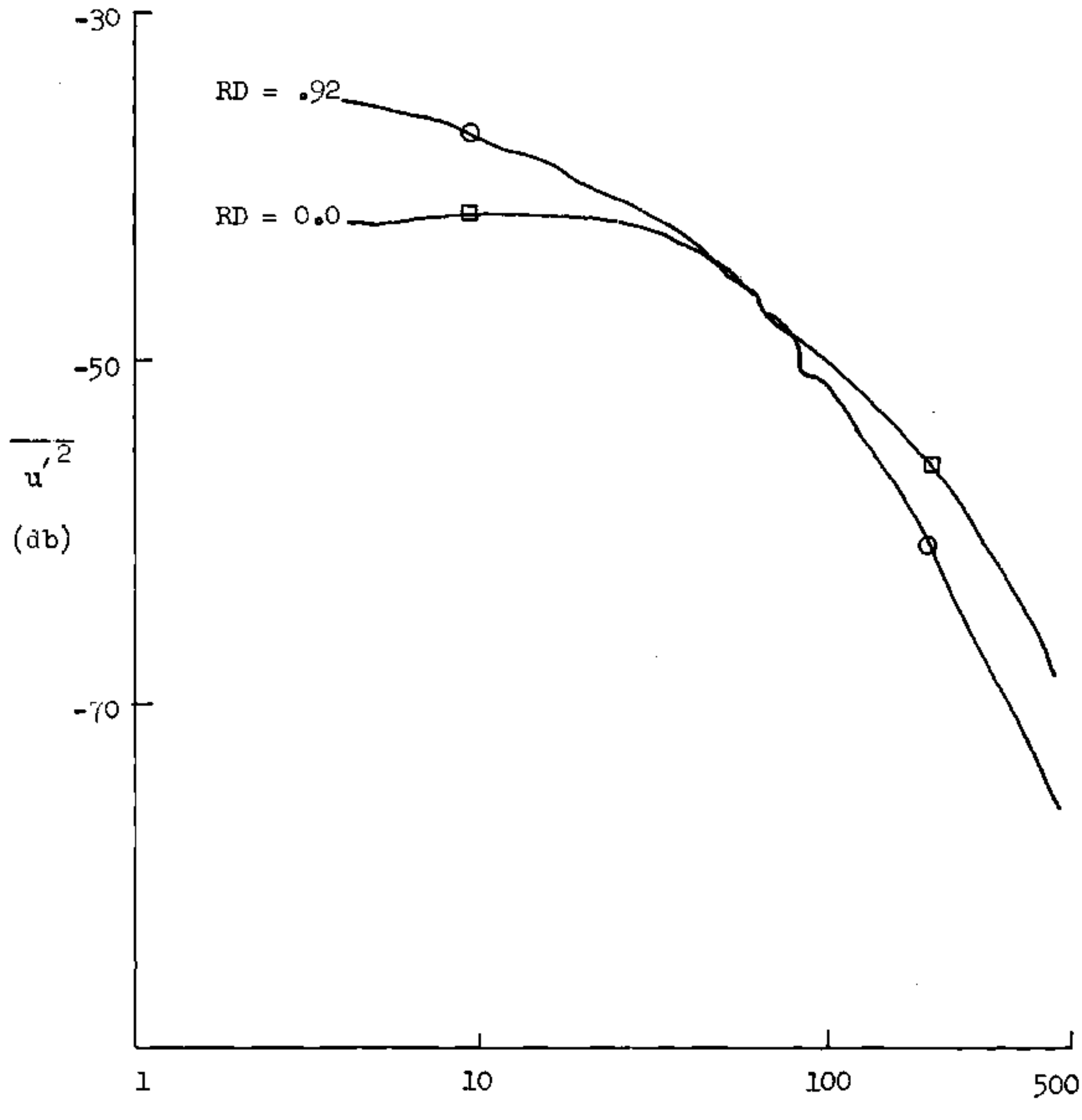

Figure 34. Energy Spectra for Water I, XD=10.0.

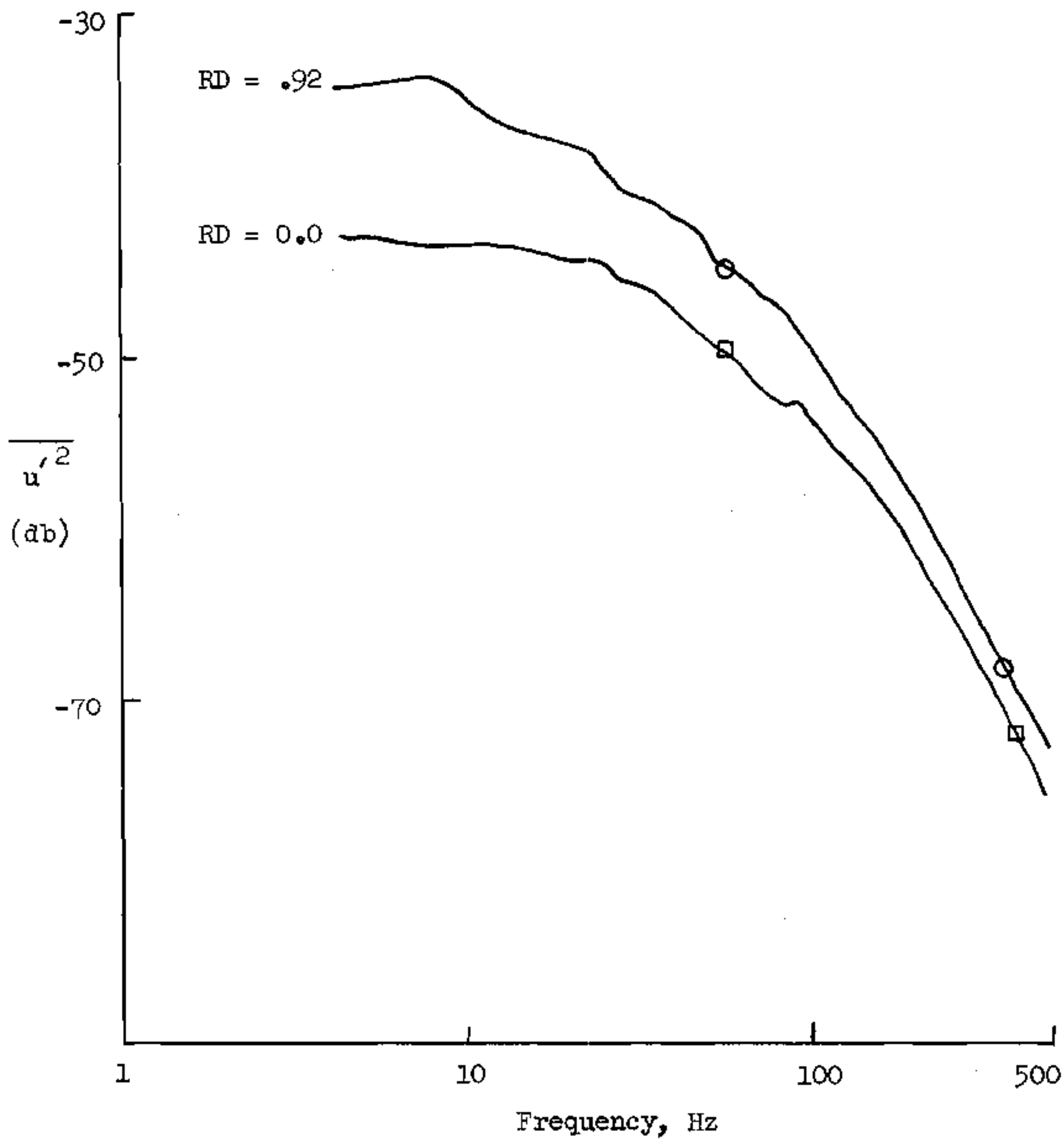

Figure 35. Energy Spectra for Water I, XD=20.0.

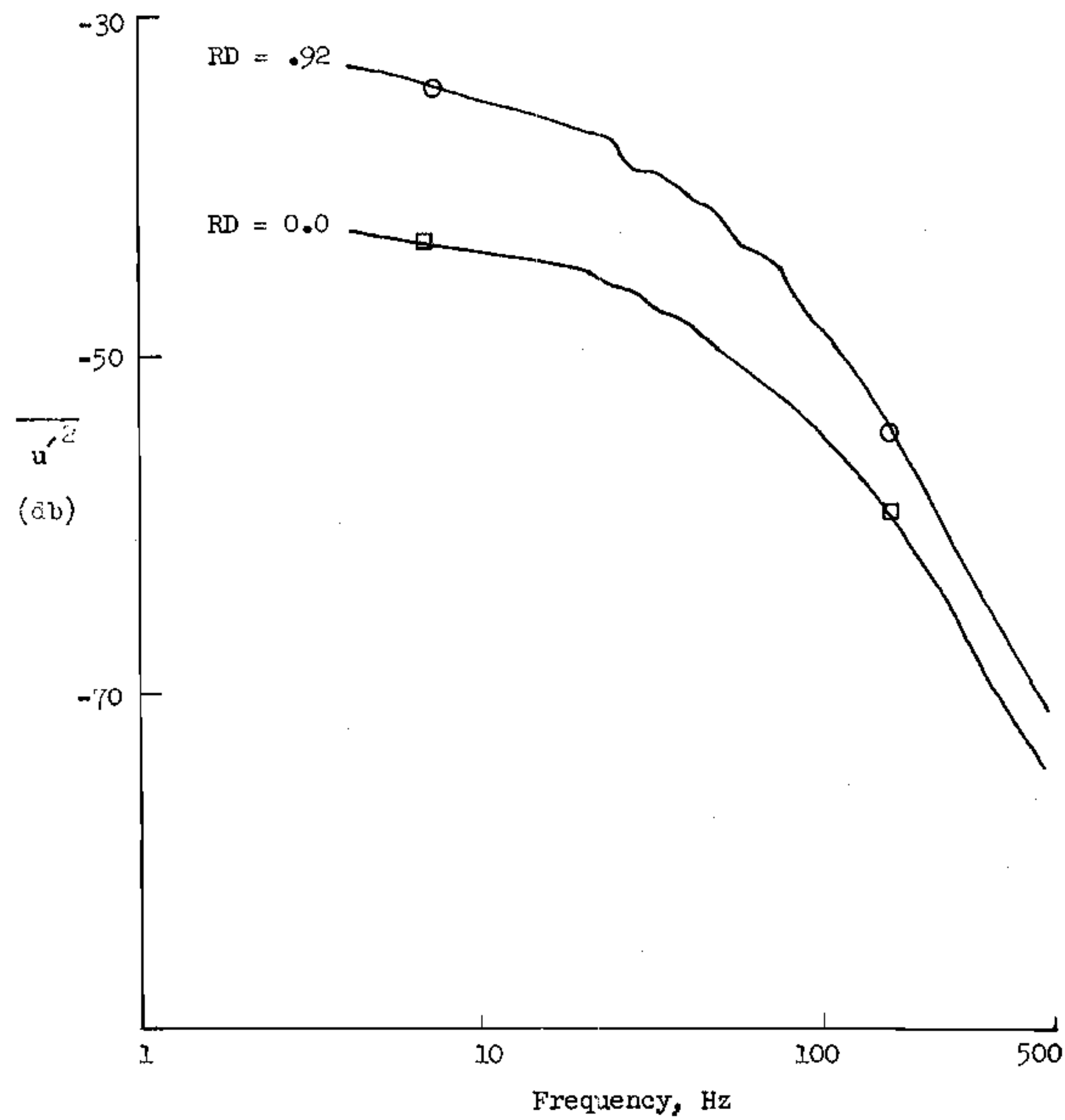

Figure 36. Energy Spectra for Water I, XD=60.

similar to those obtained for fully developed pipe flow. Figure 36 shows the spectra at the axial station farthest from the jet exit. In the frequency range of 10 Hertz to 100 Hertz the slope of the curve is approximately (-3/2). This is different from the the value for the inertial subrange observed for high Reynolds number flows. The Reynolds number for present the flow system is low (<20,000) and hence should not exhibit asymptotic behavior in the inertial subrange .

Spectra for Polymer. Figures 37 to 43 show the (u'^2) spectra obtained at seven axial stations. Figure 37 shows the spectra obtained at three radial positions at the axial location XD = 0.30. The spike in the spectra is clearly visible at RD = 0.193. This peak occurs approximately at the same frequency range as for water. Once again, the spike is indicative of the dominant eddy size in the mixing layer.

Figure 38 shows the variation of spectra at XD = 1.0. The spike in the spectra is visible here both at the center line and at RD = 0.236. Once again, the spectra close to the wall do not show much variation with distance downstream.

Figure 39 gives the spectra obtained at XD = 2.0. At this axial station the center line spectra,as for the case

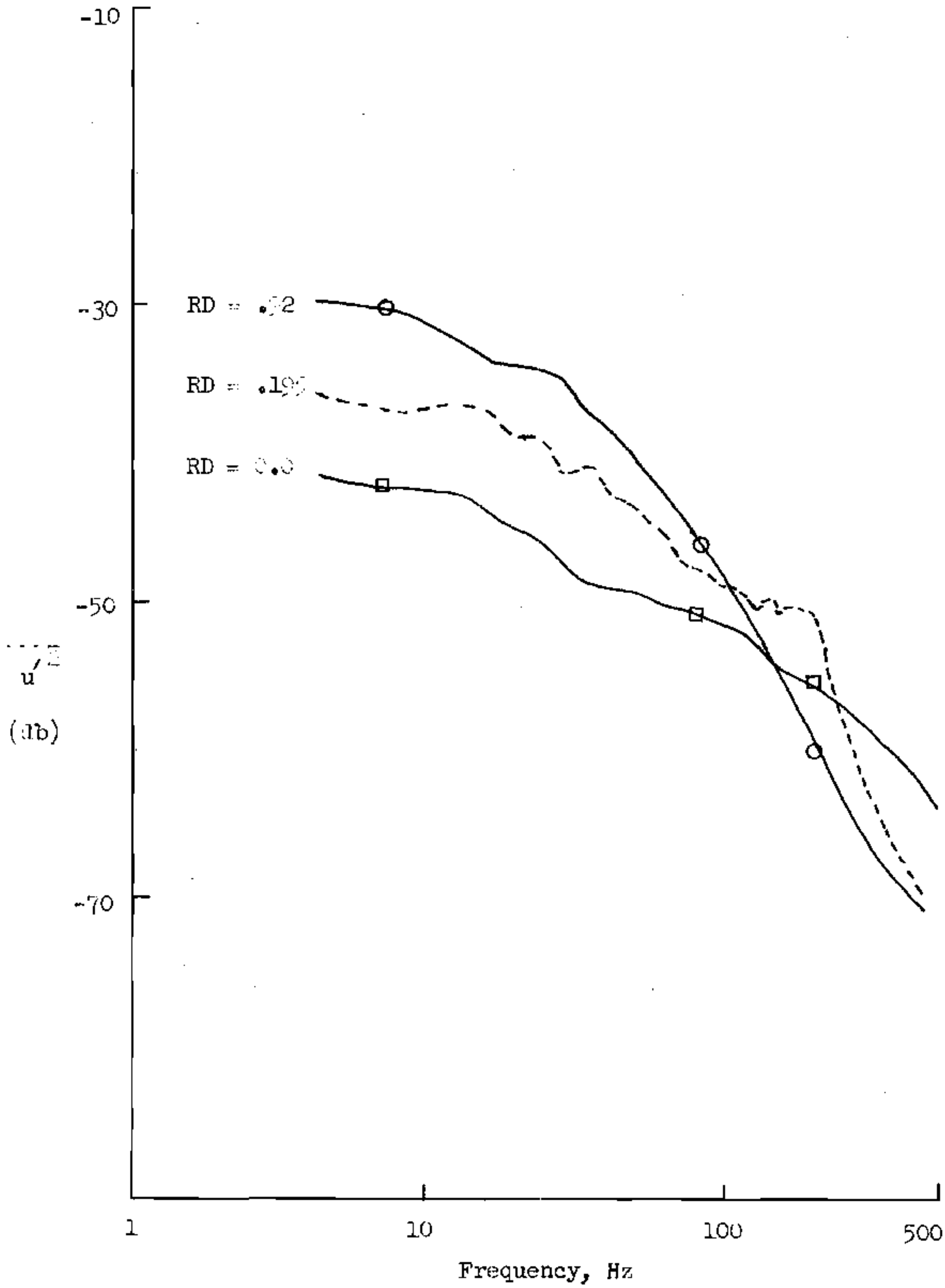

Figure 37. Energy Spectra for Polymer, XD-0.30.

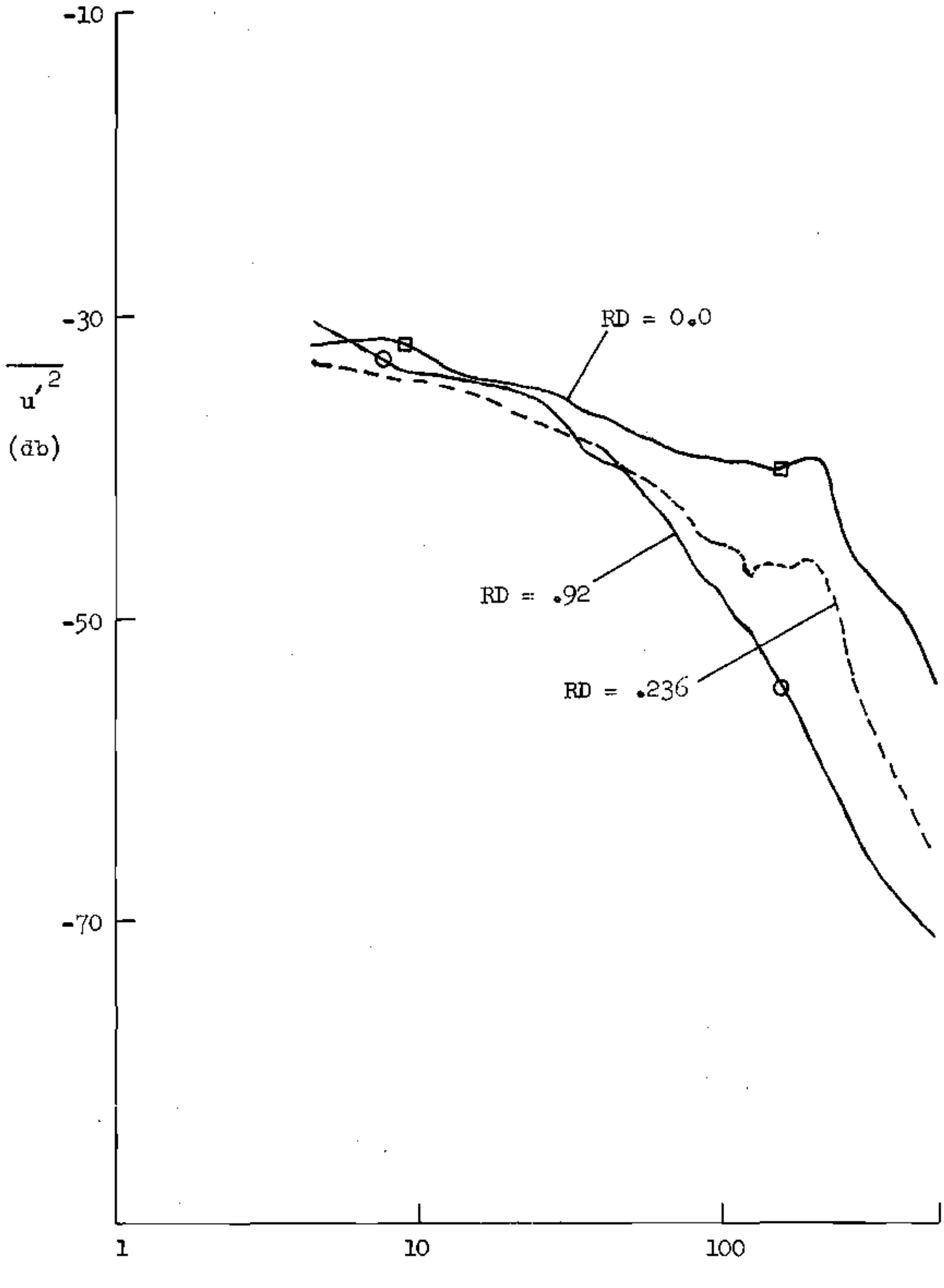

Figure 38. Energy Spectra for Polymer, XD=1.0.

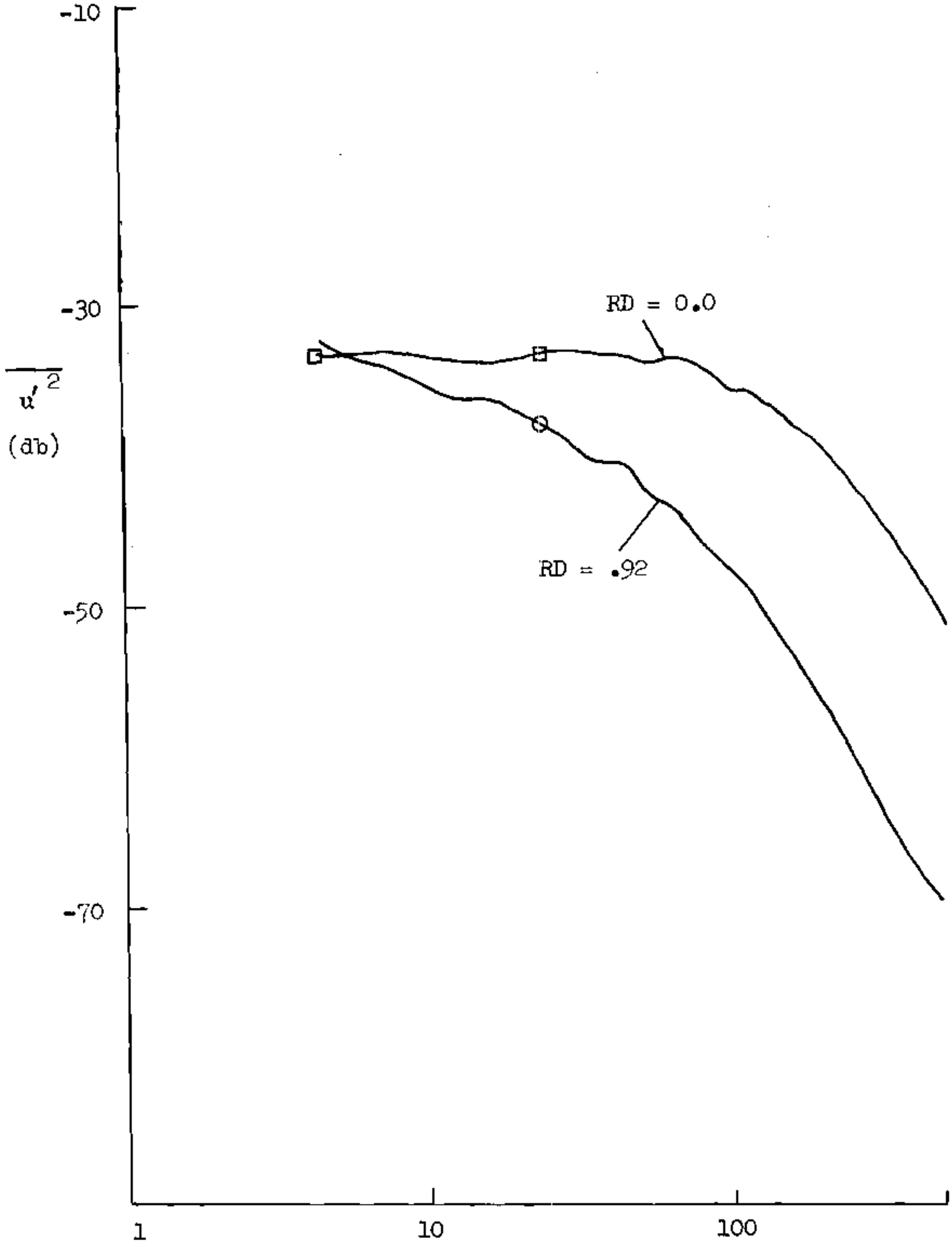

Figure 39. Energy Spectra for Polymer, XD=2.0.

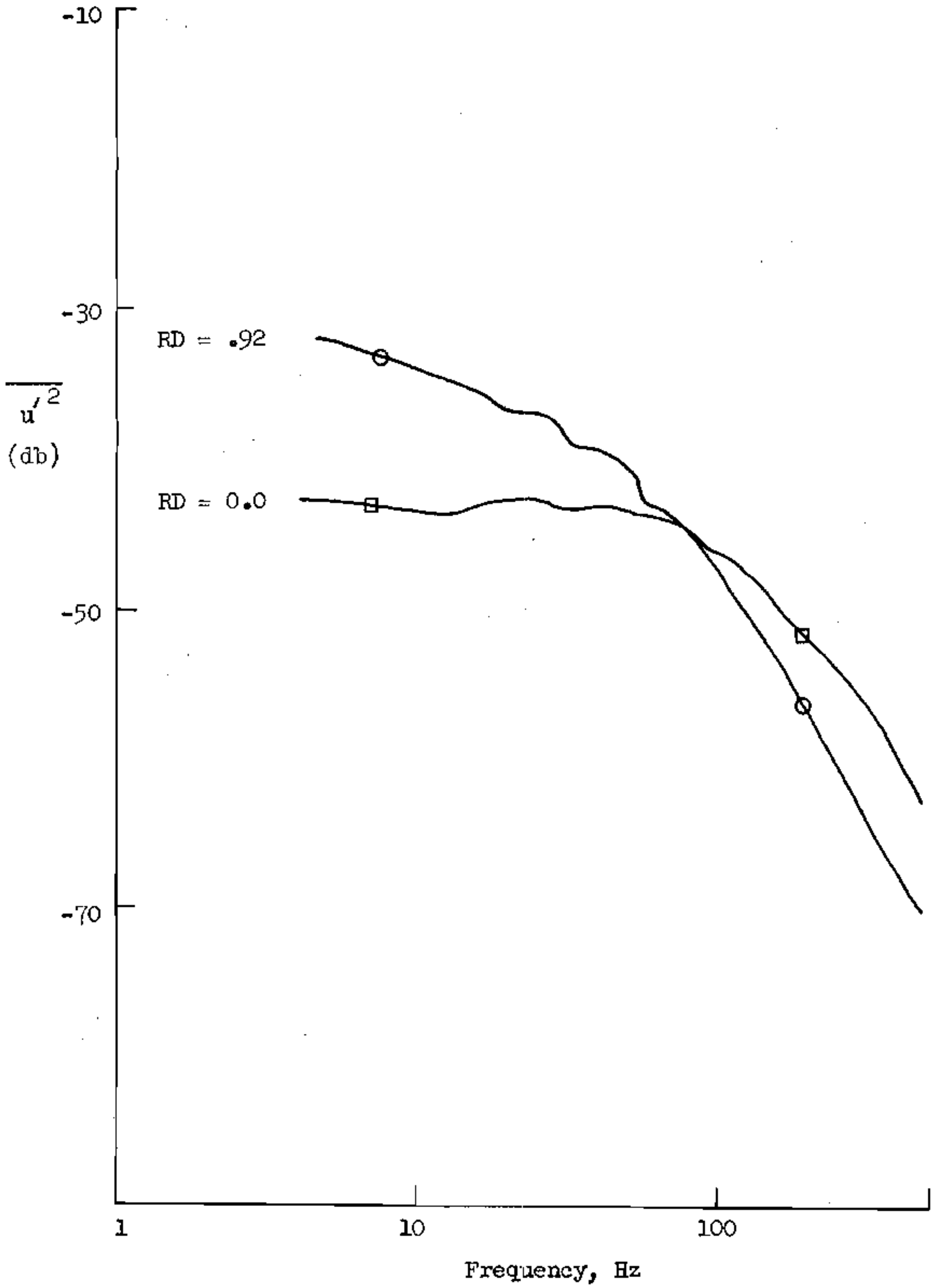

Figure 40. Energy Spectra for Polymer, XD=3.0.

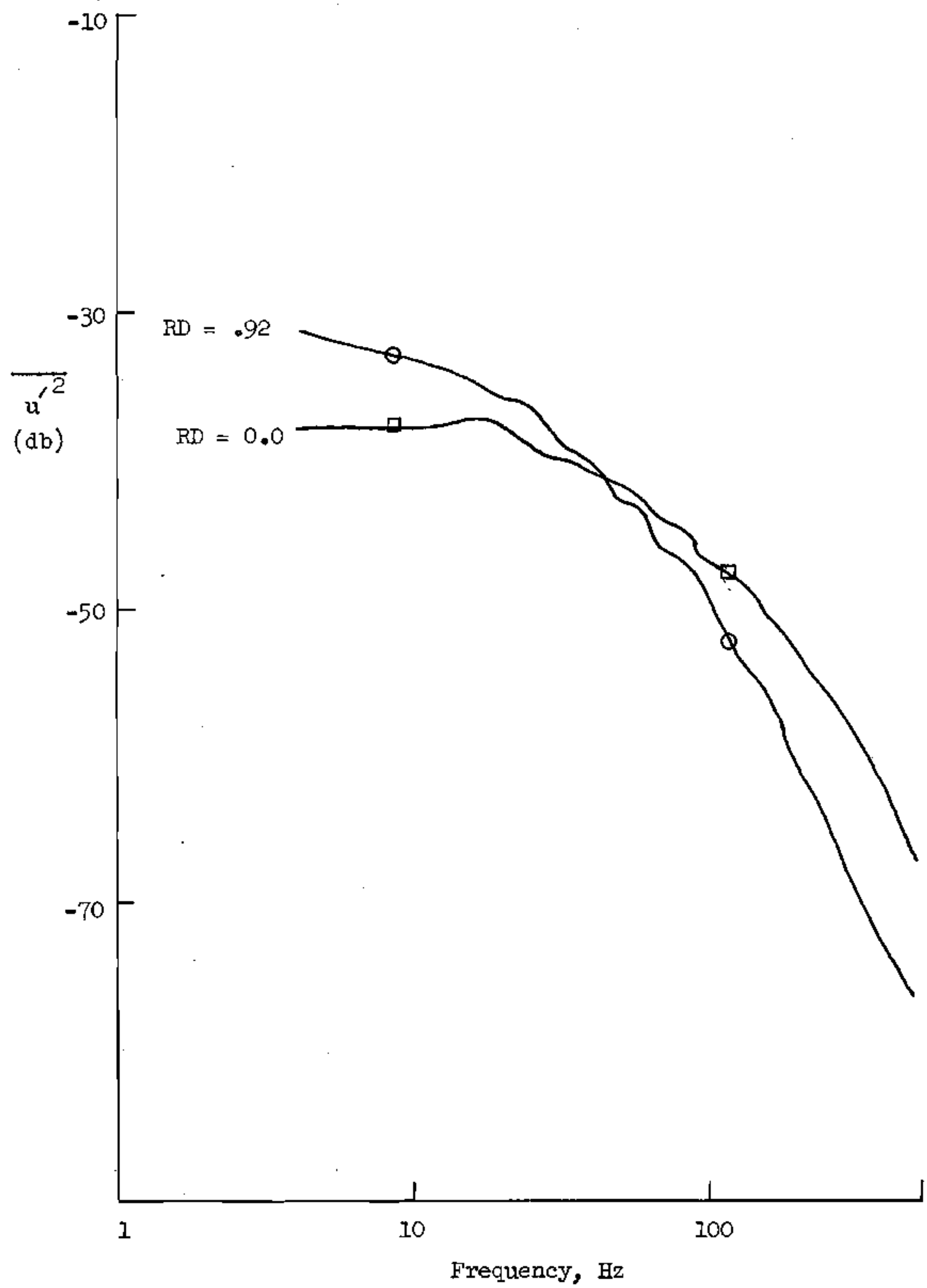

Figure 41. Energy Spectra for Polymer, XD=10.0.

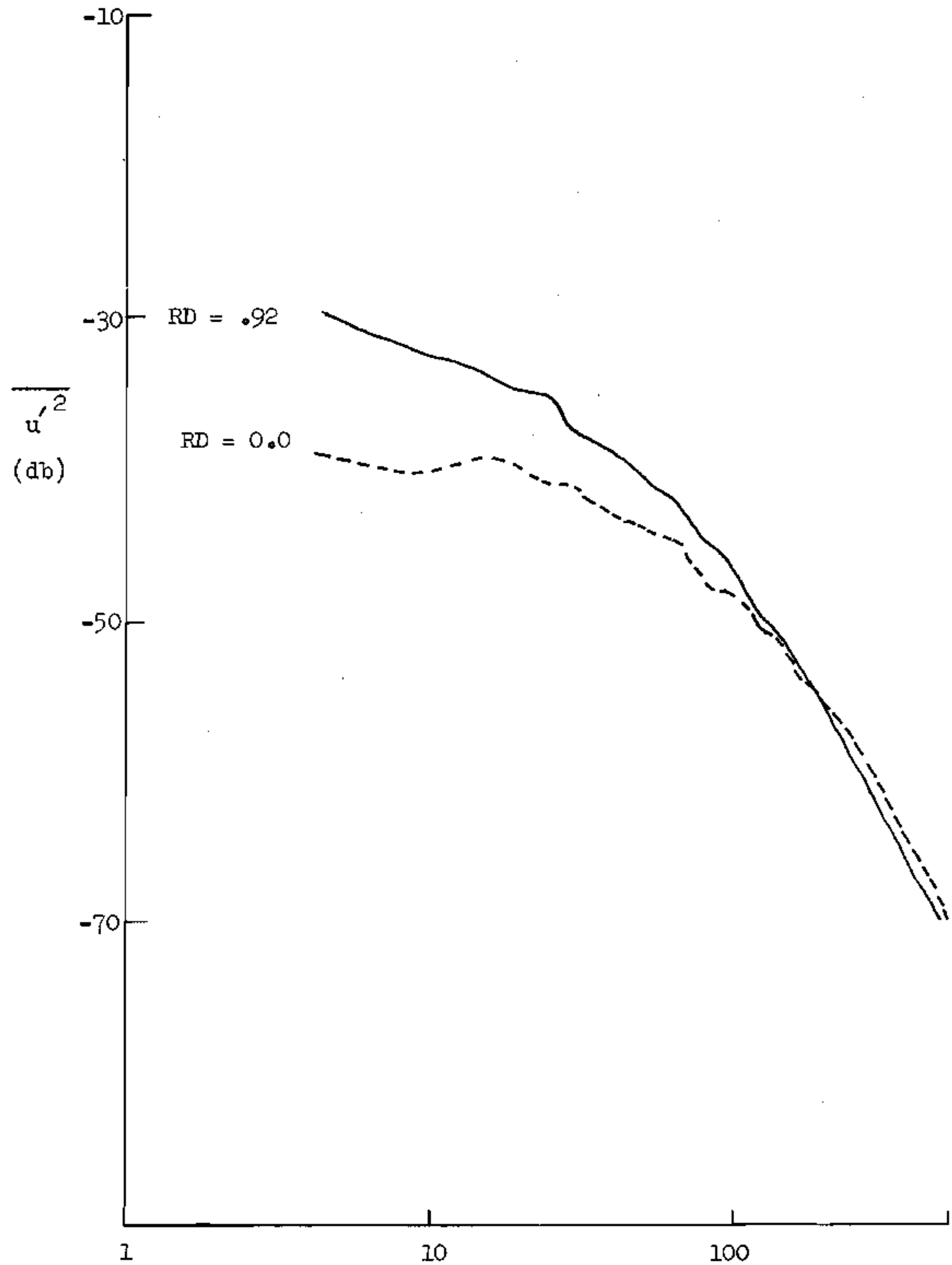

Figure 42. Energy Spectra for Polymer, XD=20.0.

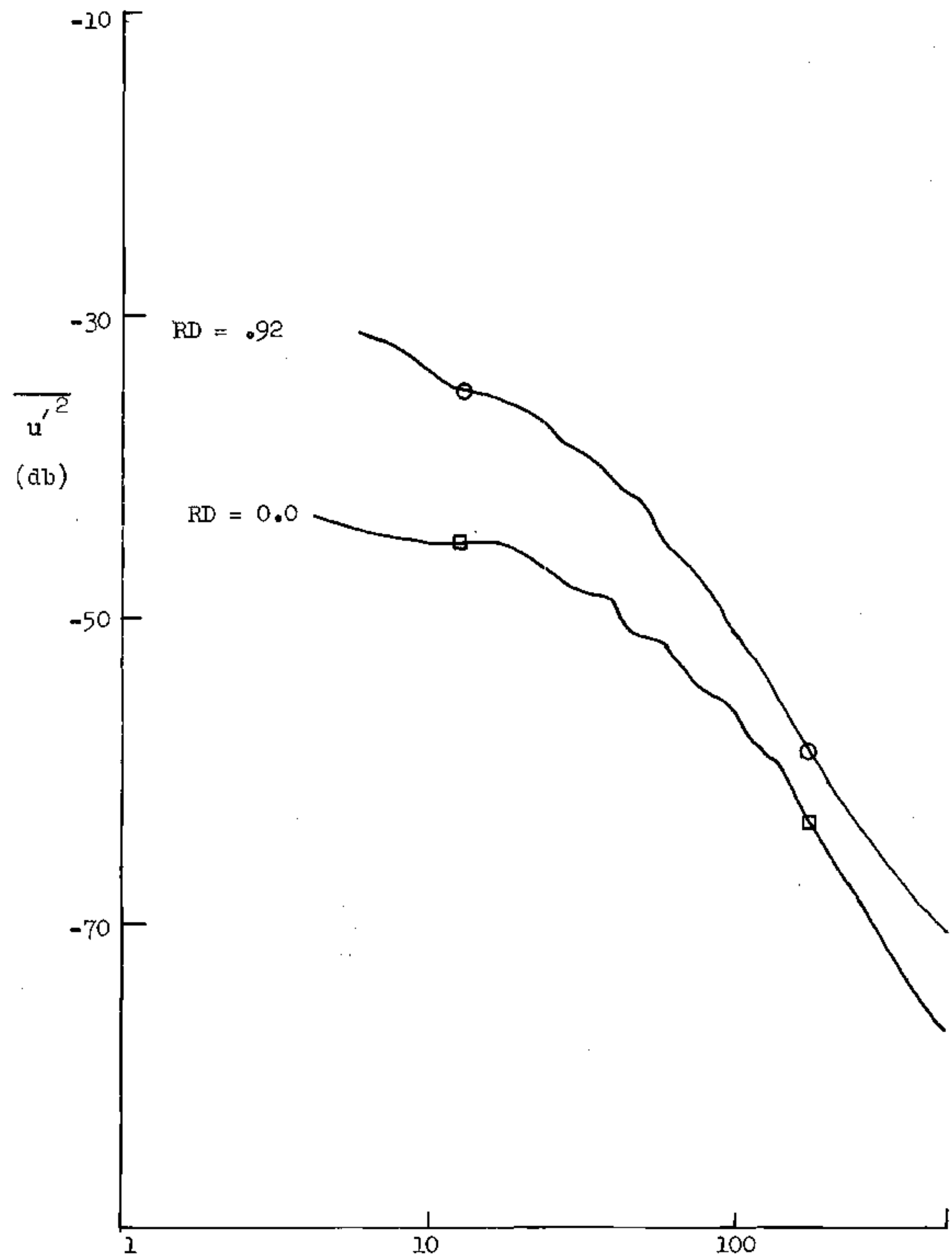

Figure 43. Energy Spectra for Polymer, XD=60.0.

for polymer and water were similar. To show the influence of the polymer on spectral shapes a direct comparison must be made. One obvious difference for the two cases was the flow rate and the initial conditions of the flow. However, Water II has a flow rate very close to that of the polymer and, therefore, comparison of these two cases would show the influence of the polymer.

The spectra obtained at a point close to the wall (RD=0.92) for water, as well polymer, at four axial locations are shown in Figures 44 - 46. They show very little difference, indicating little alteration in the energy distribution over the wave number range. As pointed out earlier, the outer flow is only slightly affected by the jet momentum, as far as mean velocity is concerned. Besides, the upstream annulus region extends for 110 duct radii providing ample time for the layer near the wall to have characteristics close to that of a wall layer. Thus, in the initial region the essential nature of the wall layer is not seriously affected by the jet flow.

Figure 44 compares the spectra for water and polymer solution at a point near the wall at the first axial station. This indicates a higher energy for polymer solution at low wave numbers than that for water I. In fact, this general trend is indicated at most of the axial

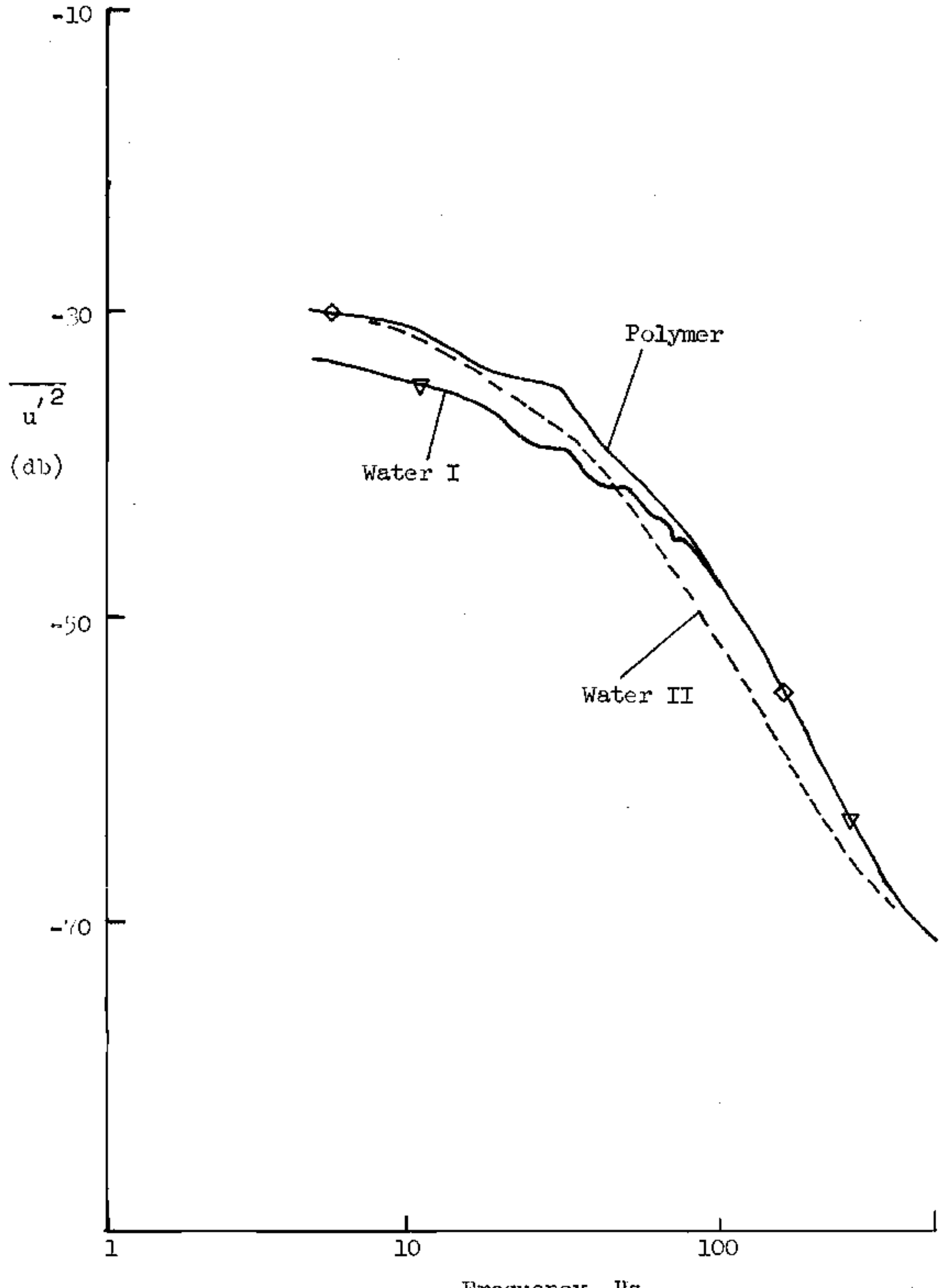

Figure 44. Energy Spectra for Water I, Water II and Polymer; RD=0.92; XD=0.30.

stations.

The spectra obtained for Water II is also plotted on Figure 44 for comparison. The curves indicate very little difference in the energy values in the low wave number range. Figures 45 - 48 provide the comparison of the spectra at a point close to the wall for axial locations XD = 1.0, 2.0, 6.0 and 60.0. The qualitative behaviour of the spectra in general is the same as in Figure 44. Figure 48 also shows the spectra obtained for Water II. This shows that the measured (u'^2) spectra is higher for the polymer solution in the low wave number range. Chung and Graebel [60] have observed the same behaviour in their study of pipe flow of polymer solution using a laser Doppler velocimeter.

The center line spectra for water obtained at the seven axial stations is shown in Figure 49. The spectra at the first three stations stations (i.e., XD $\leq$ 2) indicate an overall increase in the energy level. The spectra for the last four stations (i.e., XD $\geq$ 6) indicate a decrease in the energy level over the entire range of frequencies. In other words, the energy at the center line due to mixing in the very near field of the jet (indicated by XD=2) increases and after a certain axial station (XD=6), the energy at the center line decreases, indicating an adjustment or distribution of energy and finally reaching conditions

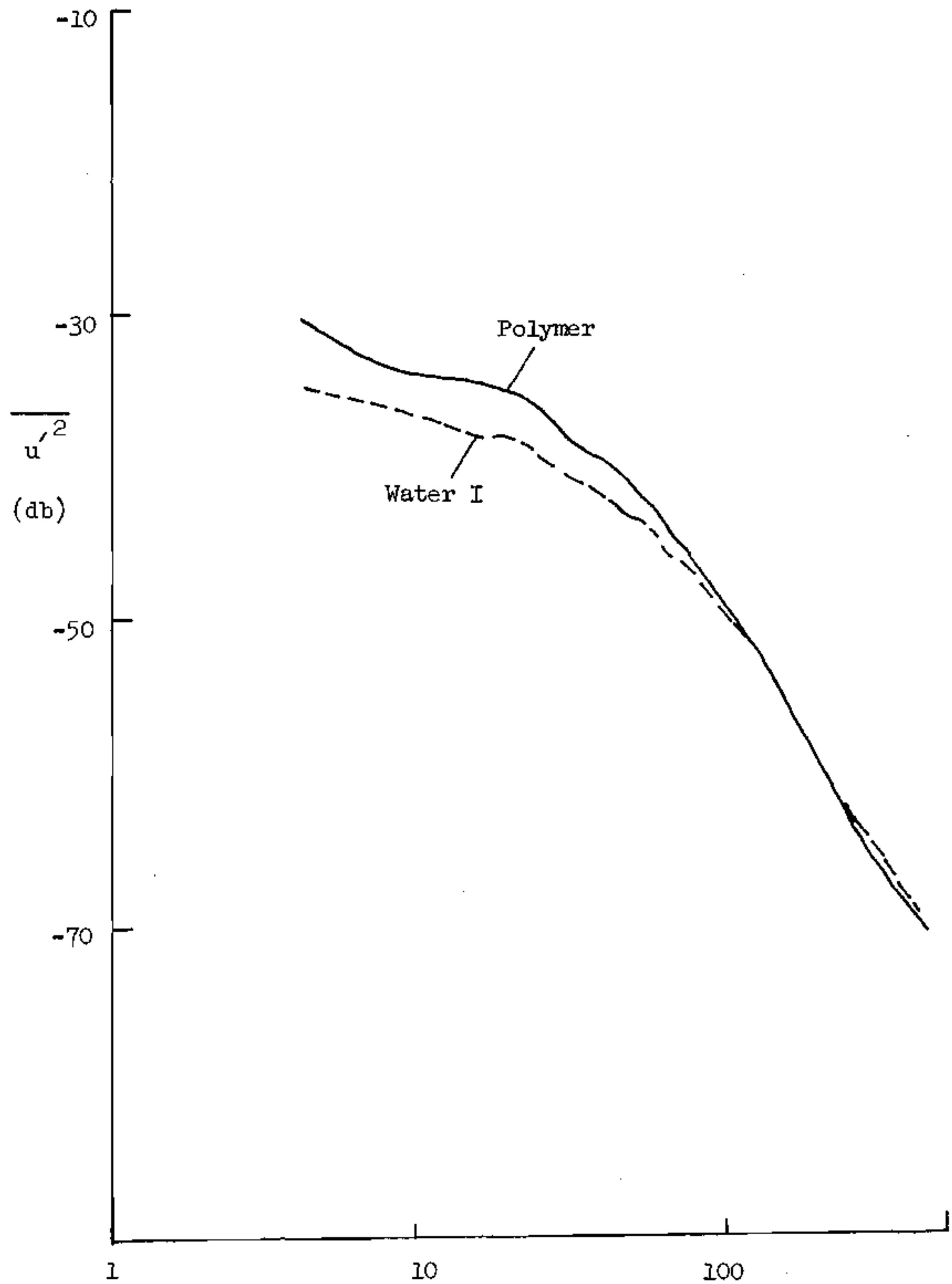

Figure 45. Energy Spectra for Water I and Polymer; RD=0.92; XD=1.0.

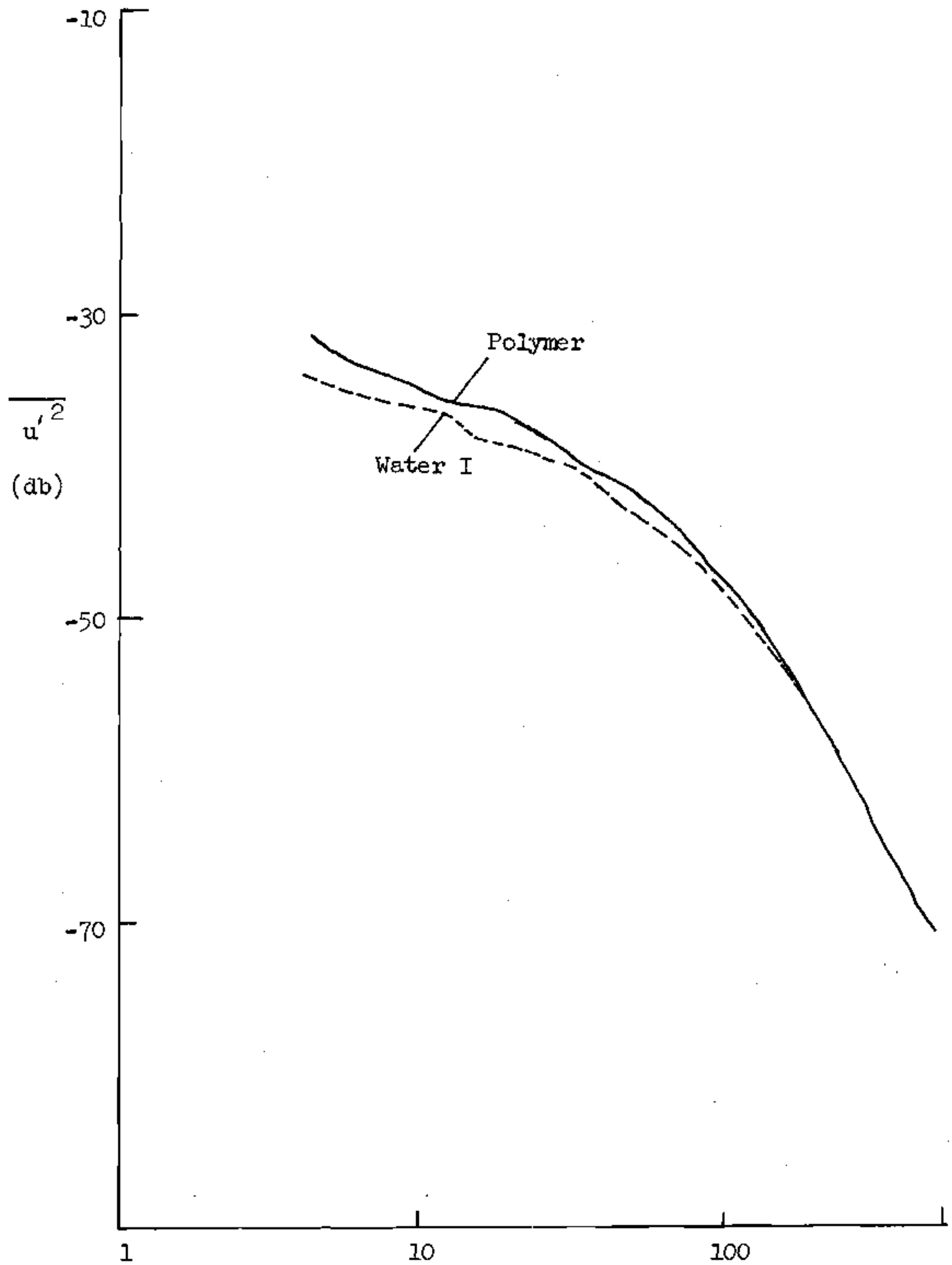

Figure 46. Energy Spectra for Water I and Polymer; RD=0.92; XD=2.0.

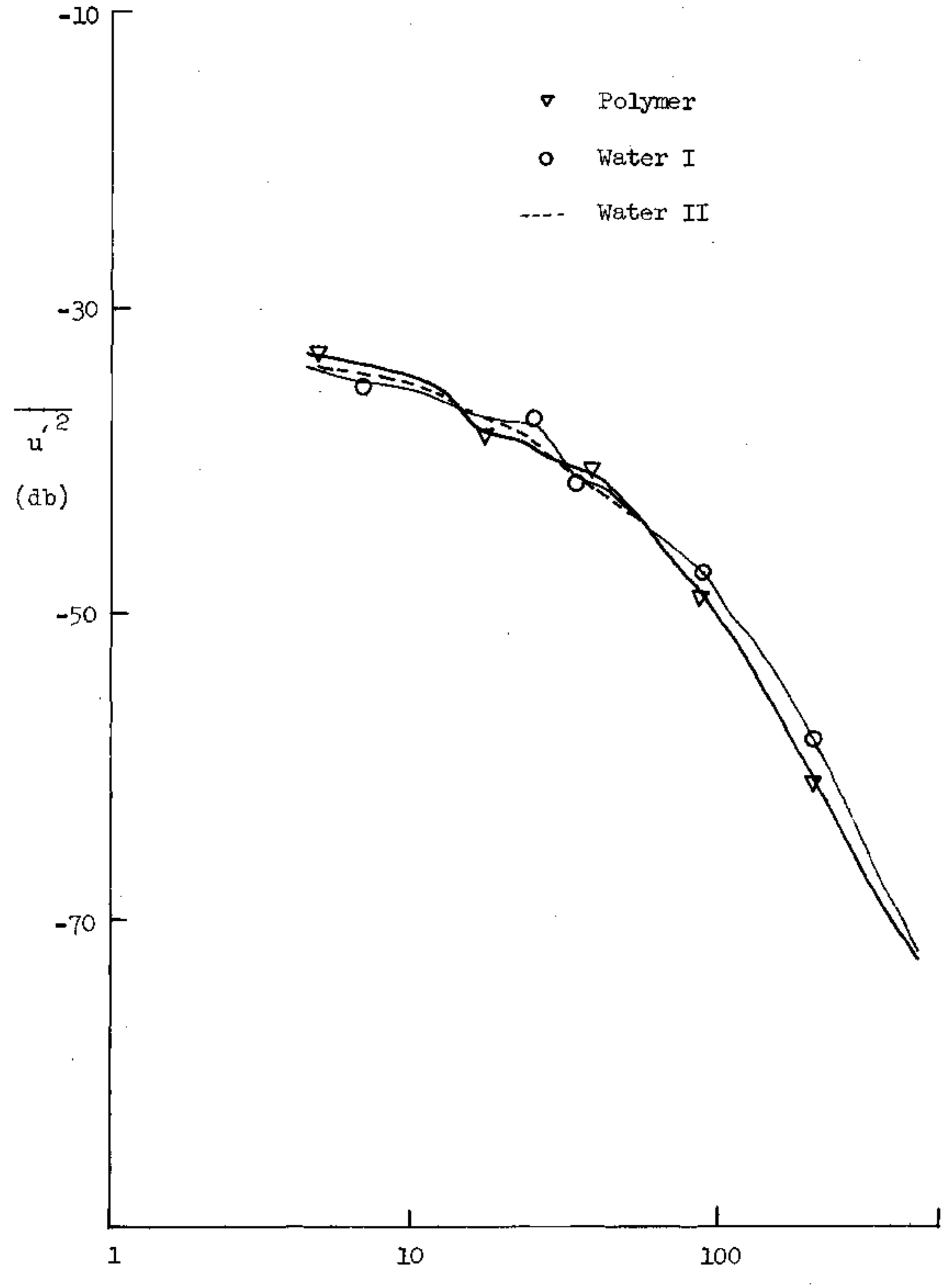

Figure 47. Energy Spectra for Water I, Water II and Polymer; RD=0.92; XD=6.0.

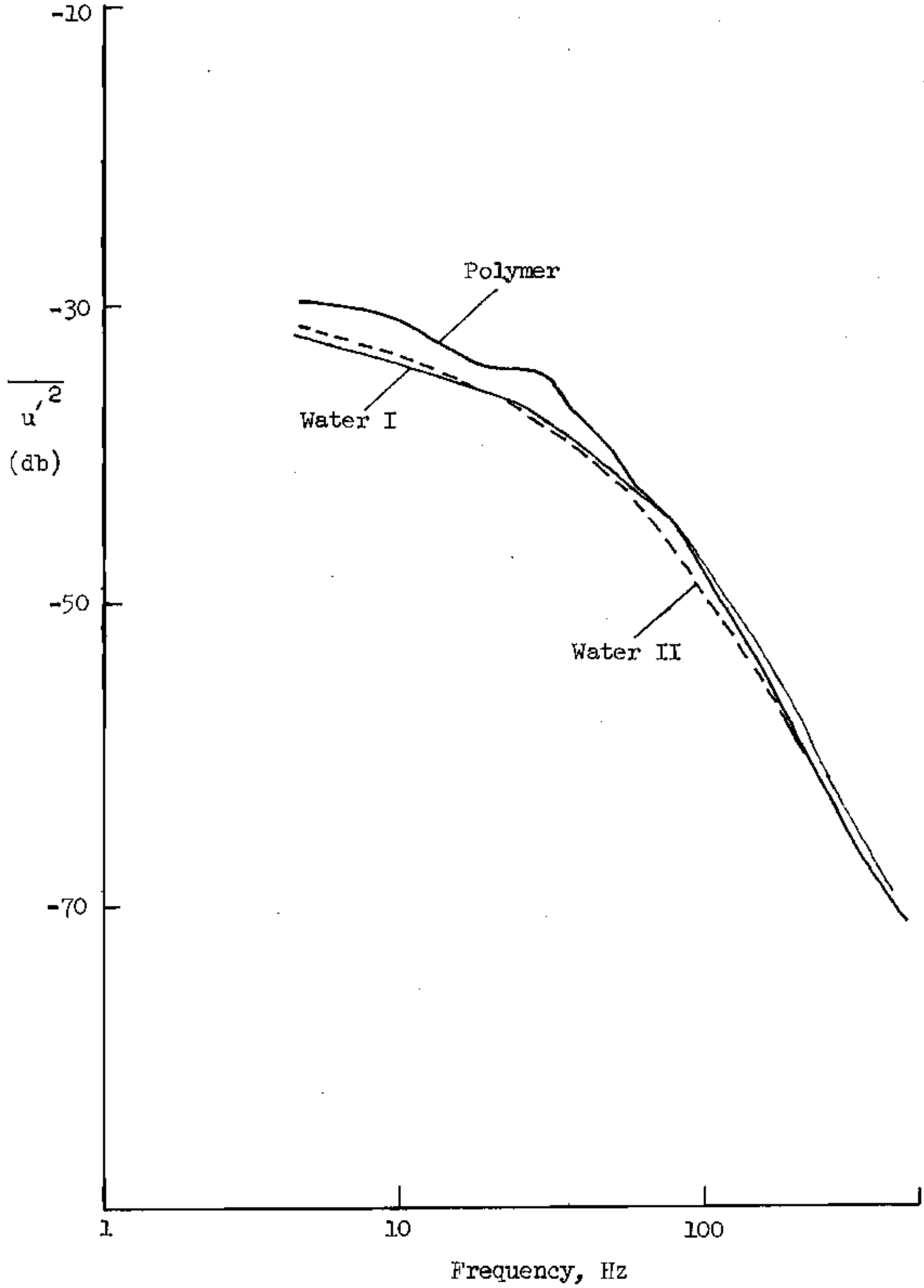

Figure 48. Energy Spectra for Water I, Water II and Polymer; RD=0.92; XD=60.0.

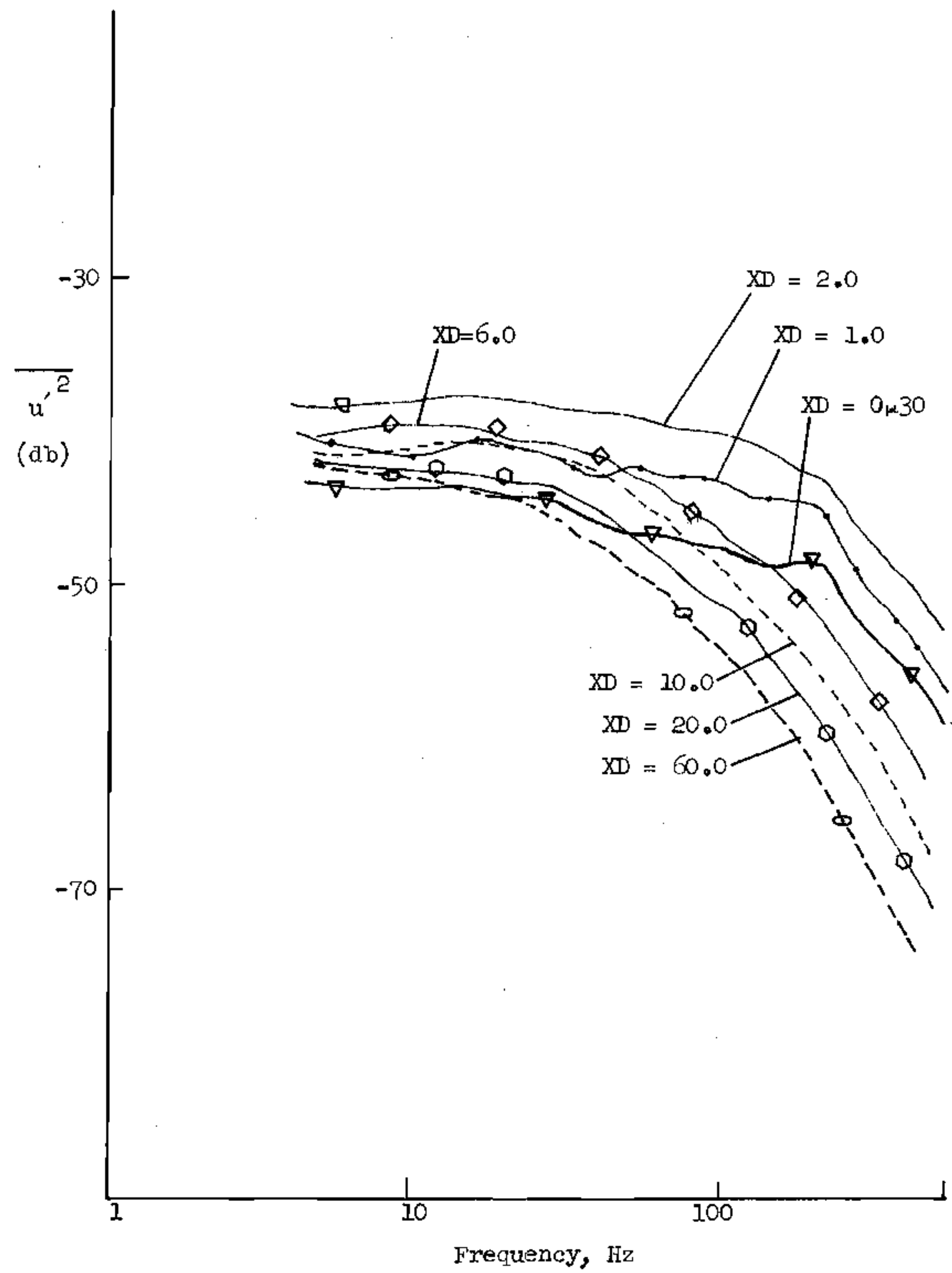

Figure 49. Energy Spectra for Water I at the axis.

corresponding to fully developed pipe flow. It is known that the output of the Fourier Analyzer provides the energy values for discrete values of the frequency and the sum of the discrete energy values would give the value of (u'^2). This coupled with the observation regarding the energy spectral level variation would suggest the centerline turbulence values $[(u'^2)^{1/2}]$ to increase first and then decrease. From Figure 18 it can be seen that turbulent intensity decreases from XD = 6 to XD = 60. Thus the spectral data and intensity measurements are consistent in this regard. Figure 49 also indicates a greater adjustment taking place at higher frequencies than at lower frequencies.

Further, it is also found from the centerline spectra of jets that the slope of the spectra in the high wave number range (ie. beyond the inertial subrange) is approximately -3.3 from the data of Gibson [61] whereas Virk's data for the pipe flow indicate approximately -4. From Figure 49 it can be seen that the slope of the spectra for the high wave number range in the initial region of flow (i.e., XD <2) is smaller than that in the region downstream of XD = 6. This suggests a jet like nature retained in the spectra at least up to XD = 2, and beyond XD = 6 the spectral shape indicates a type of flow behaviour tending toward a pipe flow.

The energy spectra at the axis for polymer solution are shown in Figure 50. The energy levels indicate an increase as the value of XD increases and reaches up to a value of 2.0. The levels then decrease as XD increases from 6.0 to 60.0. The trend also agrees with the turbulence intensity values plotted in Figure 21. Thus, the general behaviour of the spectra at XD = 1.0 and at XD = 2.0 intersect, unlike the case for water. Except for the spectra at XD = 0.30 the shape of the spectra at high wave numbers do not indicate any noticeable variation in the slope as the flow develops.

It was found that the qualitative behaviour of energy spectra at centerline for water and polymer in general are very much similar. A direct comparison of the spectra obtained for polymer and water at same axial loactions are shown in Figures 51 - 53.

Figure 51 shows the comparison of the spectra at XD = 0.30. The curves show the differnce in energy levels in the region where a spike in the spectrum was observed. This combined with the greater decay in mean velocity at centerline suggests the properties of the mixing layer to be altered due to the presence of the polymer. It could be suggested from the variation of the centerline velocity (Figure 22) that the width of the mixing layer is larger for the case of polymer solution. However, Figures 52 and 53 do

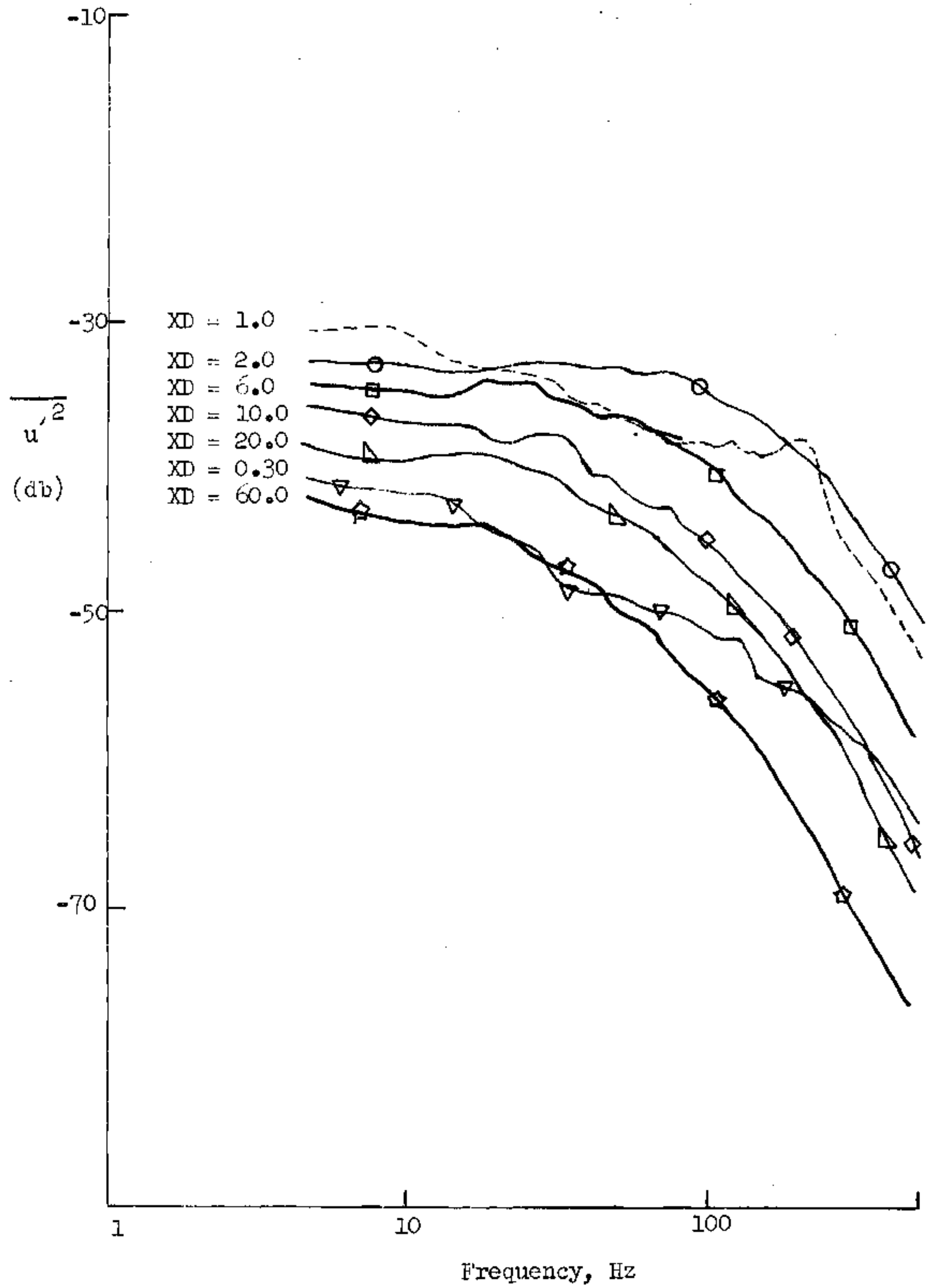

Figure 50. Energy Spectra for Polymer at the axis.

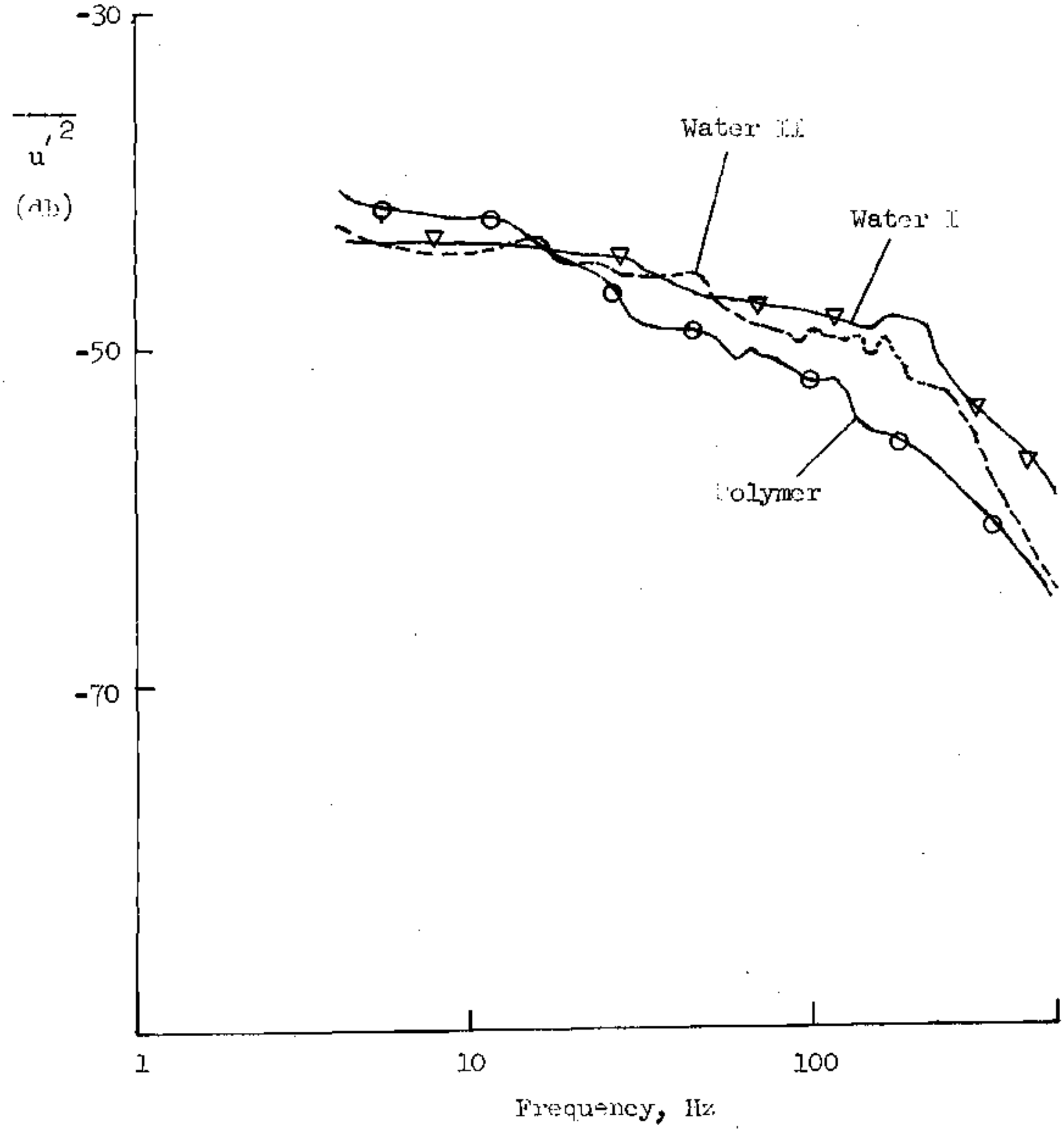

Figure 51. Energy Spectra **at** the axis for Water I, Water II and Polymer; X/D=0.30.

not indicate much difference in structure of the centerline spectra. The spectra indicated differences only in the stations before XD = 6.0. Coupled with the fact that for water, as well as polymer, XD = 6.0 was the axial station from which adjustment of the flow took place, it can be said that the influence of polymer on spectra is found in the region where the centerline turbulence intensity increases, which in turn is caused by the influence of the jet shear layer. After this, the flow adjusts to the fully developed pipe flow conditions and the presence of the polymer does not seem to affect the nature of the energy spectra. Figure 54 shows the energy spectra obtained at XD = 60.0 and indicates very little influence due to polymer. Chung and Graebel [60] also found that the spectra at centerline for polymer and water are similar.

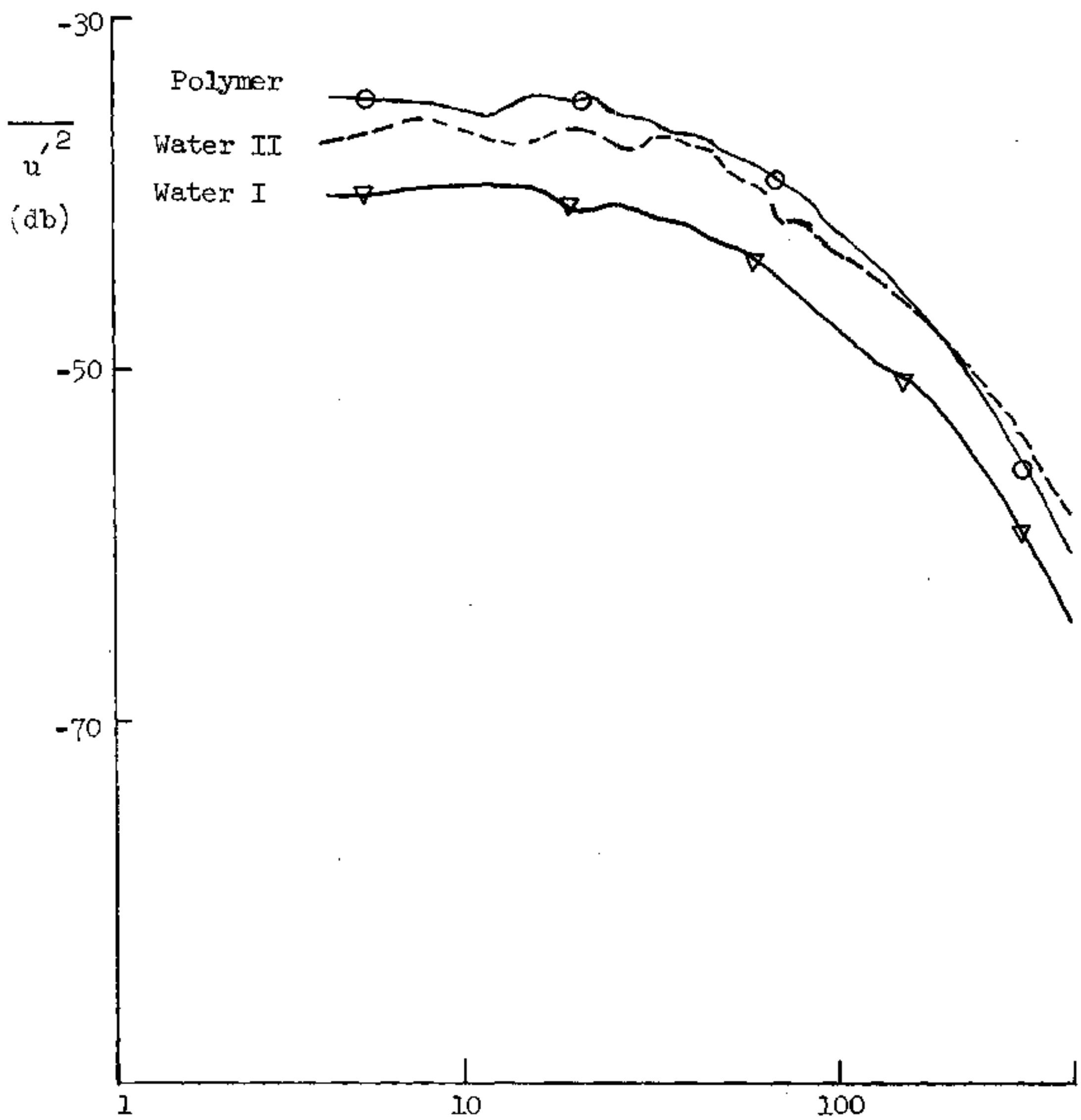

Figure 52. Energy Spectra at the axis for Water I, Water II and Polymer; XD=6.0.

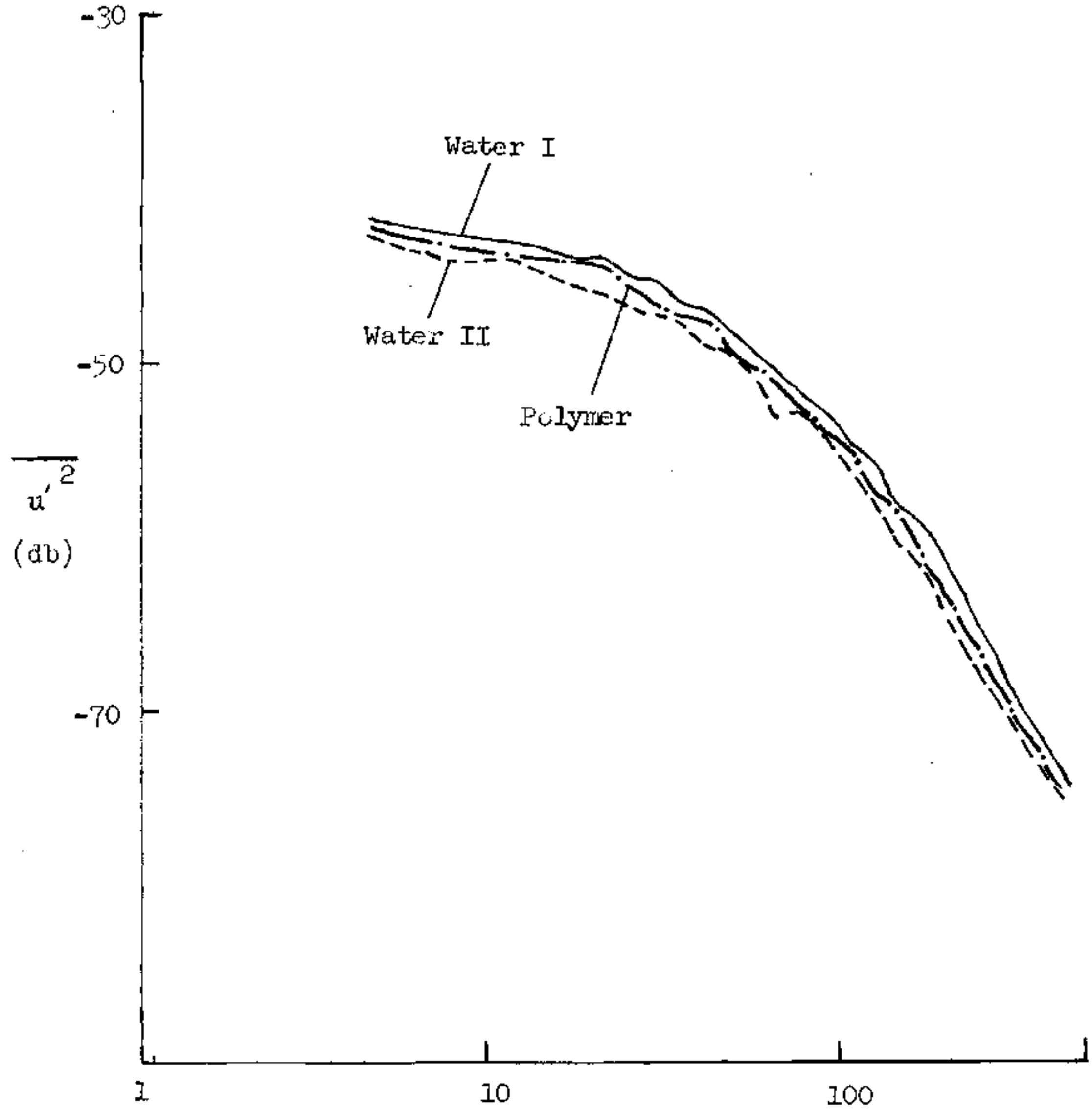

Figure 53. Energy Spectra at the axis for Water I, Water II and Polymer; XD=60.0.

CHAPTER V

CONCLUSIONS AND RECOMMENDATIONS

The turbulent, ducted jet flow problem was studied theoretically and experimentally from the near field region of the jet to stations sufficiently far down stream that fully developed pipe flow conditions were reached. Experimentally, the effects of including small concentrations of a drag reducing polymer in the fluid were also examined. The objective was to provide a fluid dynamic description of a particular type of angiographic injection procedure employed in the diagnosis of vascular disease and to determine whether polymer addition might provide any beneficial modification of the flow field such as enhanced mixing of the fluids or a reduction in turbulent intensities or wall shear stress.

Important specific observations from the study are listed below.

Analytical Studies

1. By exercising considerable care in treating the initial conditions, the k-W model was successful in predicting the flow field with reasonable accuracy for this

rather complex flow problem.

2. The computational scheme is relatively straightforward and may be implemented with a reasonable amount of computer time (approximately four minutes on CDC 3600). Thus, the method is appealing for use in analysis of high speed angiographic injection flows, provided no recirculation exists.

3. Depending upon the injection conditions relative to the duct conditions , the pressure and friction coefficients may or may not exhibit a local maximum distal to the injection plane.

4. Results predicted in the near field are somewhat sensitive to the initial conditions. This suggests, for example, that methods to improve mixing characteristics may be devised by careful manipulation of these initial conditions.

Experimental Results

1. For the specific conditions studied the jet flow momentum did not greatly alter the flow near the wall. this picture, of course, would be dramatically changed if the injection parameters were such that recirculation region was created.

2. The effect of the finite jet tube lip thickness is clearly seen in the regior immediately downstream of the jet exit plane, and the dominant eddy size in the mixing layer produces a spike in the energy spectra in the region.

3. When subjected to the same driving head of pressure, the polymer solution produces a higher jet velocity than does pure water. This is due to the drag reduction effect in the long catheter used for injection.

4. Under conditions of the same jet exit plane flow rate, the presence of the polymer results in a more rapid decay of the center line velocity than does pure water. This suggests a greater mixing between inner and outer flow.

5. The influence of the polymer is exhibited primarily in the region from the center line to the mixing zone in the developing region. For example, turbulence intensities are higher for the polymer solution than for the water in this region; and mean velocity profiles are considerably different, whereas near the wall (or outer zone) they are quite similar.

6. Beyond XD = 10.0 the polymers show only a small

effect on mean velocity or turbulence intensities. When flow is fully developed far downstream, the turbulence intensity close to the wall is slightly higher for polymer solution than for water.

7. In the developing region the polymer solution flow shows a higher energy content in large scale eddies than does the water flow. Thus, the tendency to enhance mixing may be through the mechanism of larger eddy transport.

Conclusions and Implications to Clinical Situations

The present research has examined only one small area of the overall problem of clinical angiographical injections. In addition to the obvious surgical, infectious, and biochemical complications which may arise in practice, there exist the further complexities, fluid dynamically, of retrograde and side-hole injection which have not been considered in the present work. However, despite the limitations, the study given here is the first detailed fluid dynamic investigation of a procedure which has become routine in major hospitals. The analytical results indicate that , under certain conditions, maxima in wall shear stress and pressure can occur distal to the injection when there is a large effect of the inner flow on the outer one. It has also pointed out the sensitivity of the mixing, or near field, region to the initial conditions and has provided a computational tool to aid in understanding the injection process. The experimental work has verified the analytical model and has also demonstrated that the addition of drag reducing polymers have a definite effect on the near field mixing zone in that momentum transfer between inner and outer flows is enhanced, probably by increased transfer among larger eddies. Thus, polymer addition may, in fact, aid in better X-ray contrast in angiography by improving the mixing characteristics of the contrast media.

Further, and probably more significant, is the possibility that by consideration of catheter tip design and injection parameters, improved delineation of blood vessels may result even without polymer addition.

Future Work

It was found from earlier discussions that the results obtained in the developing region of the jet were very sensitive to initial conditions. The question regarding the accuracy of the model and hence its prediction capabilities in the developing region of the jet arise in this context. Whitelaw and Durao [62] have pointed out that the variation of normal stresses, in their study of a jet in an unconfined coflowing stream, is significant. Hence, it would be interesting to see the results obtained by a more sophisticated model which takes care of this variation.

As regards measurements in polymer solutions, the most welcome next step would be to use a method of measurement which is not dependent on the concentration of the solution. A laser Doppler velocimeter would be a suitable choice for this purpose.

Clearly, the present research has made only initial inroads into an important area. Before clinical implementation of any type of potential improvement, much remains tc be accomplished. Studies of injections under a variety of conditions which span the spectrum of clinically employed parameters should be completed. It would be most interesting to study the situation where maxima in pressure and wall shear stress arise as well as cases where recirculation exists. Also, selective alterations in catheter tip geometry might be explored in an effort to discover more favorable initial jet exit plane conditions. Clearly, before any polymer additives could be introduced, enhanced optical contrast should be demonstrated in the laboratory, not to mention the problem of developing a biocompatible polymer.

APPENDIX

FOURIER ANALYZER PROGRAM

A sample program used in the Fourier Analyzer for data reduction is listed below. Mean velocity and the integral of the energy spectrum were obtained from the output [54] .

```
L     0
CL    1
L     1
RA    0     1
F
SP
#     1     50     0
:     1     50
X <   1
X >   2
W     0     0      1
$
W     0     254    256
.
```

BIBLIOGRAPHY

1. Wendeth, A. J. Jr., "Peripheral Arteriography ," CRC Reviews in Clinical Radiology and Nuclear Medicine, P.369-401, 1975.

2. Hass, W. K., Fields, W. S., North, R. R., Kricheff, I. I., Chase, N. W., and Bauer, R. B., "Joint Study of Extracranial Arterial Occlusion," Journal of the American Medical Association, Vol.203, No.11, pp.159-160, March 11, 1968.

3. Field, J. R., Robertson, J. T., and DeSaussure, R. L., "Complications of Cerebral Aniography in 2,000 Consecutive Cases," Journal of Neurosurgey, Vol. 19, pp. 775-781, Sept., 1962.

4. Giddings, J. A., "Embolism Termed a Common Result of Arteriography," Medical Tribune, May 2,1972: A brief report on workdone by J.A. Giddings, J .R. See, R.D. Lewis, and R.S. Cosby , from Pasadena Cardiovascular Research Foundation and University of Southern California School of Medicine.

5. Lonni, Y. E., Matsumoto, K. K., and Lecky J. W., "Postaortographic Cholesterol (Atheromatous) Embolization," Radiology, Vol. 93, pp. 63-65, July, 1969.

6. Toms, B. A. "Some Observations on the Flow of Linear Polymer Solutions through Straight Tubes at Large Reynolds Numbers," Proceedings of International Congress on Rhelogy, 1948, Vol. II, North Holland Publishing Co., Amsterdam, p. 135, 1949.

7. Greene, H. L., Nokes R. F., and Thomas, L. C., "Drag Reduction in Pulsed Folw of Blood," Medical Research Engineering, Vol. 9, no. 5, pp. 19-21, 1970.

8. White, W. D. and Hoyt, J. W., "The Effect of Linear, High Molecular Weight Polymers on the Turbulent Flow Properties of Human Blood," Medical Research Abstract from Proceedings of 8th International Cong. on Medical and Biological Engineering, July 22,1969.

9. Hoyt, J. W., and White, W. D., "High Polymer Additive Effect on Turbulent flow of Dextran, Saline Solution, and Plasma," Proc. of 19th Annual Conf. on Engineering

in Medicine and Biology, p. 49, 1966.

10. Squire, H. B., and Trouncer, J., "Round jets in a General Stream," ARC Reports and Memoranda No. 1974, pp. 1-23, 1944.

11. Forestall, W., and Shapiro, A. H., "Momentum and Mass Transfer in Coaxial Gas Jets," J. Appl. Mech., Vol.17, pp. 399-408, 1950.

12. Mikhail, S., "Mixing of Coaxial Streams Inside a Closed Conduit, " J. Mech. Engg: Science, Vol.2, pp.59-68, 1960.

13. Craya, A., and Curtet, R., "On the Spreading of a Confined Jet," Comptes-Rendus Academie des Sciences, Vol.241, pp.621-622, 1955.

14. Becker, H. A., Hottel, H. C., and Williams, G. C., Ninth Symposium on Combustion, p.842, 1963.

15. Curtet, R., "Confined Jets and Recirculation Phenomena with Cold Air," Combustion and Flame, Vol.2, p. 383, 1958.

16. Curtet, R., and Ricou, F. P., "On the Tendency to Self-Preservation in Axisymmetric Ducted Jets," Journal of Basic Engineering, Vol.86, pp. 765-776, 1974.

17. Abramovich, G. N., "The Theory of Turbulent Jets," M.I.T. Press, Cambridge, Mass., 1963.

18. Hill, P. G., "Turbulent Jets in Ducted Streams," Journal of Fluid Mechanics, Vol. 22, pp.161-186, 1965.

19. Alpineri, L. J., "Turbulent Mixing of Coaxial Jets," AIAA Journal, p. 1560, Vol.2, 1964.

20. Kulick, R. A., Leithem, J. J., and Weinstein, H., "Turbulence measurements in a Ducted Coaxial Flow," AIAA Journal, Vol.8, p.1694, 1970.

21. Razinsky, E., and Brighton, J. A., "Confined Jet Mixing for Nonseparating Conditions," Journal of Basic Engineering, p. 333, 1971.

22. Exley, T., and Brighton, J. A., "Flow Separation and Reattachment in Confined Jet Mixing," Journal of Basic Engineering, p. 192, 1971.

23. Brandon, H. J., "Turbulent Coaxial Jet Mixing in a

Constant Area Duct," Journal of Aircraft, Vol.9, p. 188, 1972.

24. Hedges, K. R., and Hill, P. G., "Compressible Flow Ejectors, Parts I and II," Journal of Fluids Engineering, Vol. 96, p. 272, 1974.

25. Minner, G. L., "A Study of Axisymmetric, Incompressible Ductec Jet Entrainment," Ph.D Thesis, Purdue University, January, 1970.

26. Lumley, J. L., "The Toms Phenomenon," Applied Mechanics Reviews, vol.20, p1139, 1967.

27. Lumley, J. L., "Drag Reduction by Additives," Annual Review of Fluid Mechanics, Vol. 1, p. 369, Annual Reviews Inc. 1969.

28. Hoyt, J. W., "The effect of Additives on Fluid Friction," Freeman Award Review Paper.

29. Gadd, G. E., "Friction Reduction," Encyclopedia of Polymer Science and Technology, Vol. 15, 1971.

30. Granville, P. S., "Progress in Friction Drag Reduction, Summer 1971 to Summer 1972," Microfische AD-757 012.

31. Darby, ., "A Review and Evaluation of Drag Reduction Theories," Naval Research Lab Memo. Rep. 2446, June, 1972.

32. Gadd, G. E., "Turbulence Damping and Drag Reduction Produced by Certain Additives in Water," Nature, vol.206, p463, 1965.

33. White, A., In Viscous Drag Reduction (ed. C. S. Wells), p297,Plenum Press, 1969.

34. White, D. A., "Velocity Measurements in Axisymmetric Jets of Dilute Polymer Solutions," Journal of Fluid Mechanics, vol.28, p195, 1965.

35. Smith, K. A.,Merril, E. W., Mickley, H. S., and Virk, P. S., "Anomalous Pitot Tube and Hot Film Measurements in Dilute Polymer Solutions," Chemical Engg. Science, vol.22, p619, 1967

36. Berman, N. S., Gurney, G. B.. and George, W. K., "Pitot Tube Errors in Dilute Polymer Solutions," Physics of Fluids, vol 16, p1526, 1973

37. Vlasov, S. A., Kalashnikov, V. N., Mulchenko, B. F., Rinkevichyus, B. S., and Smirnov, V. I., "The Long Range Nature of Turbulent Submerged Jets of Polymer Solutions," Fluid Mechanics- Soviet Research, vol.2, p136, 1973

38. Barker, S. J., "Laser-Doppler Measurements on a Round Turbulent Jet in Dilute Polymer Solutions," Journal of Fluid Mechanics, vol.60, p721 , 1973

39. Wells, C. S., and Spangler, J. G., "Injection of a Drag-Reducing Fluid into Turbulent Pipe Flow of a Newtonian Fluid," Physics of Fluids, vol.10, p1890, 1967.

40. Mellor, G. L., and Herring, H. J., "A Survey of the Mean Turbulent Field Closure Models," AIAA Journal, vol.11, p590, 1973

41. Launder, B. E., and Spalding, D. B., "Mathematical Models of Turbulence," Academic Press, 1972

42. Spalding, D. B., "A Two-Equation Model of Turbulence"2," VDI-Forsch-Heft 549, p5

43. Spalding, D. B., "Concentration Fluctuations in a Round Turbulent Free Jet," Journal of Chemical Engg. Science, vol.26, p95, 1971

44. Patankar, S. V., and Spalding, D. B., "Heat and Mass Transfer in Boundary Layers," Second Edition, Intertext Books, London.

45. Yajnik, K. S., and Afzal, N., "Moderate Reynolds Number Effects in Turbulent Pipe and Channel Flows," Journal of Fluid Mechanics, p25, 1974

46. Patterson, G. K., "Turbulence Measurements in Polymer Solutions with Hot Wire," Ph.D Thesis, University of Rolla, 1969

47. Rodriguez, J. M., Patterson, G. K., and Zakin, J. L., "Effects of Probe Geometry on Turbulence Measurements in Liquids Using Hot-Film Anemometry," Journal of Hydronautics, vol.4, p16, 1970

48. Warschauer, K. A., Vijge, J. B. A., and Boschloo, G. A., "Some Experiments and Considerations on Measuring Turbulence in Water with Hot Films," Applied Scientific Research, vol.29, p81, 1974

49. Koletty, J. W., "Calibration of the Conical Hot Film Anemometer Probe," Special Problem, Aerospace Engineering, Georgia Tech 1973

50. DISA Probe Manual, DISA Electronic A/S, DK2730 Herlev, Denmark

51. TSI Anemometry, Thermo-Systems Inc., 2500 Cleveland Avenue, St. Paul, Minnesota 55113

52. DISA Anemometer Manual, DISA Electronic A/S, DK2730 Herlev, Denmark.

53. DISA Linearizer Manual, DISA Electronic A/S, DK2730, Herlev, Denmark

54. Fourier Analyzer System 5451A Manual, Hewlett-Packard Company, Santa Clara, California 95050, 1972

55. Oka, S., and Kostic, Z., "Wall Proximity Influence on Hot-Wire Measurements," DISA Information no.13

56. Rudd, M. J., "Measurements Made on a Drag Reducing Solution with a Laser Velocimeter," Nature, vol.224, p587, 1969

57. Jones, B. G., Hammersly, R. J., Planchon, H. P., and Spencer, B. W., "The Turbulence Structure in the Plane Two-Stream Mixing Layer," p87, Fluid Mechanics of Mixing (ed. E.M.Ulam and V.W.Goldschmidt), 1973

58. Ko, N. W. M., and Davies, P. O. A. L., "The Near Field within the Potential Core of Subsonic Cold Jets," Journal of Fluid Mechanics, vol.50, p49, 1971

59. Virk, P. S., Merril, E. W., Mickley, H. S., and Mollo-Christensen, E. O., "The Toms Phenomenon: Turbulent Pipe flow of Dilute polymer Solutions", Journal of Fluid Mechanics, vol.30, p.305, 1967

60. Chung, J. S., and Graebel, W. P., "Laser Anemometer Measurements of Turbulence in Non-Newtonian Pipe Flows," Physics of Fluids, vol.15, p546, 1972

61. Gibson, M. M., "Spectra of Turbulence in a Round Jet," Journal of Fluid Mechanics, vol.55, p161,1972

62. Durao, D., and Whitelaw, J. H., "Turbulent Mixing in the Developing Region of Coaxial Jets," ASME Paper No. 73-FE-19, 1973

VITA

Rajagopala Menon was born in Singapura, Malaya on May 21, 1944. He attended schools in North Parur, Kerala (India), graduating in April 1959. In June 1959 he entered Union Christian College in Alwaye, where he received the degree of Bachelor of Science in Physics in June 1963.

In July of 1963, he entered Indian Institute of Technology, Kharagpur and in June 1967, graduated with a Bachelor of Technology in Aeronautical Engineering, with honors. Upon graduation, he joined Indian Institute of Technology, Kanpur, where he received the degree of Master of Technology in Aeronautical Engineering in July 1969. He worked as a Senior Research Assistant from December 1968 to July 1970. In the fall of 1970 he entered the Georgia Institute of Technology as a graduate student and research assistant in the School of Aerospace Engineering.